Lucian Mocan

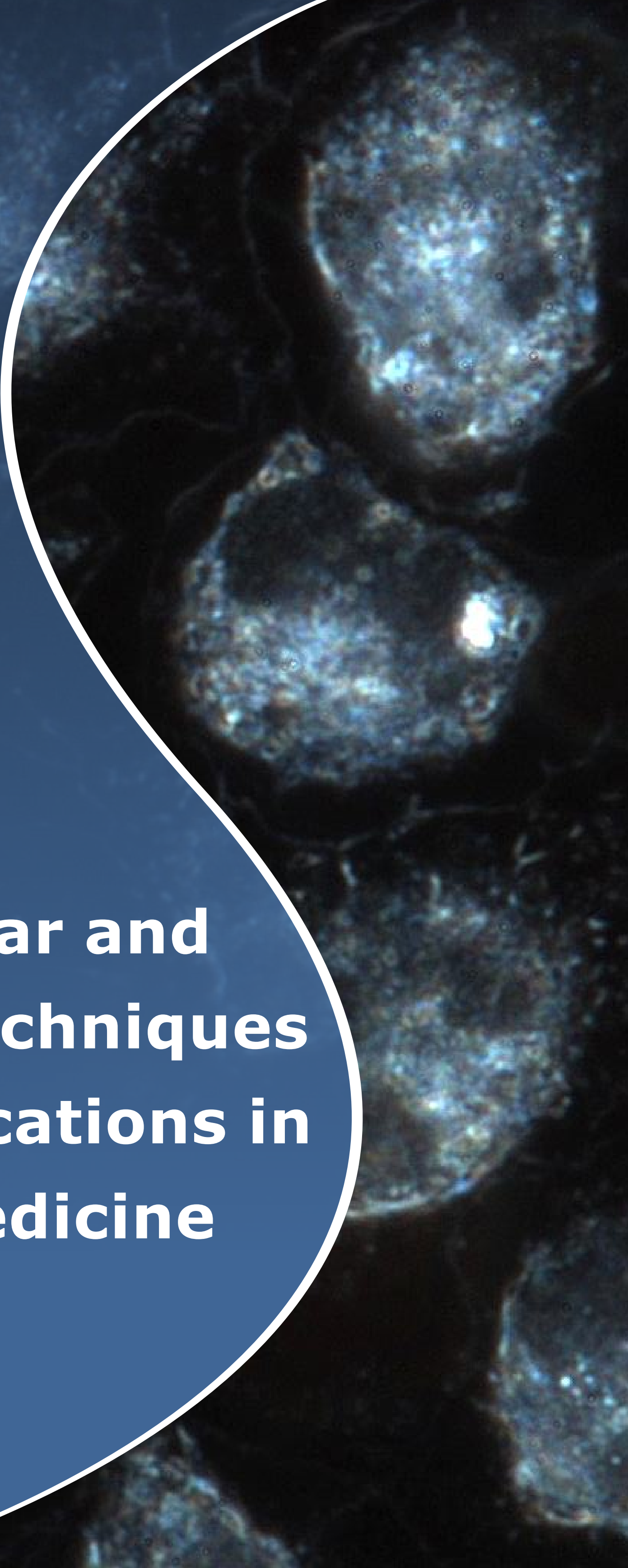

Molecular and Cellular Techniques with Applications in Nanomedicine

SciencePG
Science Publishing Group

Molecular and Cellular Techniques with Applications in Nanomedicine

Lucian Mocan

SciencePG
Science Publishing Group

Published by

Science Publishing Group

548 Fashion Avenue
New York, NY 10018, U.S.A.

http://www.sciencepublishinggroup.com

ISBN: 978-1-940366-05-0

Preface

During the past decade advances in functionalization chemistry have been one of the driving forces in the development of new classes of novel nanomaterials for applications in biology and medicine. Despite the impressive scientific efforts towards the development of novel nanomediated therapies, at the current time there is a tremendous need for standardizing cellular and molecular protocols used in Nanomedicine. To our best knowledge this is the first attempt to gather in a single book the most common molecular techniques used in Nanomedicine. Since Nanomedicine field is expanding and becomes part of the curricula in many universities, the present book with protocols will be extremely useful for the researchers, students and medical doctors.

Contents

Chapter 1

Experimental Nanophotothermolysis of Human Pancreatic Cancer Cells Using Gold Nanoparticles

Lucian Mocan[1], Lucia Agoston-Coldea[2], Teodora Mocan[3],
Cristian T. Matea[3], Flaviu A. Tabaran[4], Teodora Pop[1],
Ofelia Mosteanu[1], Cornel Iancu[1]

[1]Gastroenterology Institute; “Iuliu Hatieganu” University of Medicine and Pharmacy, 19-21 Croitorilor Street, Cluj-Napoca, Romania, 400162

[2]Department of Medical Sciences, Iuliu Hatieganu University of Medicine & Pharmacy, 2–4 Clinicilor, 400006, Cluj-Napoca, Romania

[3]Department of Physiology, "Iuliu Hatieganu" University of Medicine and Pharmacy, Clinicilor 5-7, Cluj-Napoca, Romania

[4]Department of Pathology, University of Agricultural Sciences and Veterinary Medicine, Faculty of Veterinary Medicine, 3-5 Manastur Street, 400372 Cluj-Napoca, Romania

Introduction

Pancreatic cancer (PC) represents the fourth leading cause of cancer death worldwide, having an overall 5-year survival rate of less than 5%. (1) At the current time, the surgical resection of the primary tumor is the only therapeutically approach that provides improvement in survival. Moreover, PC is also one of the most intrinsically drug-resistant of all tumors and the lack of effective cytostatics contributes to the increased mortality rates. (2)

An exciting and new approach to PC treatment is represented by the targeted therapeutics systems (an active molecule attached to a molecular carrier). The use of these biological carriers for the development of specific and sensitive site-targeted bio-nanosystems makes the selective internalization of molecules with photothermal properties in cancer cells possible. This internalization process is not possible under normal conditions (3) (4) Generally, the use of targeting molecules such as antibodies, folates and growth factors, has been specifically proposed for carrying nanomaterials to the cancer cells and tumors.

However, 100% selective internalization of nanobioconjugates in the cancer cells remains problematic.

Nanomediated photothermal therapy is a minimally-invasive treatment method in which photon energy from activated nanoparticles is converted to heat in tumor-loaded tissues (elevated to 40–43℃ and above). By using this method, highly efficient intratumoral heating can be achieved by non-radiative relaxation through electron–phonon and subsequent phonon–phonon coupling processes. The use of such particles in near-infrared PTT is highly attractive due to their rapid synthesis, facile bioconjugation, strong absorption cross-section, and tunable optical extinction. (5)

Recently, gold nanoparticles were approved on human treatment in phase 1 clinical trials, which suggests that gold can act as an effective and safe therapeutic agent. (www.clinicaltrials.gov). Furthermore, light absorbing properties of gold nanoparticles has been used to produce localized lysis to malign cells at sublethal levels by changes in cellular functions. (6)

In Vitro Treatment of Pancreatic Cancer Using Human Serum Albumin-Coated Gold Nanoparticles (HSA-GNPs)

We previously developed and published a novel system of PT for PC mediated by multiwalled carbon nanotubes (MWCNTs) bound to human serum albumin (HSA). (7, 8) This recent idea operates under the hypothesis that HSA molecules increase the effectiveness of carbon nanotubes internalization inside malign cells. Still, our published studies suggest that carbon nanotubes bound to human serum albumin exhibit a certain toxicity and are not 100% selective for malign cells. Moreover our current research in targeting pancreatic cancer with human serum albumin (HSA) bound to gold nanoparticles accepted for administration in humans that epithelial non- malign cells exhibit high uptake rates of GNP-HSA.

In this context, considering the described role of gold nanoparticles in human diagnosis and treatment applications, we reasoned that the development of novel selective targeted bio- nanosystems based on gold nanoparticles bound to novel specific antibodies, will allow us the discovery of a feasible treatment that may be successfully introduced in clinical trials on patients with PC. (9)

Synthesis of Gold Nanoparticles

Gold nanoparticles were synthesized according to standard wet chemical methods, using sodium borohydride as reducing agent. Briefly, the adding of 50 ml of aqueous solution containing 4.3 mg solid sodium borohydride to 100 ml of aqueous solution containing 100 μmol/L hydrogen tetrachloroaurate was done in a typical experiment, under vigorous stirring, continued overnight. Gold nanoparticles thus formed were filtered through a 0.22 μm filter and used for experiments.

Human Serum Albumin-Modified Gold Nanoparticles

In a few words, human serum albumin (HSA) - gold nanoparticle (GNPs) conjugates were obtained using poly-ortho-pyridyl disulfide, 2.000 Da (ethylene glycol)-N-hydroxysuccinimide as linker. Polyethylene glycol (PEG)-antibody conjugates were prepared by reacting one part 125 μM OPSS PEG-NHS with 9 parts 1 mg/ml antibody at 4 ℃ overnight. Gold nanoparticles were suspended in Milli-Q water and exposed to PEG-antibody conjugates for 1 hour, at 4 ℃, at a volume ratio of 100:1. Following antibody coupling, GNPs were reacted using a solution of mPEG-SH (5 mM, 5,000 Da), for at least 4 hours, at a temperature of 4℃ (1:200 volumetric ratio) to stabilize any exposed gold surface area. After PEG and/or antibody modification, GNPs were centrifuged to remove free molecules, aspirated and suspended in phosphate buffered saline (PBS) to an optical density of 2.0 (4.2×10^{11} particles/ml).

Universal attenuated total reflectance fourier transform infrared spectroscopy (ATR-FT-IR) was performed using a Perkin-Elmer Spectrum Two® instrument with an UATR single reflection diamond. Baseline corrections and spectra proccesing were done using the intruments Spectrum 10™ software.

Atomic force microscopy measurements were carried out on a Workshop TT-AFM® (AFMWorkshop, CA, USA) in vibrating mode using ACTA-SS cantilevers (AppNano, CA, USA). Samples were deposited on a mica substrate using a KLM® SCC spin coater. The recorded data was processed with the aid of Gwyddion® 2.36 software.

The obtained HSA stabillized gold nanoparticles were subjected to UV-Vis and DLS measurements.

AFM measurements were conducted on the GNP-HSA sample in order to further investigate the size and shape of the obtained nanoparticles. Figure 1 A. shows a 2D representation of GNP-HSA, spherical nanoparticles can be observed with an average diameter of ~41nm.

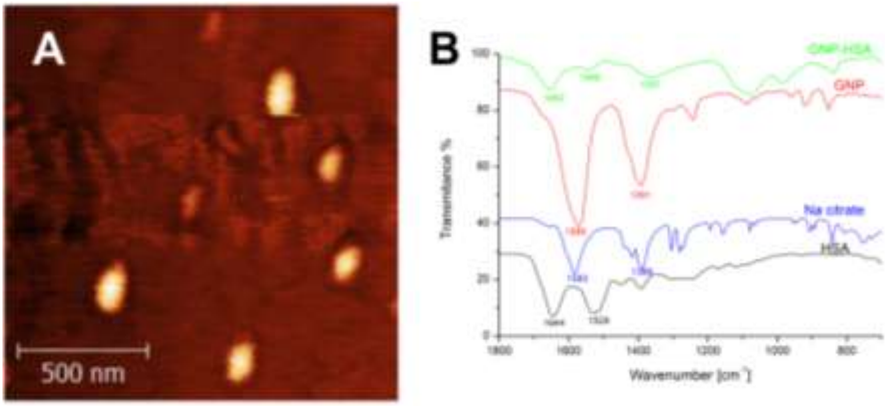

Figure 1. *AFM measurements of GNP-HSA: A. 2D image of HSA functionalized GNPs; B. FT- IR spectra of HSA functionalized gold nanoparticles (GNP-HSA), citrate stabilized GNP, Na citrate and HSA protein.*

In order to confirm the successful attachment of HSA on the gold nanoparticle surface, ATR-FT- IR spectroscopy measurements were undertaken. Figure 1B depicts FT-IR spectra of GNP-HSA, GNP, sodium citrate and HSA. For the GNP-HSA sample the two characteristic bands of HSA can be observed at 1652 cm^{-1} and 1546 cm^{-1} attributed to the amide I and amide II, respectively. The band at 1652 cm^{-1} is attributed to C=O stretching from the albumin, while the band at 1546 cm^{-1} is a coupling of C-N stretching and N-H bending modes in the protein. In the case of citrate capped GNPs the bands corresponding to the symmetric and antisymmetric stretching of COO^- of the citrate ions, can be observed at 1391 cm^{-1} and 1569 cm^{-1}, respectively. Figure 1 indicates that the citrate ions from the GNPs surface were replaced by HSA during the functionalization step of the gold nanoparticles. This phenomena can be explained by the fact that HSA has a tertiary structure stabilized by 17 internal disulphide bonds between 34 cysteine residues which accounts for the higher affinity of the protein for gold nanoparticles, compared to that of citrate ions.

Development of the *in Vitro* Test Platform

The human pancreatic adenocarcinoma 1.4E7 cell line was used for the experiments. This is a stable hybrid cell line formed by the electrofusion of human pancreatic islets with the human pancreatic ductal carcinoma cell line (PANC-1 cells), purchased from the European Collection of Cell Cultures (ECACC). Cells were grown in 25 cm^3 plastic flasks and maintained (in a humidified 37 ℃ 5% CO_2 incubator) in RPMI containing 10% fetal bovine serum with 1% penicillin-streptomycin. Cells were kept in logarithmic growth phase by routine passage every 2-3 days. On reaching confluence, cells were separated after being washed with phosphate buffered saline and they were detached using trypsin. For the experiments, cells were grown to confluence on glass Lab-Tek 4 chamber slides (No.177399). Albumin-coated gold nanoparticles were further delivered to adherent cell cultures, after removal of the cell culture medium, and incubated for gradually increased periods of time (1 minute, 30 minutes, 1 hour, 5 hours, 24 hours) at increasing concentrations: 1 mg/L, 5 mg/L, 20 mg/L, 50 mg/l. For each concentration, all experiments were carried out in triplicate. Figure 2 shows the intracellular "uptake" of gold nanoparticles (appearing on phase contrast microscopy as black intracytoplasmic conglomerations) functionalized with human serum albumin into malignant pancreatic cells. As suggested by the images below, we have observed (by both phase contrast microscopy and fluorescence microscopy) an intracellular internalization directly proportional to the concentration of nanoparticles in the solution administered. In addition, the quantification of intracellular gold nanoparticles conglomerations using fluorescence (by marking the nanobioconjugate with fluorescent molecules of fluorescein isothiocyanate) shows the selectivity of the uptake process compared to the simple FITC-labeled GNP solution.

For immunohistochemistry, Lab-Tek chamber slides were used for in situ observation of glass- adherent cells (walls were removed and the AuNP medium/solution cleared). Thus, no cell transfer was necessary before visualization/staining. After administration and irradiation, cells were washed 3 times with 1 x PBS and then fixed with 10% formaldehyde solution for 10 minutes, washed three times with PBS and subjected to chemical immunostaining. Cultured cells were examined with an inverted phase contrast microscope (Olympus FSX100, Munich, Germany).

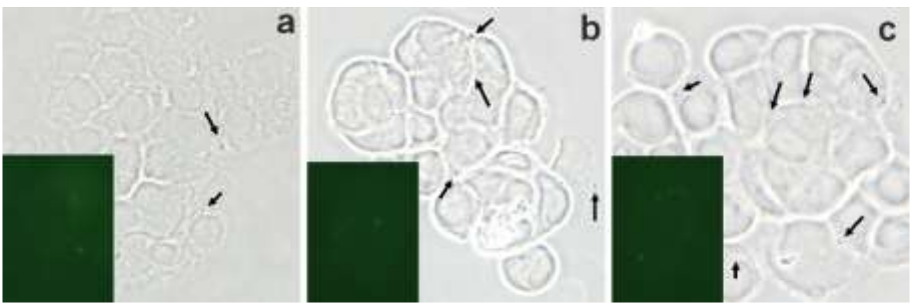

Figure 2. *1.4E7 pancreatic cancer cells incubated for 30 minutes with 1 mg/L-a, 5 mg/L of HSA-GNPs, visualized by phase contrast microscopy (x400 magnification); bottom left: quantification using an inverted fluorescence microscope, green filter, 455 nm.*

Laser Treatment

A 2W laser (Apel Laser, Bucharest, Romania) operating at 808 nm was used for a 2-minute irradiation of a cell monolayer placed on a glass substrate (laboratory glass slides, after removal of secondary walls and discharge of HSA-coated AuNP solution), after having been incubated with nanomaterials for various time periods. The laser diode was positioned vertically, 2 cm away from the surface of the microtiter plate. For ex vivo preactivation of nanoparticles, the AuNP solution was placed in a Lab-Tek 177399 slide and similarly irradiated for different time periods (5, 10, 20 minutes). AuNP solution temperature was measured using a digital thermometer (Digitron 1804).

Cell Proliferation

Following treatment, the MTT assay was performed to determine cell proliferation (3-[4,5-Dimethyl-2-thiazolyl]-2,5-diphenyl-2H-tetrazolium bromide). Briefly, 1.4E7 cells were plated at a seeding density of 4×10^4 cells/ml in 96-well plates. After being treated with different concentrations of nanoparticle solution (pre-irradiated or simple) at different time intervals, 10 μl of MTT (5 mg/ml) were added to each well. Cultures were returned to the incubator and incubated for 4 hours at 37℃. Further, the solution was removed and each well was added 100 μl of MTT solvent. After stirring for 30 minutes, absorbance was measured at wavelengths of 570 nm by spectrophotometry, using a microplate reader (MW-520).

Cytotoxicity Studies: Oxidative Stress Detection

The Total ROS/superoxide detection kit (Enzo Life Sciences, Plymouth Meeting, Pa, USA) was used to stimulate the production of reactive oxygen species (ROS) and/or reactive nitrogen species (RNS) in the cells exposed to GNPs, before and after treatment. 1.47 adherent cells were incubated with GNPs for 30 minutes at 37℃. Following incubation with GNPs (pre- activated/simple) +/- laser irradiation, cells were treated with reagent for oxidative stress detection for 30 minutes. Finally, cells were subjected to trypsinization and suspended with 0.5 ml of 10% FBS in 1 × wash buffer. Green fluorescence, an indicator of cellular production of different ROS/RNS types, was present in treated cells and visualized using the FACSCalibur flow cytometer (Becton Dickinson, San Jose, CA, USA) in the green FL1 channel (530 nm). All parameters considered for analysis were collected at low speed, in logarithmic mode (approx. 15 microliters min^{-1}), in order to maintain the counting level under 1,000 events per second. Characterization of cell population concentration was performed using both CellQuest software and PaintAGate. In addition, the accumulation of hydrogen peroxide was measured using CM- H2DCFDA (Invitrogen) and detected in the green channel (525 nm). Green fluorescent images were collected using the Olympus FSX100 fluorescence microscope. ROS species detection kit, Enzo Life Sciences, for flow cytometry, was used for the monitoring of real time release of reactive oxygen species and/or reactive nitrogen species (ROS/RNS) in 1.4E7 cells, before and after treatment. The kit contains the reagent for oxidative stress detection (green) as a marker detecting cell-penetrating ROS, which reacts with many reactive species, such as hydroxyl radical and hydrogen peroxide.

Analysis of the Mitochondrial Function

1.4E7 cells were grown to confluence on Lab-Tek 4 chamber glass slides. A pre-heated (37 ℃) dye solution containing MitoTracker® (Invitrogen) was added for 30 minutes, after removal of the culture medium (10). After staining was completed, cells were examined with an Olympus FSX100 microscope in the red channel. In order to further measure total mitochondrial mass, stained slides were scanned at a resolution of 100 μm by means of a proteomics imaging system (ProXPRESS 2-D, Perkin-Elmer, Boston, MA) with 480-nm excitation and 620-nm emission filters. The exposure time was adjusted to achieve a pixel intensity value of 55,000 to 63,000 on the more intense spots on the slides. Images were subsequently analyzed using Progenesis Discovery software, 2003 version. (Nonlinear Dynamics, Ltd., Newcastle upon Tyne, Great Britain). MitoTracker Red CMXRos is a red fluorescent dye (with a slightly thiol-reactive chloromethyl fraction), which stains mitochondria in living cells and thus, its passive intracellular diffusion depends on the membrane potential function. Once the mitochondria are functionalized, cells can further be fixed with aldehyde-based fixative.

Table 1. *Cytotoxic effects of different incubation times (%).*

Cytotoxicity of HSA-GNPs at various concentrations and various incubation times				
	1 min	**1 hour**	**3 hours**	**24 hours**
HeLa Control	0%	0.4%	0.5%	1.7%
1.4E7 Control	0%	0.3%	0.7%	2.1%
HeLa 1 mg/L	0.3%	0.7%	1.6%	3.2%
1.4E7 1 mg/L	0.7%	1.1%	2.1%	3.4%
HeLa 5 mg/L	0.6%	1%	2.4%	4.5%
1.4E7 5 mg/L	0.5%	0.9%	2.3%	4.1%
HeLa 20 mg/L	0.8%	1.4%	3.2%	4.2%
1.4E7 20 mg/L	0.9%	1.4%	2.2%	4.1%
HeLa 50 mg/L	0.7%	1.3%	2.4%	4.5%
1.4E7 50 mg/L	1.4%	1.6%	2.2%	5.8%

Assessing the Efficacy of Nanophotothermal Therapy

Cells grown in 6-well plates were treated with drugs for 48 h and incubated with 5 II Annexin V-Rhodamine in functionalization-compatible buffer (10 mM HEPES, 140 mM NaCl, 2.5 mM $CaCl_2$, pH 7.4) for 15 minutes, in the dark, in accordance with the manufacturer’s protocol. Cells were further washed in buffer, counterstained with propidium iodide and analyzed immediately using the Becton Dickinson FACSCalibur flow cytometer (488 nm and 585 nm excitation). Annexin V-Alexa Fluor 488, propidium iodide, or both, have been omitted for negative controls.

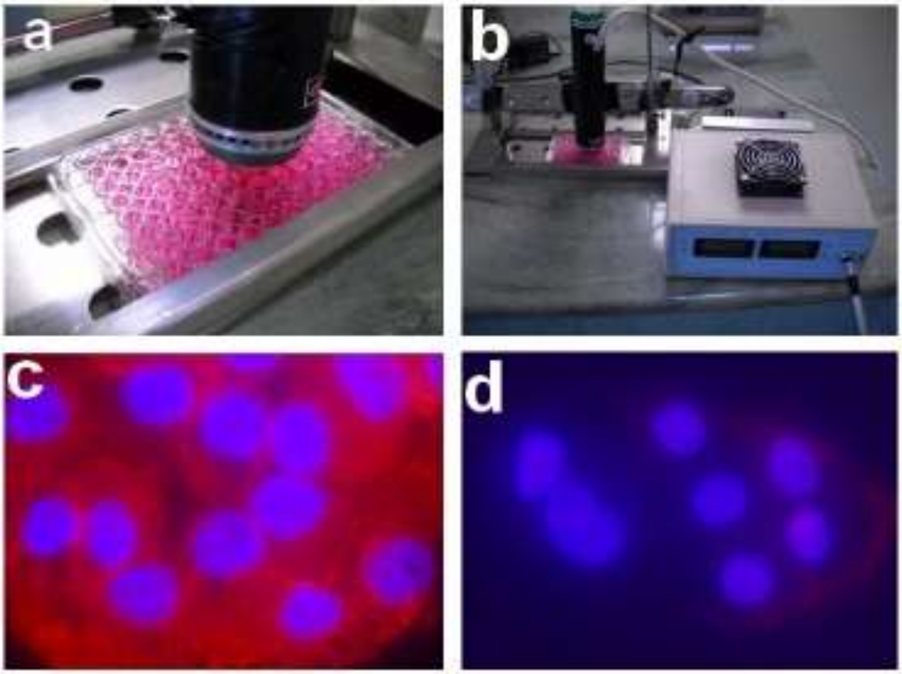

__Figure 3.__ Nanophotothermal therapy of PANC-1 cells mediated by HSA-GNPs. a-b System settings c-d Annexin V expression in PANC-1 cells and CRL-4020 respectively (60 minutes exposure, 20 mg/L).

For the 30 minute assessment, cell necrosis increased from 58.34% (1 mg/L) to 90.34% (50 mg/L). In normal epithelial cells, the values obtained for the 30 minute samples were lower for all exposure concentrations. The significance of cytotoxicity threshold for CRL-4020 cells was set for a p value of <0.0001, for the 30 minute assessment, values ranging from 8.77% to 68.86% in all the concentration groups (1-50 mg/L).

Moreover, the values recorded for the 30 minute exposure period ranged from 6.08% to 62.23% for different concentrations for the PANC-1 group exposed to MWCNTs alone. The following levels of significance were calculated for the 30-minute exposure period and for 5 mg concentrations: PANC-1/CRL-4020:

70.78%/9.89% ($p<0.001$). As seen in Fig. 3, c-d, the optimal apoptotic effect after incubation with HSA-GNP was obtained for 5 mg/l. (PANC-1/CRL-4020: 56.1%/11.4% for the 60-second exposure period, and 75.34%/14.67% for the 30-minute exposure period. After 60 minutes of incubation, the difference in apoptosis was also big between the two cell lines at low/average GNP-HSA concentrations (80.12% - 1 mg/L, 86.14% - 5 mg/L, 85.82% - 20 mg/L for PANC-1, 15.56% -1 mg/L, 21.34% - 5 mg/L, 52.14% - 20 mg/L for CRL-4020.) Cell lysis values for high nanomaterial concentrations were roughly similar (100% - PANC-1, 84.13% - CRL-40420).

Thaken all these data togheter, we showed here a novel method of treatment for human pancreatic cancer with specifically immunolabelled gold nanoparticles with high selectivity for pancreatic cancer cells for further thermal activation by external laser field. We estimate that the proposed practical approach will allow us to advance the designed nanocompounds in phase 1 clinical trials on human patients with pancreatic cancer.

References

[1] Jemal A, Bray F, Center MM, Ferlay J, Ward E, Forman D. Global cancer statistics. CA Cancer J Clin 2011 Mar-Apr;61(2):69-90.

[2] Patra CR, Bhattacharya R, Wang E, Katarya A, Lau JS, Dutta S, et al. Targeted delivery of gemcitabine to pancreatic adenocarcinoma using cetuximab as a targeting agent. Cancer Res 2008;68(6):1970-1978.

[3] Yang F, Jin C, Subedi S, Lee CL, Wang Q, Jiang Y, et al. Emerging inorganic nanomaterials for pancreatic cancer diagnosis and treatment. Cancer Treat Rev 2012;38(6):566-579.

[4] Borja-Cacho D, Jensen EH, Saluja AK, Buchsbaum DJ, Vickers SM. Molecular targeted therapies for pancreatic cancer. Am J Surg 2008 Sep;196(3):430-441.

[5] Mocan L, Ilie I, Tabaran FA, Dana B, Zaharie F, Zdrehus C, et al. Surface plasmon resonance-induced photoactivation of gold nanoparticles as mitochondria-targeted therapeutic agents for pancreatic cancer. Expert opinion on therapeutic targets 2013(0):1-11.

[6] Hainfeld JF, O'Connor MJ, Lin P, Qian L, Slatkin DN, Smilowitz HM. Infrared-transparent gold nanoparticles converted by tumors to infrared absorbers cure tumors in mice by photothermal therapy. PloS one 2014;9(2):e88414.

[7] Iancu C, Mocan L, Bele C, Orza AI, Tabaran FA, Catoi C, et al. Enhanced laser thermal ablation for the in vitro treatment of liver cancer by specific delivery of multiwalled carbon nanotubes functionalized with human serum albumin. International Journal of Nanomedicine 2011;6:129.

[8] Mocan L, Tabaran F, Mocan T, Bele C, Orza A, Lucan C, et al. Selective ex-vivo photothermal ablation of human pancreatic cancer with albumin functionalized multiwalled carbon nanotubes. International Journal of Nanomedicine 2011 28 April 2011;6(1):915-928.

[9] Iancu C, Mocan L. Advances in cancer therapy through the use of carbon nanotube-mediated targeted hyperthermia. International Journal of Nanomedicine 2011;6:1675.

[10] Ohno M, Oka S, Nakabeppu Y. Quantitative analysis of oxidized Guanine, 8-oxoguanine, in mitochondrial DNA by immunofluorescence method. Methods Mol Biol 2009;554:199-212.

Chapter 2

Nanotherapeutic Strategies for the Selective Ablation of Human Liver Cancer Cells

Teodora Pop[1], Teodora Mocan[2], Lucia Agoston[3], Flaviu A. Tabaran[4], Cristian Matea[5], Ofelia Mosteanu[1], Cornel Iancu[5], Lucian Mocan[5]

[1]3rd Medical Clinic, University of Medicine and Pharmacy Cluj Napoca

[2]Department of Physiology, “Iuliu Hatieganu” University of Medicine and Pharmacy, 19-21 Croitorilor Street, Cluj-Napoca, Romania, tel/fax: +40264-439696

[3]Department of Medical Sciences, Iuliu Hatieganu University of Medicine & Pharmacy, 2–4 Clinicilor, 400006, Cluj-Napoca, Romania

[4]Department of Pathology, University of Agricultural Sciences and Veterinary Medicine, Faculty of Veterinary Medicine, 3-5 Manastur Street, 400372 Cluj-Napoca, Romania

[5]Gastroenterology Institute; “Iuliu Hatieganu” University of Medicine and Pharmacy, 19-21 Croitorilor Street, Cluj-Napoca, Romania, 400162

Introduction

Hepatocellular carcinoma (HCC) is one of the leading causes of cancer deaths worldwide. Despite recent findings on screening and early detection of HCC, it has a rapid clinical course with an average 6-month survival rate and a 5% five-year overall survival rate. (1)

Most data suggest that nanotechnology could play a major role in developing novel therapies against cancer. Some of the most extensively studied methods to treat cancer using nanoparticles include the nanoparticle-based thermal approach, nanoemulsion, pH-sensitive nanoparticles, nanoparticles combined with laser irradiation and the use of nanovectors for drug delivery. (2-6)

The ability of gold nanoparticles (GNPs) to convert near infrared (NIR) radiation into heat, due to photon-phonon and electron interaction, provides the opportunity to create a new generation of immunoconjugates for cancer phototherapy, with high performance and efficiency for selective cancer thermal ablation, and for the use of nanotechnology in molecular diagnostics (nano- diagnosis). (5)

The working hypothesis at this stage was based on literature data showing that proliferative tumors have the ability to create albumin deposits. (7-9, 9-12) Reports have shown that liver cancer cells have excessive specific human serum albumin receptors and are able to internalize large quantities of albumin through caveolae-dependent endocytosis. Resulting amino acids are further used for the synthesis of various substrates necessary for tumor growth. Considering all these data together, the use of gold nanoparticles functionalized with human serum albumin (HSA) is recommended at this stage for selective targeting and laser necrosis of liver cancer cells. To our knowledge, this is the first demonstration of selective targeting through gp 60 receptors located on the membrane of malignant liver cancer cells, using gold nanoparticle functionalized with human serum albumin.

Our previous research supports the involvement of certain peptide antibodies (such as human serum albumin and insulin growth factor) in the nanomediated selective targeting of liver and pancreatic cancer. This implication is supported by the fact that these biostructures act as specific intracellular carriers inside the cell line. Previous data from our studies suggest that carbon nanotubes functionalized with human serum albumin could be selectively delivered and internalized (see section: preliminary results) into liver cancer cells. However, due to concerns regarding toxicity and biological interactions within the human biological system, we intend to clinically adapt our research, using synthesized biocompatible gold nanoparticles in order to develop a novel photothermal therapy with selective targeting for liver cancer, which can be safely used in humans. (13)

Our goal in the future is to develop specific receptor antibody-conjugated gold nanoparticles for targeted delivery into liver cancer cells in vivo, using this antibody as a carrier for delivery and the antagonist receptor located on the malignant cell membrane as the targeting half. Our hypothesis argues that, due to the level of expression of certain receptors on the surface of malignant cells, these nanobiomolecules will selectively target malignant lesions. We reasoned that the external treatment by laser irradiation/radiofrequnecy using these targeted biocompatible gold nanoparticles, where the specific ablation will allow for effective tumor destruction, may be a novel and successful method for the treatment of liver cancer.

One potential concern regarding the clinical applications of our sensitive nanobiosystem proposed to fight liver cancer is the systemic toxicity of gold nanoparticles that are going to be functionalized. Therefore, our main strategy for the proposed research is the use of high-purity gold nanoparticles for detection of liver cancer, currently approved for treatment in humans.

We believe that by using these nanomaterials, we can easily transfer the designed nanobiosystem for approval and implementation in clinical trials to treat patients with advanced liver cancer using laser-nanomediated photothermolysis in our department of surgery and, therefore, on the market.

At this stage, we initiated targeting experiments against liver cancer using antibodies (epidermal growth factor) that have already proven their specificity for this type of cancer. We decided to attach specific antibodies on the surface of GNPs for selective cellular uptake and to optimize the response of functionalized nanoparticles to NIR radiation, so that they could produce the necessary heat to destroy cancer cells by laser irradiation, but in low concentrations, to avoid their possible undesirable systemic toxicity.

From our clinical perspective, in order to obtain a selective nanomediated photothermal ablation of advanced liver cancer in humans, our purpose within this research was to develop a novel nanobiosystem based on nontoxic gold nanoparticles that can safely be administered in clinical trials.

In Vitro Treatment of Pancreatic Liver Cancer Using Human Serum Albumin-Coated Gold Nanoparticles (HSA-GNPs)

Synthesis and Characterization of Gold Nanoparticles

Gold nanoparticles were synthesized according to standard wet chemical methods, using sodium borohydride as reducing agent. (4-6) Briefly, the adding of 50 ml of aqueous solution containing 4.3 mg of solid sodium borohydride to 100 ml of aqueous solution containing 100 μmol/L hydrogen tetrachloroaurate was done in a typical experiment, under vigorous stirring, continued overnight. (4) Gold nanoparticles thus formed were filtered through a 0.22 μm filter and used for experiments. (AFM and UV-Vis spectroscopy)

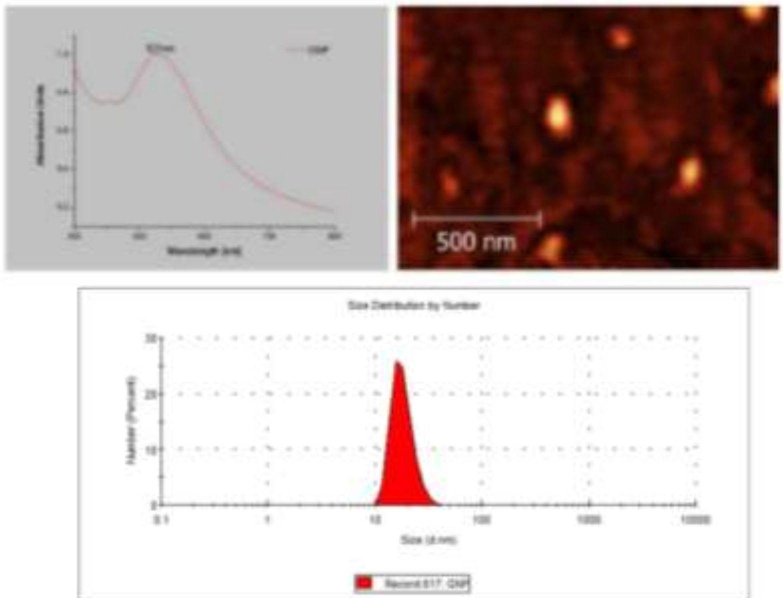

Figure 1. *Characterization of synthesized nanoparticles used for experiments. UV-Vis spectroscopy (top left), atomic force microscopy (top right), dynamic light scattering (DLS) (center).*

UV-Vis Spectroscopy Analysis

Characteristic surface plasmon resonance (SPR) of gold nanoparticles was observed using ultraviolet-visible spectroscopy (mini Shimadzu spectrophotometer 1240), confirming the presence of spherical gold nanoparticles. (Figure 1, red spectrum). The size of the functionalized nanoparticles was assessed using atmic force microscopy (AFM), showing an average 42 nm diameter (TT-AFM microscope from the Department of Nanomedicine, Regional Institute of Gastroentherology and Hepatology, Cluj-Napoca).

DLS (Dynamic Light Scattering) Analysis

Gold nanoparticles (GNP) were subjected to dynamic light scattering (DLS) measurements using the Zetasizer Nano Series S90 system (He-Ne laser 633 nm). The bottom chart in Figure 1 shows the relative light scattering percentage of nanoparticles (Y axis) according to their size (X axis). As indicated, nanoparticle size increased significantly for the functionalized complexes, suggesting a significant attachment of albumin molecules onto their surface.

Culture of the Malignant Liver Cells

The main purpose of this investigation was to develop and test a novel method of treating human hepatocellular carcinoma (HCC). Preliminary data from the literature support the overexpression of epidermal growth receptor on the surface of malignant liver cells and hence, its use in targeting experiments.

C3A cell line was used for initial in vitro experiments, purchased from the European Collection of Cell Cultures (ECACC). Cells were grown in 25 cm^3 plastic flasks and maintained (in a humidified 37 ℃ 5% CO_2 incubator) in MEM containing 10% fetal bovine serum with 1% penicillin-streptomycin. Cells were kept in logarithmic growth phase by routine passage every 2-3 days. On reaching confluence, cells were separated after being washed with phosphate buffered saline and they were detached using trypsin. For the experiments, cells were grown to confluence on glass Lab-Tek 4 chamber slides (No.177399). A HeLa cell line was used as control and maintained by standard protocols. Albumin-coated gold nanoparticles were further delivered to adherent cell cultures, after removal of the cell culture medium, and incubated for gradually increased periods of time (1 minute, 30 minutes, 1 hour, 5 hours, 24 hours) at increasing concentrations: 1 mg/L, 5 mg/L, 20 mg/L, 50 mg/l. For each concentration, all experiments were carried out in triplicate.

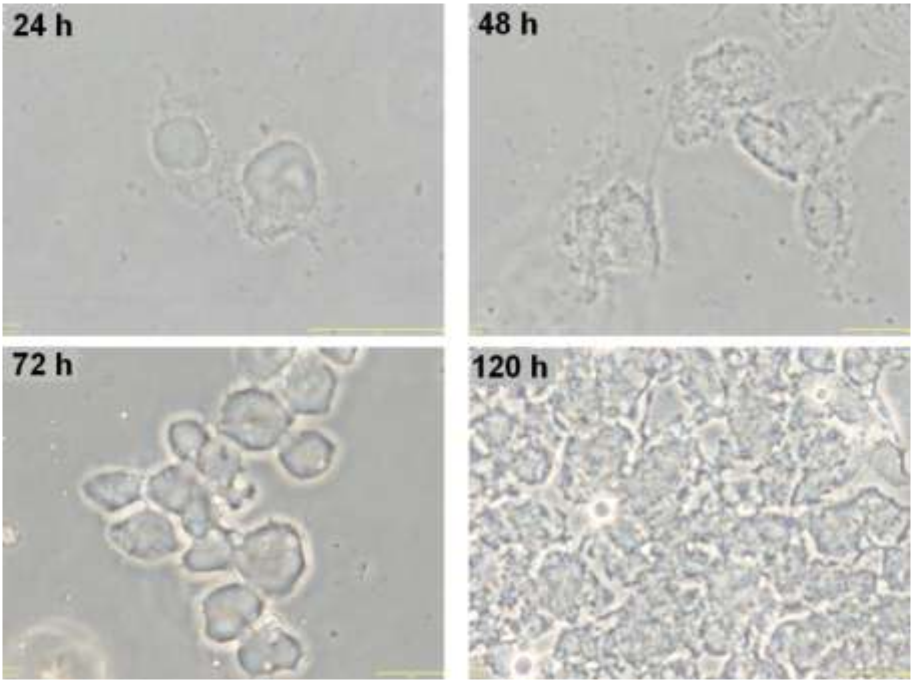

Figure 2. *C3A cells used in the experiment. Dynamic phase contrast microscopy at different time intervals.*

For immunohistochemistry, Lab-Tek chamber slides were used for in situ observation of glass- adherent cells (walls were removed and the AuNP medium/solution cleared). Thus, no cell transfer was necessary before visualization/staining. After administration and irradiation, cells were washed 3 times with 1x PBS and then fixed with 10% formaldehyde solution for 10 minutes, washed three times with PBS and subjected to chemical immunostaining. Cultured cells were examined with an inverted phase contrast microscope (Olympus FSX 100, Munich, Germany).

For the investigation of the toxicity of the nanoconjugates, different concentrations of C3A and HeLa cells (control) were exposed and incubated with HSA-GNPs for different periods of time, in order to assess their cytotoxic potential. Consistent with other findings, we demonstrated that only high concentrations of AuNP bioconjugates have cytotoxic effects. However, being a serious obstacle in the use of gold nanoparticles in clinical applications, toxicity can be minimized by administration of low doses of nanoconjugates.

Initiation and Growing of C3A and HeLa Malignant Liver Cells (Control)

HSA-GNP-induced Cytotoxicity

The possible cytotoxic effect induced by the administration of gold nanoparticles was investigated before testing the in vitro response of the cells treated with HSA-GNPs to laser irradiation. C3A cells and epithelial cells were treated with various concentrations of HSA- GNPs for different incubation periods. A Rev-Science direct blade count flow cytometer was employed to study the effects of AuNP bioconjugates on cell viability.

Table 1. *The cytotoxic effects on C3A and HeLa cells induced by different concentrations of nanobiomaterial, at different incubation times.*

HSA-GNP	**Cytotoxic effects of different incubation times (%)**					
concentration	**1min**	**30min**	**1h**	**3h**	**5h**	**24h**
HELA controls	0.1%	0.2%	0.3%	0.4%	0.9%	1.6%
C3A controls	0.1%	0.1%	0.3%	0.5%	1.1%	1.3%
1 mg/L HELA	0.3%	0.5%	0.7%	1.9%	2.4%	3.8%
1 mg/L C3A	0.5%	0.8%	0.9%	2.2%	2.5%	3.6%
5 mg/L HELA	0.6%	0.9%	1%	2.4%	3.1%	4.2%
5 mg/L C3A	0.4%	0.7%	0.8%	2.6%	3.2%	4.4%
20 mg/L HELA	0.7%	0.8%	1.2%	3%	3.1%	4.8%
20 mg/L C3A	0.8%	1.2%	1.2%	2.6%	2.8%	4.5%
50 mg/L HELA	0.6%	0.8%	1.8%	2.2%	2.8%	4.9%
50 mg/L C3A	1.4%	1.5%	1.6%	2.2%	2.8%	6.2%

Internalization of HSA-GNP Complexes in Malignant Liver Cells

The capacity of FITC-functionalized HSA-GNP bioconjugates to internalize in C3A cells was assessed using confocal fluorescence microscopy.

The results presented in Figure 3 show that, at low concentrations and short exposure, HSA- GNPs accumulate inside C3A cells. The imaging evidence shows that HSA can act as a carrier for GNPs and, as we could not identify any fluorescence in hepatocytes under identical exposure conditions, HSA-GNP bioconjugates have specific affinity for liver cancer cells.

Immunocytochemistry Staining of Target-Receptors for the Newly Generated Therapy

Phase contrast microscopy was additionally used to demonstrate the presence of gold nanoparticles inside C3A cells after administration of HSA-GNPs. As shown in Figure 3 (bottom right), intracellular GNP aggregates appear as dark signals, optically dense, associated with a refractive signal for phase contrast microscopy. Furthermore, we could not identify any aggregates inside hepatocytes treated similarly. (top right)

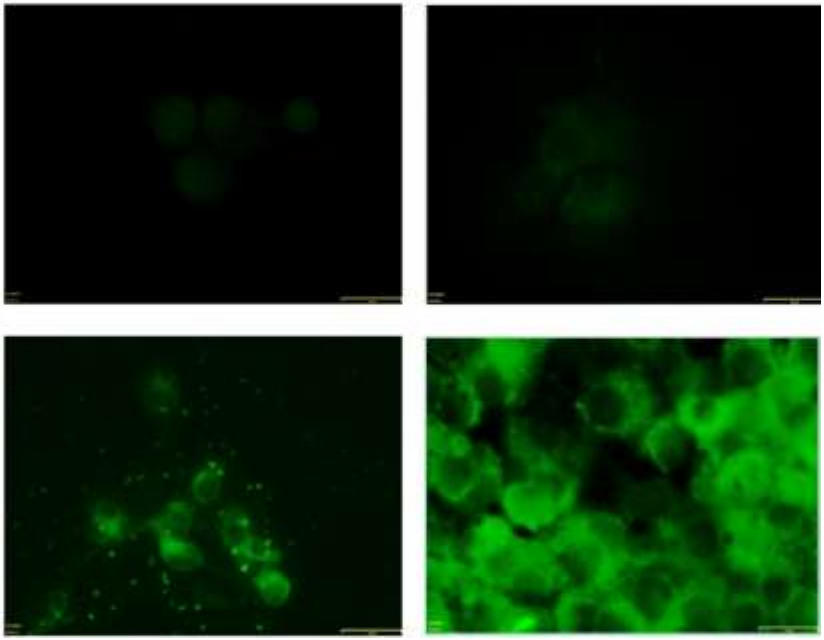

Figure 3. *Internalization of gold nanoparticles functionalized with fluorescently labeled albumin inside malignant liver C3A cells (bottom row) or benign HeLa hepatocytes (top row).*

Selective Internalization of Gold Nanoparticles Functionalized with Human Serum Albumin (HSA-GNPs) in Liver Cancer Cells

In order to highlight the molecular mechanisms involved in the specific uptake of HSA-GNPs in C3A cells, we investigated the possible implication of the 60 kDa glycoprotein, gp60, recognized for its role in albumin transcytosis in malignant cells, in the selective uptake of albumin-coated gold nanoparticles.

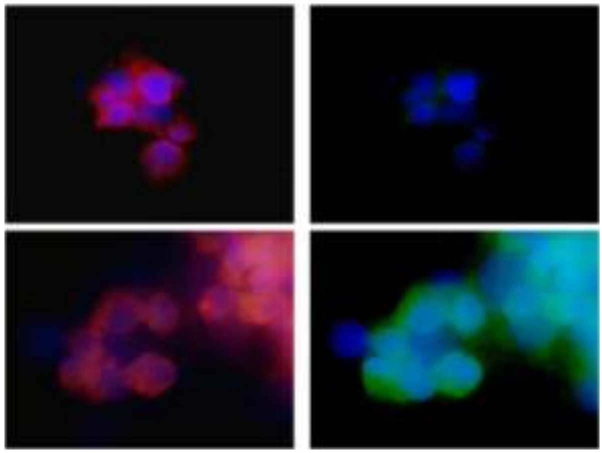

Figure 4. *In vitro endocytosis of HSA-GNPs in human liver cancer cells: colocalization of Cy-gp60 antibody and FITC-HSA-GNPs in HeLa epithelial cells (top row); colocalization of Cy-gp60 antibody and FITC-HSA-GNPs in C3A cells (bottom row).*

In order to achieve this, we allowed cells previously treated with 5 mg/L HSA-GNPs for one hour, to incorporate Cy3-anti-gp60 antibodies for 30 minutes at 37℃. Therefore, we obtained fluorescent images proving internalization of Cy3 fluorescence (Figure 4, middle images).

Simultaneously, we showed that C3A cells internalized with GNPs functionalized with albumin (stained with FITC fluorescent dye) were distributed in punctate structure inside the cells (Figure 4, right images). Nuclei were stained using 4'-6-diamidino-2-phenylindole (DAPI), known to form fluorescent complexes with natural double-stranded DNA. Figure 4, bottom right, shows the obvious and almost complete colocalization of FITC fluorescence (green image) and Cy3 fluorescence (red image) using yellow color in the overlaid image. This finding suggests that GNPs functionalized with albumin were incorporated into the plasmalemmal vesicles, containing gp60 as membrane protein, further validating the HSA-GNP specificity for gp60 receptors. Importantly, as shown in Figure 4, top right, threre was no significant colocalization of Cy3-gp60 antibody and HSA-FITC-GNPs in hepatocytes (HeLa), incubated under the same circumstances.

Therefore, based on these data, we showed that HSA-GNPs can act as nanosystems with specific and sensitive targeting of a specific location against the gp60 receptor located on the membrane of liver cancer cells.

The Association of Caveolin-1 with Vesicles Containing FITC-HSA-GNPs

Most data indicate that caveolae-mediated endocytosis in cancer cells is stimulated by the binding of albumin to gp60, a receptor located in the caveolae.

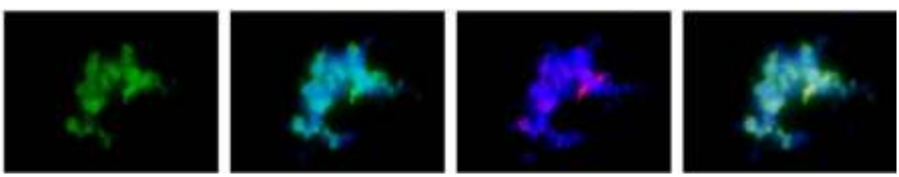

Figure 5. *Colocalization of anti-caveolin-1-Cy3 antibody (red) with HSA-FITC-GNPs (green). Nuclei were stained using DAPI immunoblotting.*

Considering these data and the described caveolae-mediated endocytosis, we proposed the hypothesis that the mechanism of HSA-GNP internalization in C3A cells was similar. To test this hypothesis, we immunostained C3A cells with Cy3-anti-caveolin-1 antibody. As shown in Figure 5, confocal visualization revealed that most plasmalemmal vesicles containing FITC-HSA-GNPs stained for caveolin-1 used this monoclonal fluorescent anti-caveolin-1 antibody. Taken together, these data demonstrate that HSA-GNPs selectively internalize into human liver cancer cells through caveolae-mediated endocytosis, by binding of the albumin carrier to gp60, a specific albumin-binding protein.

Quantification of Cell Death After Administration of the GNP-Ab Complex in Cultured C3A Cells Followed by Laser Treatment

Cytotoxicity Induced by Laser Irradiation or Administration of HSA-GNPs

Before testing the in vitro response to laser irradiation of cells treated with HSA-GNPs, we investigated the possible effect of the cytotoxicity induced by the administration of gold nanoparticles in cells. C3A cells and epithelial cells were treated with various concentrations of HSA-GNPs for different incubation times. Annexin V assay for the detection of cell death was used to assess the effect of GNP bioconjugates on cell viability.

After incubation for 24 hours, C3A cells exposed to 50 mg/L HSA-GNPs showed a 4.71% decrease in viability, as compared to 1.6% ($p<0.02$) (Table 1). Human hepatocytes (HeLa) exposed to 50 mg/L HSA-GNPs showed a 2.8% drop in viability, compared to the untreated sample with 98.7% viable cells ($p<0.001$). Statistical data showed that exposure to small and medium concentrations of nanomaterials did not induce significant cytotoxic effects ($p>0.05$ for all comparisons).

Figure 6. *Annexin V expression after HSA-GNP-mediated nanophotothermolysis of liver cancer cells (5 mg/L.).*

The next step in eliminating any possible error was the 2 minute irradiation of a sample of cells without nanoparticles, using 2W 808nm laser diode. There was no cell lysis after irradiation. This demonstrates C3A transparency for NIR beam.

Cell Death Evaluation After Laser Treatment and Administration of HSA-GNPs

Initially, the first stage consisted in assessing mitochondrial function and oxidative stress products using Mitotracker Red.

As shown in Figure 7 (red fluorescence, mitochondrial function assessment kit CM-H2XRos), mitochondria in cells treated with GNPs alone present bright branched fluorescence, evenly spread throughout the cytoplasm, strongly suggesting normal mitochondrial function. In contrast, as shown in the same figure (middle image), exposure to 5 mg/L HSA-GNPs for 30 minutes caused a large decrease in fluorescence, with only few mitochondria visualized. Furthermore, treatment with HSA-GNPs induced the intracytoplasmic dissipation of mitochondrial fluorescence - a strong indicator of mitochondrial disintegration to such an extent that it produced the rupture of the outer mitochondrial membrane. In addition, mitochondrial localization was different in C3A cells treated with HSA-GNPs. There was a specific migration of mitochondria towards cell membrane observed in most activated cells treated with GNPs. Quantification of data obtained by flow cytometry (BD FACSCalibur cytometer, from all cells (red FL3 channel) revealed a significantly lower fluorescence (Chi square test <0.05), suggesting decreased mitochondrial activity in malignant pancreatic cells treated with HSA-GNPs, compared to controls (treated with GNPs alone).

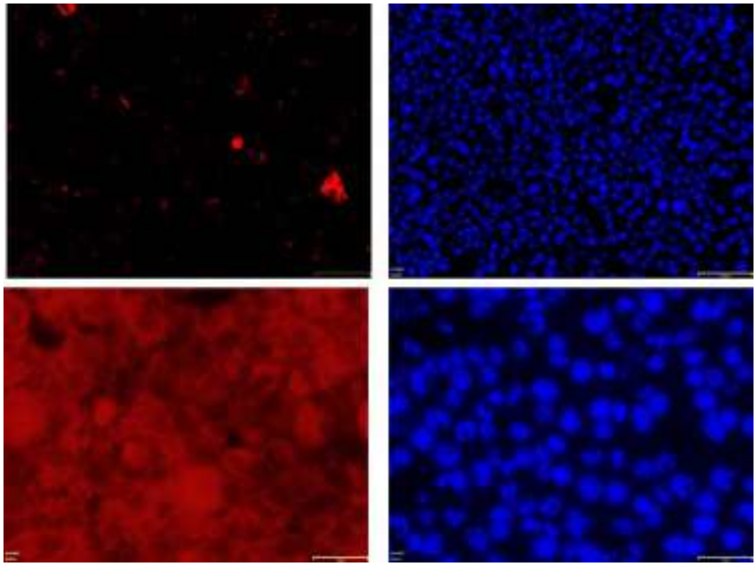

Figure 7. *Assessment of cell status after nanophotothermal therapy with HSA-GNPs (top row) and GNPs (bottom row) by analyzing mitochondrial function using Mitotracker Red.*

Studies on Apoptosis and Necrosis After Nanophotothermal Therapy

Necrosis was assessed using Annexin V-Cy5 for flow cytometry (BD FACSCalibur cytometer from the Department of Nanomedicine,) and apoptosis using fluorescence microscopy (Olympus FSX100 high-performance microscope from the Department of Nanomedicine) to indicate the effect of laser photoactivated HSA-GNPs on pancreatic cancer cells. As shown in Figure 6, there was an increased number of apoptotic cells in the group treated with HSA-GNPs. Moreover, the percentage of Annexin V-positive cells was directly proportional to ROS quantification by flow cytometry. There was no intermediate Annexin V staining in C3A cells, suggesting that these apoptotic cells rapidly lose their phospholipid asymmetry in the plasma membrane, followed by phosphatidylserine exposure on cell surface. At longer incubation times, there was an increase in annexin V-positive cells and in cells with condensed nuclei.

The rate of HSA-GNP-treated C3A cell lysis post-irradiation ranged from 36.15% (for 1 mg/L) to 86.24% (for 50 mg/L), for 60 seconds ($p<0.001$), while for the 30-minute period, the necrotic rate increased from 61.24% (1 mg/L) to 90.24% (50 mg/L), $p<0.001$. We obtained significantly lower apoptotic rates in irradiated epithelial cells treated for 60 seconds and 30 minutes, at concentrations ranging from 1 mg/L to 50 mg/L (5.28%-61.42% for 60 seconds, 9.89%-70.78% for 30 minutes). Thus, optimal necrotic effect of malignant cells after incubation with HSA-GNPs was obtained at an optimal concentration of 5 mg/L. (C3A/HEPB5: 64.8%/10.14% for 60 seconds, 76.14%/15.7% for 30 minutes). After one hour of incubation, there was a also statistically significant difference in the percentage of necrotic cells between C3A and HeLa cells for small/medium concentrations of HSA-GNPs (80.1% - 1 mg/L, 87.14% - 5 mg/L, 86.9% - 20 mg/L for C3A; 13.6 % - 1 mg/L, 20.4% - 5 mg/L, 50.4% - 20 mg/L for HeLa). P values were <0.001 for comparisons between different types of nanomaterials. There were no significant differences ($p=0.143$) between the apoptotic rates of C3A and HeLa cells treated with HSA-GNPs (100% - C3A, 82.3% - HeLa) at high concentration of nanomaterial (50 mg/L).

After 3 to 5 hours of incubation, there was significant apoptotic rate of the two cell lines only when they were treated with low concentrations of nanomaterial (<20 mg/L). There was a non-significant difference in the effect of cell lysis between the two cell lines for higher concentrations ($p=0.196$ for 20 mg/L, $p=0.213$ for 50 mg/L).

After 24 hours of incubation, C3A cells treated with 1 mg/L HSA-GNPs were 100% lysed, necrotic after laser irradiation, compared to 53.2% of HeLa cells treated similarly. For very low concentrations of HSA-GNPs, there was a clear difference in the percentage of necrotic cells between the two cell lines. ($p<0.045$). Cell lysis rates of irradiated cells incubated with more than 5 mg/L nanomaterial for 24 hours, were almost similar in the two cell lines. (100% versus 84.8%)

On the other hand, there were no significant differences in the percentage of viable cells between the two cell lines when using non-functionalized GNPs ($p>0.05$ for all comparisons and each exposure period). Moreover, for C3A cell lines, there was a significant difference between the groups treated with HSA-GNPs and GNPs alone at low concentrations (1 mg/L 5 mg/L, 20 mg/L) and short exposure (60 seconds, 30 minutes, 1 hour, 3 hours, 5 hours).

The main purpose of this investigation was to develop and test a novel method of treatment for human hepatocellular carcinoma (HCC). Preliminary data from the literature support the implication of albumin in tumor growth. This is due to the fact that albumin enhances tumor extension, being used for synthesis in different cellular compartments.

In order to investigate the toxic effects of nanoconjugates, epithelial cells and C3A cells were exposed and incubated with various concentrations of HSA-GNPs at different incubation periods. Consistent with other findings, it was shown that only high concentrations of GNP bioconjugates have cytotoxic effects. However, toxicity, which is a major obstacle to the use of gold nanoparticles in clinical applications, can be minimized by administration of low doses of nanoconjugates. (14-17)

HSA-GNPs were further used as heat-inducing agents under laser radiation during the process of nanophotothermolysis. This method is based on the presence and grouping of HSA-GNPs inside cells, as well as their high optical absorption capacities, responsible for inducing thermal effects, especially under NIR irradiation, where biological systems have low absorption and high transparency. Optoelectronic transitions in graphitic structures of bundles of GNPs generate heat, which rapidly spreads in subcellular compartments, where nanoconjugates are present.

Nanophotothermolysis of liver cancer cells containing HSA-GNPs, induced by laser irradiation, can be used in two main modes: pulsed and continuous. The pulsed mode produces localized damage (a few µm) of individual cancer cells by laser-induced micro and nanobubbles around overheated nanoparticles, without harmful effects on the surrounding healthy cells. It is particularly favored for in vivo necrosis of circulating tumor cells using only nanosecond laser pulses. The second mode requires more time (several minutes of exposure) and results in thermal denaturation and coagulation as major mechanisms of cell damage. It is more appropriate for the treatment of primary tumors with sizes of up to several mm.

At this stage in the study, pulsed and continuous wave laser irradiation highlighted significant differences in the percentage of apoptotic C3A cells ($p<0.05$) after irradiation at concentrations below 20 mg/L, for 60 seconds and 30 minutes, compared to apoptotic HeLa cells. It is obvious that in the case of low concentrations of HSA-GNPs (e.g. plasma levels after intra-arterial administration) necrosis rate is significantly higher when combining nanoparticles with molecular carriers. Caveolae-mediated endocytosis was shown to be the C3A albumin absorption mechanism, similar to other ligands, such as cholesterol or folic acid. This particular type of endocytosis is a distinctive form of transport, being fundamentally different from independent or clathrin-mediated endocytosis. The mechanism consists in the internalization of caveolae together with nanobiomolecules, biomaterials being accumulated caveosomes, a distinct type of organelles.

Data in the literature have highlighted the potential of folic acid in specific therapies. Thus, significant results were obtained after conjugation of nanoparticles wrapped in polyethylene glycerol (PEG) with folic acid as target receptor (folate receptor). As previously mentioned, clathrin-mediated endocytosis was the preferred process of internalization, as it is a non-degrading mechanism using pH-dependent chemotherapy. Nowadays, a combination of cytostatic drugs and albumin, called Trexall, is prescribed for the treatment of metastatic liver cancer in humans. In a similar manner, we aim to develop highly efficient nanobiomolecules for nanophotothermal therapy. The literature has already suggested new ideas for therapy that could eliminate the destructive lysosomal transit and, therefore, provide a higher level of protection for drug compounds. A specific endothelin receptor associated with the mechanism of absorption described is gp60. Using phase contrast microscopy and immunofluorescence microscopy, we showed that the absorption of HSA- GNPs in C3A cells occurs via caveolae-mediated endocytosis, initiated by the binding of gp60 (albondin). (18) (Figure 4)

The treatment of C3A cells with high concentrations of HSA-GNPs for more than 5 hours showed that the percentage of necrotic cells was not significantly different from that of epithelial cells. This finding suggests the non-selective passive intracellular diffusion of nanomaterial inside cells, when exposed to high concentrations of nanomaterial for long periods of time.

On the other hand, selective lysis of C3A cells treated with HSA-GNPs was obtained for periods of incubation of less than 30 minutes, regardless of concentration. In cellular systems, molecular membrane association/dissociation processes are very short, ranging from seconds to a few minutes. (19)

References

[1] Jemal A, Bray F, Center MM, Ferlay J, Ward E, Forman D. Global cancer statistics. CA Cancer J Clin 2011 Mar-Apr;61(2):69-90.

[2] Iancu C, Mocan L. Advances in cancer therapy through the use of carbon nanotube-mediated targeted hyperthermia. International Journal of Nanomedicine 2011;6:1675.

[3] Brannon-Peppas L, Blanchette JO. Nanoparticle and targeted systems for cancer therapy. Adv Drug Deliv Rev 2012.

[4] Conde J, Doria G, Baptista P. Noble Metal Nanoparticles Applications in Cancer. Journal of Drug Delivery 2012;2012.

[5] Dreaden EC, Austin LA, Mackey MA, El-Sayed MA. Size matters: gold nanoparticles in targeted cancer drug delivery. Therapeutic delivery 2012;3(4):457-478.

[6] Hamdy S, Haddadi A, Ghotbi Z, Hung RW, Lavasanifar A. Part I: targeted particles for cancer immunotherapy. Curr Drug Deliv 2011 May 1;8(3):261-273.

[7] Wan X, Zheng X, Pang X, Zhang Z, Zhang Q. Incorporation of lapatinib into human serum albumin nanoparticles with enhanced anti-tumor effects in HER2-positive breast cancer. Colloids and Surfaces B: Biointerfaces 2015;136:817-827.

[8] Jeanbart L, Ballester M, de Titta A, Corthesy P, Romero P, Hubbell JA, et al. Enhancing efficacy of anticancer vaccines by targeted delivery to tumor-draining lymph nodes. Cancer Immunol Res 2014 May;2(5):436-447.

[9] Wang Y, Ni Y. Combination of UV–vis spectroscopy and chemometrics to understand protein–nanomaterial conjugate: A case study on human serum albumin and gold nanoparticles. Talanta 2014;119:320-330.

[10] Nanda R, Chennamaneni P, Gibson J, Koetter K, Libao B, Skor M, et al. Abstract P2-16-21: A randomized phase I trial of nanoparticle albumin bound paclitaxel (nab-paclitaxel, Abraxane®) with or without mifepristone for advanced breast cancer. Cancer Res 2013;73(24 Supplement):P2-16-21-P2-16-21.

[11] Guarneri V, Dieci MV, Conte P. Enhancing intracellular taxane delivery: current role and perspectives of nanoparticle albumin-bound paclitaxel in the treatment of advanced breast cancer. Expert Opin Pharmacother 2012;13(3):395-406.

[12] Barshtein G, Arbell D, Yedgar S. Hemolytic Effect of Polymeric Nanoparticles: Role of Albumin. NanoBioscience, IEEE Transactions on 2011(99):1-1.

[13] Iancu C, Mocan L, Bele C, Orza AI, Tabaran FA, Catoi C, et al. Enhanced laser thermal ablation for the in vitro treatment of liver cancer by specific delivery of multiwalled carbon nanotubes functionalized with human serum albumin. International Journal of Nanomedicine 2011;6:129.

[14] Li JJ, Hartono D, Ong CN, Bay BH, Yung LY. Autophagy and oxidative stress associated with gold nanoparticles. Biomaterials 2010 Aug; 31(23):5996-6003.

[15] Puvanakrishnan P, Park J, Chatterjee D, Krishnan S, Tunnell JW. In vivo tumor targeting of gold nanoparticles: effect of particle type and dosing strategy. Int J Nanomedicine 2012;7:1251- 1258.

[16] Boisselier E, Astruc D. Gold nanoparticles in nanomedicine: preparations, imaging, diagnostics, therapies and toxicity. Chem Soc Rev 2009;38(6):1759-1782.

[17] Male KB, Lachance B, Hrapovic S, Sunahara G, Luong JHT. Assessment of cytotoxicity of quantum dots and gold nanoparticles using cell-based impedance spectroscopy. Anal Chem 2008;80(14):5487-5493.

[18] Tiruppathi C, Song W, Bergenfeldt M, Sass P, Malik AB. Gp60 activation mediates albumin transcytosis in endothelial cells by tyrosine kinase-dependent pathway. J Biol Chem 1997 Oct 10;272(41):25968-25975.

[19] Fesce R, Meldolesi J. Peeping at the vesicle kiss. Nat Cell Biol 1999;1(1):E3-E4.

Chapter 3

Development of an in Vitro Anticancer Vaccine Platform Using Gold Nanoparticles Immunoconjugates

Teodora Mocan[1], Flaviu A. Tabaran[2], Cristian Matea[3], Teodora Pop[3], Diana Gonciar[3], Ofelia Mosteanu[3], Lucian Mocan[3], Dana Bartos[3], Lucia Agoston-Coldea[4], Cornel Iancu[3]

[1]Department of Physiology, "Iuliu Hatieganu" University of Medicine and Pharmacy, Clinicilor 5-7, Cluj-Napoca, Romania

[2]Department of Pathology, University of Agricultural Sciences and Veterinary Medicine, Faculty of Veterinary Medicine, 3-5 Manastur Street, 400372 Cluj-Napoca, Romania, tel/fax: +40264-593792

[3]Gastroenterology Institute; “Iuliu Hatieganu” University of Medicine and Pharmacy, 19-21 Croitorilor Street, Cluj-Napoca, Romania

[4]Department of Medical Sciences, Iuliu Hatieganu University of Medicine & Pharmacy, 2–4 Clinicilor, 400006, Cluj-Napoca, Romania

Introduction

Colon cancer is a major cause of deaths worldwide, and it is expected to rise in the coming years. Current therapeutic strategies in colon cancer treatment include surgical resection of the primary tumor, chemotherapeutic drugs and radiotherapy. (1, 2)

The development of nanoscale drug delivery systems represents an exciting and new approach to cancer treatment. (3) A strong goal in the use of nanoscale drug delivery systems is to deliver high doses of active bio-nanomolecules at specific sites while simultaneously reducing systemic toxicity. Very recent clinical trials suggest that nanoscale drug delivery systems such as Doxil® (doxorubicin encapsulated in liposomes (4) and Abraxane® (paclitaxel attached to nanoparticles) (5) could prolong survival in advanced cancer. One remarkable property of these nano-systems is represented by the activation of the immune system, which could form an attractive basis for cancer vaccine development. Although such drug delivery systems hold a tremendous potential for the future prevention of cancer, the research for a true anticancer vaccine remains elusive. Nanotechnology has already brought to light promising results in the field of anticancer vaccines. For instance, inert nanobeads, recombinant virus-like particles (VLPs), and immunostimulating complexes, are being used in cancer vaccine research due to their efficacy at eliciting both cellular and humoral immune responses.

During the last decade, advances in functionalization chemistry have been one of the driving forces in the development of new classes of nanoparticles for applications in biology and medicine. (9). Due their unique physical and chemical properties nanosize particles hold great hopes for drug delivery and cancer therapy. (10). There are several encouraging data that some classes of nanostructures may be used in initiating and maintaining immune responses. (11). When bound to tumor antigens, they elicit a specific antitumor response in animal models. (12) Furthermore, data shown that peptide-functionalized nanoobjects can act as proficient immunomodulators and consequently generate specific antibody responses. (13) Moreover, ex vivo clonal expansion of T cells with antibody-linked nanoparticles results in T-cell activation and might lead to the development of novel immunotherapies. (14).

It has been shown in animal models that significant lymphocytes proliferation and secretion of cytokines may help to rebuild the host`s immunity against cancer and consequently to generate obvious antitumor immunity. Despite their proven role in proliferation of T lymphocytes, especially the proliferation of $CD8^+$ lymphocytes (cytotoxic T lymphocytes) (14) which constitutes the main part of antitumor effector cells (15), (16) there are currently no studies that explore the concept of cancer prophylaxis mediated by gold nanoparticles.

Recent literature data supports the role of embryonic stem cells (ESC) as cellular cancer vaccine that stimulates the biological systems to destroy colon cancer cells by eliciting an immune boost. (17). The implication is supported by the fact that ESC prevent and control the proliferation and expansion of malign tumors in vivo by formation and development of CD^{+} and $CD8^{+}$ T lymphocytes (18). Considering all these data together we have been recently able to demonstrate that combined administration of both ESC and multi walled carbon nanotubes can function as powerful nanobiosystem to induce and rebuild antitumor immunity in colon tumor animal models. (Figure 1). The proposed administration led to significant antitumor responses and enhanced tumor rejection in mice with subcutaneous inoculation of colon malign cells. (19) The paper was published in Journal of American Society for Nanomadicine and was the first paper that introduced a novel concept in the field: that of nano-mediated anti-cancer vaccine.

Still, toxicity issues regarding carbon nanotube-living organism interaction, have been suggested by our data (20-25) and other research groups reports. (26, 27) Reports suggest carbon nanotubes might be unnappropriate for long-term human usage. Recently, gold nanoparticles were approved on human treatment in phase 1 clinical trials, which suggests that gold can act as an effective and safe agent for human-intend applications. (www.clinicaltrials.gov). Present project proposes tailoring of research from a clinical perspective by using gold nanoparticles (that are approved for human treatment) in order to develop a novel prophylaxy method for colon cancer.

Moreover, preliminary obtained results suggest that nanostructures may function as antigen presenting molecules. We have, therefore, reasoned that binding of a low immunogenic peptide antigen onto the gold nanoparticle could lead, by presentation to MHC molecules of dendritic cells, to an essential mount in immune response intensity. We reason that MUC1 (CD227), a membrane-tethered mucin glycoprotein that is normally expressed on the apical surfaces of normal glandular epithelia, could become an adequate conjugator for Gold-NPs., capable to produce the expected effect. It has been previousely stated that MUC 1 is over expressed and aberrantly glycosylated in >70% of human colon cancer. (28) Recent description of MUC1 as a target for cytotoxic T lymphocytes (CTLs) has raised interest in using this protein as a possible target for immunotherapy, suggesting a good potential for its application of nanomediated colon cancer vaccine. (29-31)

Additionaly, based on previous experiments, we reason that changing the initial vaccine formulation through in vitro pre-pulsing of embryonic stem cells to facilitate dendrite cell differentiation would make a difference in the final desired in vivo effect following administration.

We therefore hypothesize that a novel vaccine nano-formulation, containing MUC-1- functionalized GoldNPs and stem cell-derived dendritic cells could lead to potent antitumor lymphocyte activation, thus opening new avenues in the prophylaxy of colon cancer.

Motivation

MUC1 (CD227) is a membrane-bound glycoprotein expressed in normal glandular epithelial cells under basal conditions. Existing studies in the literature suggest MUC1 overexpression and aberrant glycosylation in more than 70% of colorectal cancers. Recent studies focus on its potential to serve as target for cytotoxic T lymphocytes. The use of MUC1 in immunotherapy as a specific target gives way to potential applications in nanoparticle-mediated therapies for colorectal cancer.

Exposure of dendritic cells to MUC1-gold nanoparticle conjugates aims to stimulate MUC-1 antigen presentation to specific immune cells (lymphocytes), regulated by the major histocompatibility complex (MHC). The intended response is to induce peptide-specific immune activation with improved anticancer effect. The final formula of the vaccine against colorectal cancer combines the effect of three factors which have already proven their efficacy in immunostimulation: gold nanoparticles, dendritic cells and the tumor-specific peptide (MUC1).

A MUC1-specific proteic product (ab 80082) was selected for the experiment. Product selection was based on similar experiments in the literature, employing structure-based binding methods. The presence of a histidine residue (His) in the selected molecule makes the functionalization of gold nanoparticles with bio-ligands theoretically approachable and guarantees future binding success.

Microscopic Assessment of Dendritic Cell Cultures

Analysis of Dendritic Cell Cultures by Optical Microscopy

Cell culture plates and adherent dendritic cell cultures on port object slides were examined using an optical microscope (Olympus BX51). Simple optical and phase contrast microscopy images were obtained using an Olympus SP-350 camera and processed with Cell B Olympus and Olympus Stream Basic programs.

Analysis of Dendritic Cell Cultures by Laser Scanning Confocal Microscopy

Dendritic cell cultures obtained were analyzed and characterized using Zeiss LSM 710 confocal microscope mounted on an inverted microscope (Axio Observer Z1). EC plan neofluar 10x/0.30M27 objectives were used to obtain an overview of cell cultures and plan apochromat 63x/1.40 objectives were used to observe structural details of dendritic cells. The lasers used to obtain specific fluorochrome excitation emitted light at 488 nm and 633 nm. Both argon laser and helium-neon laser were set to 5.0% of their light potential. Laser beam aperture (aperture/"pinhole") was fixed at 39 µm (1 Airy unit) for images obtained with x10 objectives and 50 µm for 63x objectives.

For images obtained with the 63x objective, the main acquisition for fluorescence channel 1 (green channel-FITC) was 945, and 570 for channel 2 (red DRAQ5).

For images obtained with 10x objective, the main acquisition for fluorescence channel 1 (green channel-FITC) was 834, and 871 for channel 2 (red DRAQ5). Digital amplification of the fluorescent signal was 15 for Ch1 and 1 for Ch2.

Laser beams were generated at 492-629 nm for fluorescence channel 1 and 661-757 for fluorescence channel 2.

Histochemical and Immunohistochemical Staining of Dendritic Cell Cultures for Laser Scanning Confocal Microscopy

Immunocytochemistry (indirect immunofluorescence) was employed to examine CD68 cell membrane antigen expression, using an anti-CD68 polyclonal antibody (IgG) (product Linaris Biologische Produkte, catalog no. MAK0341Q). Visualization was performed via fluorescent staining with fluorescent secondary antibody conjugates. Annex 1 shows the immunocytochemical staining protocol used. Histochemical labeling with fluorochrome DRAQ5® was used in order to visualize nuclei from the cell culture (Cell Signaling Technology Product, Cat. No. 4084).

The cytoskeleton was viewed using selective labeling of actin fibers. Labeling was performed by incubating fixed cells permeabilized with phalloidin (isolated from Amanita phalloides) and conjugated with FITC fluorochrome (Sigma-Aldrich product, Cat. No. 5282). Annex 2 shows the phalloidin labeling protocol used.

Results

Analysis of Dendritic Cell Cultures by Optical Microscopy

Cell cultures analyzed using simple optical microscopy and phase contrast or dark field microscopy reveal the presence of stellate cells (dendritic) with 3-5 branches (most cells observed) or fusiform cells (rare), adherent to culture flask walls (Figure 1). Cell growth occurs in a single and relatively uniform layer, with different degrees of confluence depending on the duration of the growth process. Cellular extensions have different lengths, from a few microns, which give a scalloped aspect to the edge of the cell, to over 20 μm. Rare cells are spherical or oval. Most cells are large, with an average length of 40-70 μm, including dendritic extensions. Cell body varies in volume, with a bulky round or oval central nucleus. Bilobed-reniform nuclei were rare. Some cells contain two adjacent nuclei (binucleated cells). The cytoplasm of cells with dendritic morphology is finely granular or, in some cases, finely vacuolated. There was a small percentage of suspension cells, generally oval-shaped.

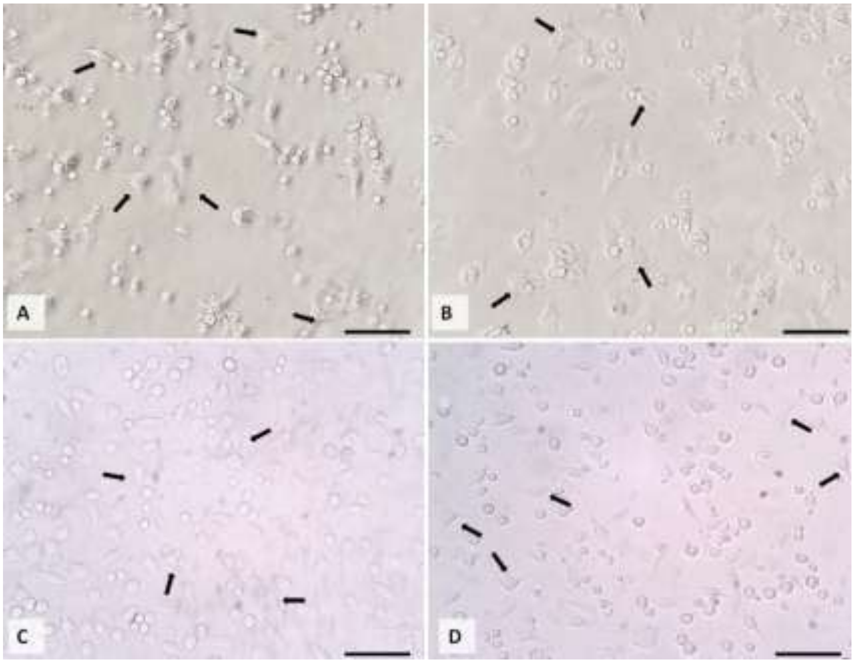

Figure 1. *Images of phase contrast microscopy (images A and B) and simple optical microscopy (images C and D) of isolated dendritic cell cultures. The arrows indicate cells with morphology that is characteristic of dendritic cells. Scale: 100 µm.*

Analysis of Dendritic Cell Cultures by Laser Scanning Confocal Microscopy

Cell culture analysis using laser scanning confocal microscopy confirms the dendritic morphology observed by optical microscopy, but adds essential data regarding cell structure. Dendritic extensions contain large numbers of actin filaments, following the path of these extensions along their entire length (Figure 2). These extensions sometimes end with a fine edge of side branches also containing actin in the cytoskeleton. The nucleus is oval, with compact or coarse chromatin and variable nucleolus (invisible for about half of the cells analyzed). Actin clusters can sometimes appear on the dendritic cell body (small size, 1-2 µm), giving cells a granular appearance.

Monolayer cell growth is generally observed on the entire surface of the culture plates, with the exception of certain outbreaks where dendritic cells are overlapped, with a bud-pattern aspect (colonies), consisting of 5 to 20 cells. Cellular debris with globular appearance, containing traces of DNA and actin (apoptotic bodies), are rarely observed.

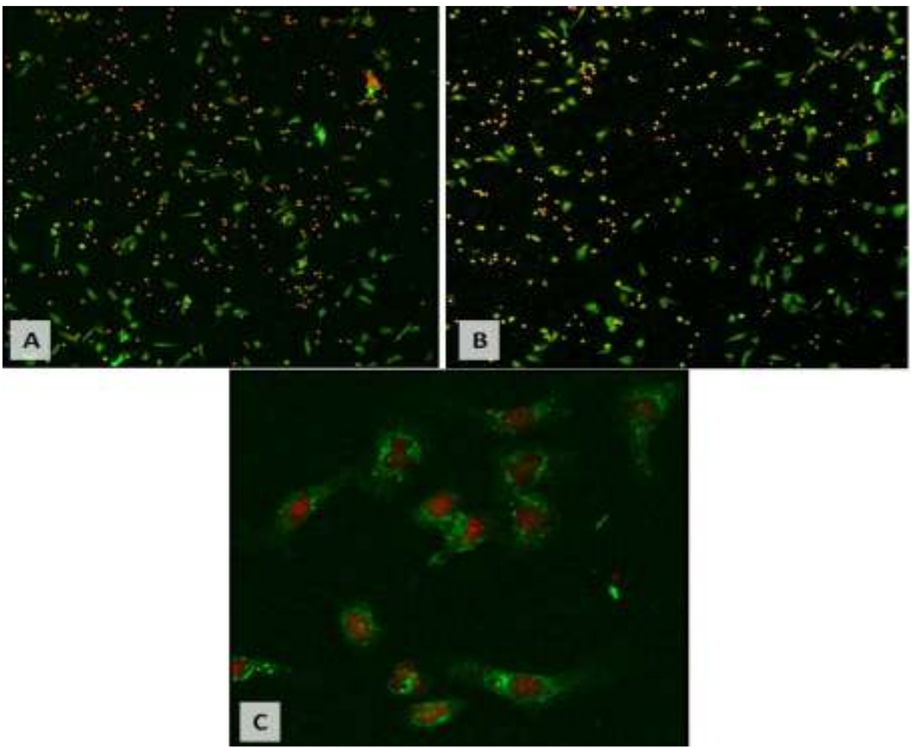

Figure 2. *Laser confocal microscopy images of dendritic cell cultures. The specific fluorescence of fluorochrome-labeled (DRAQ5) cell nuclei is observed in the red fluorescent channel. The fluorescence of phalloidin-conjugatedFITC-labeled actin fibers is observed in the green channel. Images A and B were obtained with a Plan Neofluar 10x/0.30 M27 Objective, and image C with a Plan Apochromat 63x/1.40 Objective.*

Expression of dendritic cells for CD68 antigen was stable and obvious for most cells analyzed. In terms of distribution, the antigen had a typical location, in the membrane, sometimes granular and insular. There was a small or medium amount of antigen expression for most cells with dendritic morphology. CD68 antigen expression also occurred for spherical or oval cells (Figure 3).

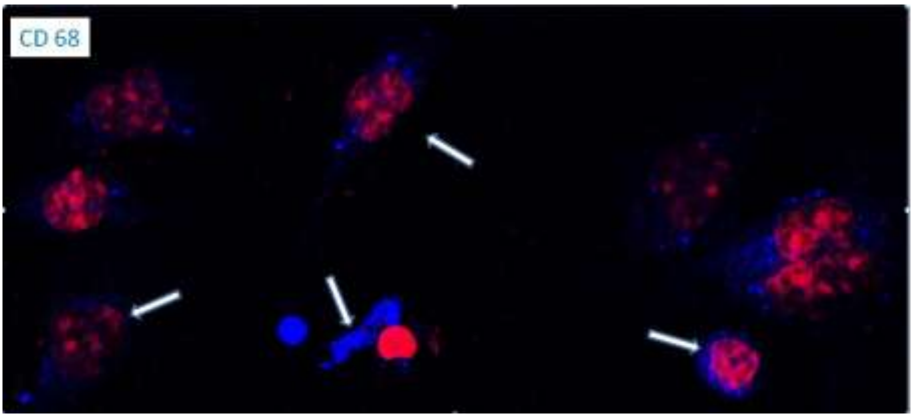

Figure 3. *Laser scanning confocal microscopy images of dendritic cell cultures immunocytochemically labeled with CD68 antigen. Blue fluorescence channel shows the positive CD68 antigen expression by cells with dendritic morphology. Red fluorescence channel shows the specific fluorescence of fluorochrome-labeled (DRAQ5) cell nuclei. Plan Apochromat 63x/1.40 Objective.*

Annex 1. *Immunocytochemical staining for CD68 antigen.*

1	Fixation with anhydrous acetone at -20 ℃	5 minutes
2	Phosphate buffered saline (PBS) washing	3 x 1 minute
3	Blocking non-specific binding by incubation with 3% BSA in phosphate buffered saline (PBS)	10 minutes
4	Incubation with primary antibodies (anti-CD 68)	3 hours at 37 ℃
5	Phosphate buffered saline (PBS) washing	3 x 1 minute
6	Incubation with secondary antibodies	30 minutes at 37 ℃
7	Phosphate buffered saline (PBS) washing	3 x 1 minute
8	Incubation with DRAQ5®	5 minutes
9	Phosphate buffered saline (PBS) washing	3 x 1 minute
10	Adding Mowiol mounting medium	

Discussion

Dendritic cells are antigen-presenting cells playing a key role in regulating the adaptive immune responses, achieving peripheral antigen uptake and processing. Further, by blood or lymphoid migration into lymphatic tissues rich in T lymphocytes, they present antigens to lymphocyte populations undergoing the execution stage of immune responses. Besides controlling the induction of the primary immune response, DCs are also essential for the induction of immunological tolerance.

Mature dendritic cells are isolated and characterized based on their key morphological properties in vivo and in vitro, as well as on the expression of different functional antigens. Considering that there is not only one antigen identifying dendritic cells, their phenotyping implies the characterization of a broad package of molecules. Dendritic cells and their subtypes are characterized by the presence or lack of major histocompatibility complex class II molecules, CD68 antigens, CD83, p55, S100b, M342i, MIDC-8, CD11c, CD123 and the absence of certain antigens such as CD3, CD14, CD19, CD56 and CD66b.

Regarding the expression of CD68 antigen expression found here, it is an important tool in diagnosing monocytes/macrophages and dendritic cells. Even if it is usually used to identify monocytes/macrophages, this antigen is also expressed by other cells, such as endothelial cells or fibroblasts, but in a variable quantity, much smaller than macrophages or dendritic cells. Thus, a powerful expression of this antigen is a characteristic of macrophage cells and dendritic cells derived from the myeloid cell line. Moreover, not only the expression, but the location of CD68 is suggestive for immunophenotyping. While macrophages are mainly located intracytoplasmically or around the cell membrane, dendritic cells have a predominant perinucelar CD68 location.

From a morphological point of view, one of the most important features employed for the identification and characterization of dendritic cells, is represented by the multiple cytoplasmic extensions that give a stellate appearance to these cells. The number and characteristics of these extensions vary depending on the degree of maturity (differentiation) and the medium where cells are described (in vivo/in vitro). Mature dendritic cells in culture flasks visualized by phase contrast microscopy have various cell extensions (over 10 µm long) giving cell edges a veil look. The morphological aspect observed by means of optical and confocal microscopy is suggestive of dendritic cell characteristics. The long multiple or branched extensions are typical dendritic cell characteristics, and even more, they are characteristics of semi-mature or mature dendritic cells.

Actin fibers reinforce the cell skeleton, becoming one of the most important consolidation elements for dendritic cell extensions spines bet on our case. Because of this, actin skeleton analysis brings important information on cellular ramifications. Furthermore, due to its major role in cell mobility and dendritic cell development, the amount of actin is suggestive of the movement capacity and of the ability to infer the prevailing phagocitary activity or antigen presentation.

Even if both immunocytochemical and microscopic observations are characteristic of dendritic cells, complementary immunophenotyping studies are required for complete phenotyping and determination of the degree of maturity/differentiation.

Conclusion

Optical and laser scanning confocal microscopy observations of culture plates suggest dendritic cell morphology under various stages of differentiation/maturity.

Analyzed cells exhibit intense immunopositivity for CD68 antigen, a typical property of monoblast-derived cells, namely dendritic cells and monocytes/macrophages.

Functionalization of Gold Nanoparticles with MUC1

Synthesis of gold nanoparticles was performed in aqueous medium using the Turkevich method, with a few minor changes. Briefly, 48 mg of $HAuCl_4$ (Sigma-Aldrich code 520918) were dissolved in 100 mL bidist H_2O. Further, 100 mg sodium citrate (Sigma-Aldrich code S4641) were dissolved in 5 mL bidist H_2O, the resulting solution being subjected to ultrasounds for 15 minutes. The citrate solution obtained was heated to 100 ℃ and then the $HAuCl_4$ solution was quickly added, under continuous magnetic stirring. Under the action of temperature and citrate,

Au (III) was reduced to Au^0 (metallic gold). The reaction was allowed to proceed to reflux for 2 hours. Then, the solution was cooled to room temperature, subjected to centrifugation (15,000 rpm for 30 minutes) and redispersed in bidist H_2O using a sonicator. Assessment of citrate-stabilized gold nanoparticles (GNPs) was performed using a Shimadzu 1800 UV-Vis spectrophotometer. Synthesized gold nanoparticles showed a reddish coloration and a maximum absorption of λmax = 523nm.

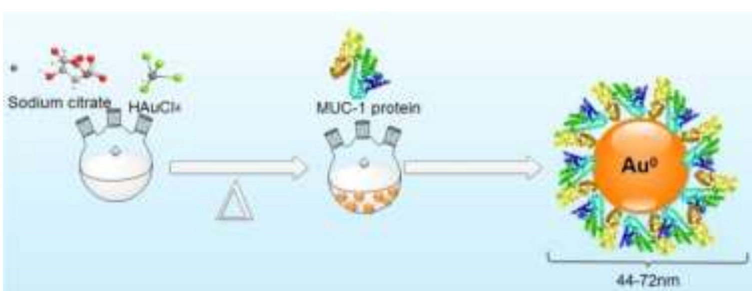

Figure 4. *Functionalization of gold nanoparticles with MUC1.*

For functionalization of gold nanoparticles with MUC1, the latter was reduced in the presence of dithiothreitol (DTT). Briefly, 150 µL MUC1 solution (conc. 1 µg/µL) were dispersed in 1 mL bidist H_2O, to which 400 µL 100 mM

DTT solution (pH=8.5) were added and the sample was incubated for 1 hour at room temperature. The reduction step is designed to break the disulfide bonds inside the protein and to expose thiol groups (-SH), groups with affinity for the synthesized gold nanoparticles. Further, the reduced MUC1 solution was combined with 5 mL GNP solution, pH was adjusted to ≈7 and the reaction was allowed to proceed for 2 hours at room temperature. It is now that the sample color changed from red to blue (Figure 5). This change in color is due to MUC1 attachment to gold nanoparticles.

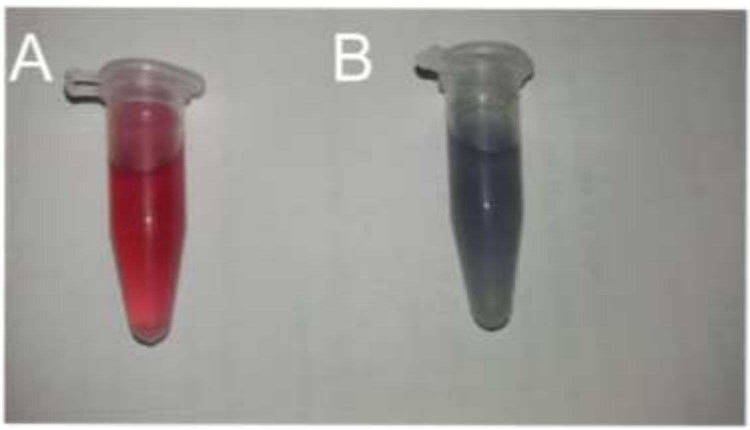

Figure 5. *A - GNP solution; B - GNP solution in reaction to reduced MUC1.*

Gold nanoparticles functionalized with MUC1 (MUC1-GNPs) were subjected to centrifugation (15,000 rpm for 15 minutes) and re-dispersed by sonication in bidist H_2O to remove secondary reaction products.

Characterization of the Newly Obtained MUC1-GNP Compounds

The MUC1-GNP solution was characterized using spectral methods (UV-Vis) and atomic force microscopy (AFM).

UV-Vis spectra of GNPs and MUC1-GNPs were recorded using a Shimadzu 1800 spectrophotometer and normalized using OriginLab ™ software.

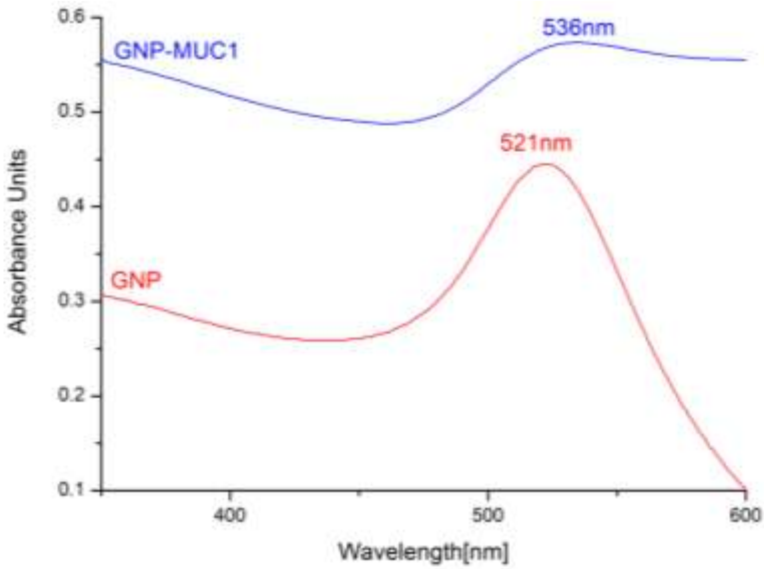

Figure 6. *UV-Vis spectra of GNPs and MUC1-GNPs.*

Figure 6 shows that the spectrum of GNPs exhibits a GNP-specific absorption maximum of λmax=523 nm. The absorption maximum for MUC1-GNPs suffers a bathochromic effect, with a λmax = 536 nm.

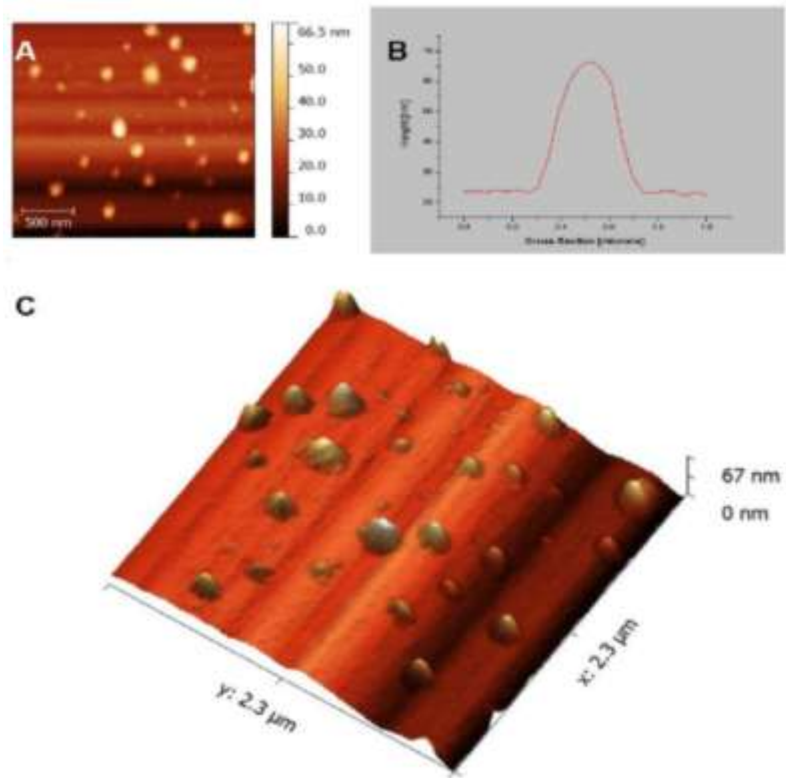

Figure 7. *AFM images of MUC1-GNPs. A - 2D topographic image; B - MUC1-GNP profile; C -3D representation.*

Nanoparticles functionalized with MUC1 were analyzed using atomic force microscopy (TT- AFM Workshop™ microscope). Samples were previously dispersed with a in-sample sonicator and deposited on a Mica structure. Data acquisition was performed under non-contact mode (vibrating mode). Data were processed using Gwyddion® software. Nanoparticle size was calculated based on profiles extracted from images, MUC1-GNP ranging between 44 and 72 nm (Figure 7B). Figure 7C shows a three-dimensional representation of functionalized nanoparticles.

Exposure of Dendritic Cells to MUC1-GNPs in Vitro

Cell Culture Preparation

For the microscopic examination of cells, seeding was performed (after trypsinization, detachment and passage) on slides with 4 separate chambers (four well-chamber), corresponding to the four groups. After cell reattachment and growth in specific medium (0.5 ml/chamber), cells were serially counted, identifying the exponential growth phase.

Cell cultures carried out to test cell proliferation were obtained by cell seeding in 96-well plates (50 microliters/well).

Cell Exposure to the Material

At the appropriate time, cells were exposed by adding 0.5 ml of test solution in each chamber on the microscope slide, and 50 microliters in each well of the 96-well plate, as follows:

1 Group 1 - unexposed (culture medium)

2 Group 2 - exposed to MUC1-GNPs in low concentration (5 micrograms/mL)

3 Group 3 - exposed to MUC1-GNPs in average concentration (10 micrograms/mL)

4 Group 4 - exposed to MUC1-GNPs in high concentration (20 micrograms/mL)

Incubation with the corresponding test solution was performed for 2 hours under standard conditions (37 ℃, 5% CO_2).

For the quantification of cell proliferation, experiments were carried out in triplicate, each group being assigned three wells out of the existing 96 wells on the plate.

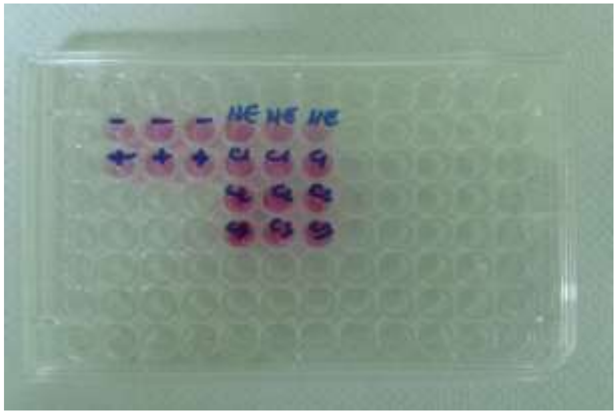

Figure 8. *Aspect of 96-well-plate including MUC-1-GNPs- exposed and non-exposed groups, as well as positive and negative controls.*

Quantification of Cell Proliferation/Viability

The assessment of the effects of cell exposure to various solutions on cell viability was performed using MTT Assay protocols. The

MTT reagent (3-(4,5-dimethyl-2-thiazolyl)-2,5-diphenyl-2H-tetrazolium bromide) is a compound that undergoes reduction processes in metabolically active cells (viable cells). The resulting compound, formazan, can be solubilized and quantified using spectrophotometry. The specific protocol of the manufacturer (ATCC) was used in order to assess cell viability and proliferation. Briefly, it follows the succeeding growth steps using specific culture media mentioned above, with MTT reagent addition, incubation for 2-4 hours until the formation of visible precipitates, addition of detergent substances, maintaining the solution in the dark for 2 hours at room temperature. Finally, counting was done spectrophotometrically at 570 nm. The results were expressed as a percentage of the levels reported for the control samples.

Results

After exposure, the cell culture aspect was examined microscopically.

The quantification of the level of cell proliferation/viability was also performed, considering 100% absorbance of the non-exposed batch (OD 570 nm).

As shown in the figure below, the levels of proliferation were constant, without significant differences between any of the 2 groups (p>0.05).

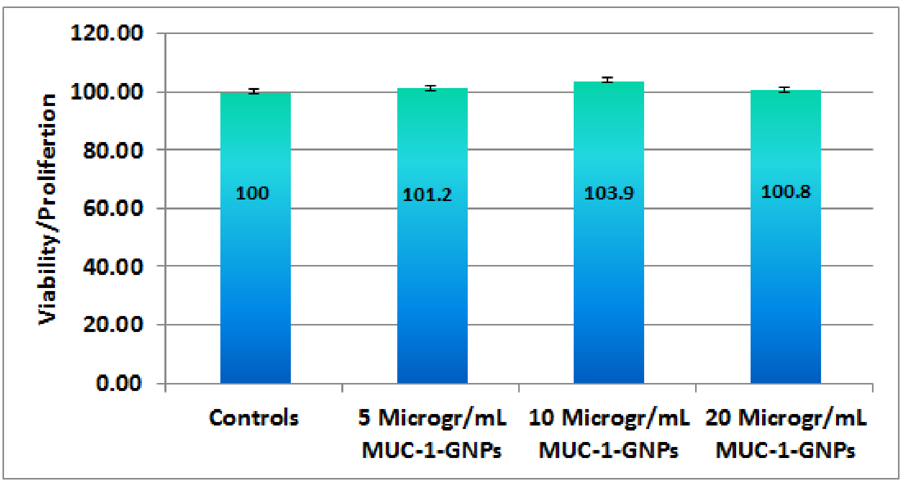

Figure 9. *MTT assay results for the exposed groups.*

Discussion

The experiments in the literature show mixed results regarding the cytotoxicity of the compounds obtained by covalent conjugation of gold nanoparticles with protein molecules. Thus, some studies indicate a definite toxicity, evidenced by the level of the half maximal inhibitory concentration measured by MTT and LDH assays. PCR experiments, as well as ATP depletion dosage, suggest the induction of both intrinsic and extrinsic apoptotic cell damage. Strictly dependent on the attached molecules and other features of the nanomaterial, gold nanoparticles can interact with cellular DNA, redox balance, mutagenesis, and protein synthesis.

Other evidence suggests the absence of toxic effects on gold nanoaparticles of different sizes and functionalization agents: biotin, cysteine, glucose, etc., as demonstrated by the MTT assay (6).

The effects of gold nanoparticles on dendritic cells have recently been studied. The study demonstrates the lack of cytotoxic effects on this cell type of major importance in both humoral and cell-mediated immunity. The absence of any phenotypic change in dendritic cells suggests the absence of dendritic cell activation. However, an interesting observation of the study is provided by the intense changes in cytokine profile, which might induce future activation. (7).

Current experiments demonstrate the high level of biocompatibility of the newly synthesized product. The interaction between MUC1-GNPs and dendritic cells does not induce significant levels of apoptosis. This is particularly useful when intended to build a combined vaccine (cells + nanomaterial). It is also notable that in the absence of cytotoxic effects, the presence of MUC1 and the altered cytokine profile, already demonstrated in the literature, may contribute to cell activation required for immunostimulation.

Conclusion

Quantification of cell viability after exposure of PANC 1 cells indicates the lack of cytotoxic effects of the newly generated MUC1-GNPs nanoconstruct.

Assessment of MUC1-GNP Basal Cytotoxicity in Dendritic Cells

Both optical microscopy and confocal microscopy were used to assess the toxic changes and cell damage that may occur following exposure of dendritic cells to the test compound.

Optical microscopy observed that the analyzed cells retained their typical dendritic morphology after exposure to gold nanoparticles functionalized with MUC1. Furthermore, there were no changes in cell adhesion or cell morphology following exposure to 10 µg or 20 µg doses of MUC1-GNPs, cells also maintaining a similar morphology to control cultures (Figure 4).

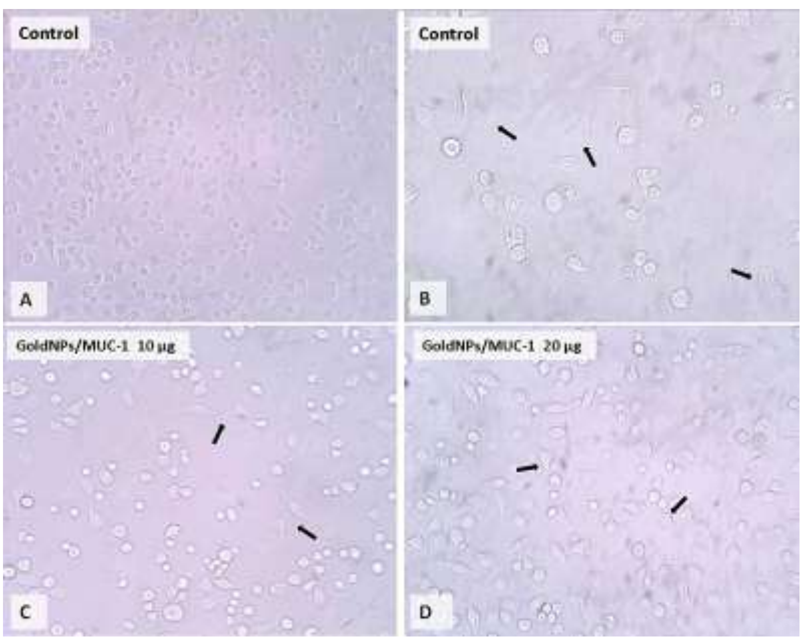

Figure 10. *Images of dendritic cell cultures isolated after exposure to different doses of gold nanoparticles functionalized with MUC1 (MUC1-GNPs), provided by optical microscopy. Arrows indicate cells with characteristic dendritic morphology in control cell cultures and following exposure to the test compound.*

Laser confocal analysis of dendritic cell cultures is in agreement with the information provided by optical microscopy. There were no changes suggesting a cytotoxic effect (i.e. cytoplasmic or nuclear vacuolation, cell ballooning, detachment from the adherent surface, cell wall fragmentation or decrease in the number or length of dendritic extensions). Therefore, dendritic cells retained their structure unchanged following exposure to 10 µg or 20 µg doses of MUC1-GNPs (Figure 11).

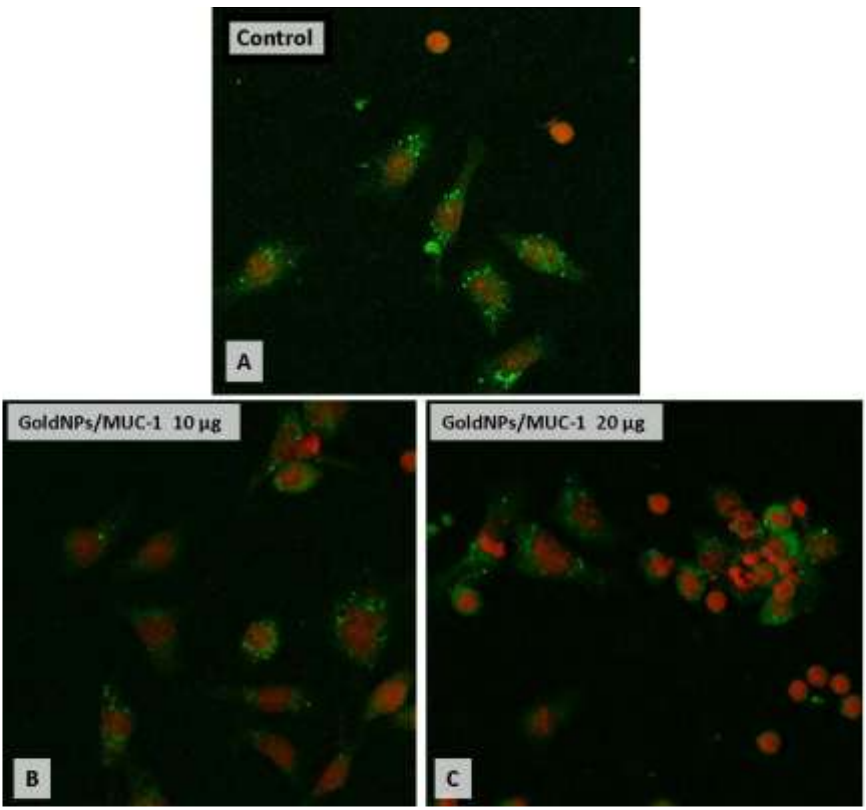

Figure 11. *Images of dendritic cell cultures isolated after exposure to different doses of gold nanoparticles functionalized with MUC1 (MUC1-GNPs), provided by laser confocal microscopy. Specific dendritic cell nuclei fluorescence (histochemically labeled with DRAQ5) is observed in the red fluorescence channel. Actin fiber fluorescence (labeled with FITC-conjugated phalloidin) is observed in the green channel. Images were acquired with a Plan Apochromat 63x/1.40 Objective.*

Conclusion

The microscopic analysis carried out after exposure suggests the high cellular biocompatibility of the newly synthesized product.

Annex 2. *Histochemical labeling of actin fibers in the dendritic cell cytoskeleton.*

1	4% paraformaldehyde fixation	10 minutes
2	Phosphate buffered saline (PBS) washing	3 x 1 minute
3	Tween 20 permeabilization (10% in PBS)	5 minutes
4	Phosphate buffered saline (PBS) washing	3 x 1 minute
5	Incubation with phalloidin (FITC) working solution	40 minutes in the dark
3	Phosphate buffered saline (PBS) washing	3 x 1 minute
8	Incubation with DRAQ5® for nuclei labeling	5 minutes
9	Phosphate buffered saline (PBS) washing	3 x 1 minute
10	Adding Mowiol mounting medium	

Conclusion

1. Experiments resulted in the generation and complex characterization of an innovative bionanocomposite product, MUC1-GNP.

2. When in contact with dendritic cells, key components of the future anti-cancer vaccine, the new product acts as a low-cytotoxic agent, recommended for cell/living tissue applications in a concentration of 0-20 micrograms/mL.

References

[1] Jemal A, Bray F, Center MM, Ferlay J, Ward E, Forman D. Global cancer statistics. CA Cancer J Clin 2011 Mar-Apr;61(2):69-90.

[2] Segal NH, Saltz LB. Evolving treatment of advanced colon cancer. Annu Rev Med 2009;60:207-219.

[3] Subramani K, Hosseinkhani H, Khraisat A, Hosseinkhani M, Pathak Y. Targeting nanoparticles as drug delivery systems for cancer treatment. Current Nanoscience 2009;5(2):135-140.

[4] ElBayoumi TA, Torchilin VP. Tumor-targeted nanomedicines: enhanced antitumor efficacy in vivo of doxorubicin-loaded, long-circulating liposomes modified with cancer-specific monoclonal antibody. Clinical Cancer Research 2009;15(6):1973.

[5] Miele E, Spinelli GP, Miele E, Tomao F, Tomao S. Albumin-bound formulation of paclitaxel (Abraxane® ABI-007) in the treatment of breast cancer. International Journal of Nanomedicine 2009;4:99.

[6] Bachmann MF, Jennings GT. Vaccine delivery: a matter of size, geometry, kinetics and molecular patterns. Nature Reviews Immunology 2010.

[7] Wang E, Monaco A, Monsurro V, Sabatino M, Pos Z, Uccellini L, et al. Antitumor vaccines, immunotherapy and the immunological constant of rejection. IDrugs 2009 May;12(5):297-301.

[8] Scheerlinck JPY, Greenwood DLV. Virus-sized vaccine delivery systems. Drug Discov Today 2008;13(19-20):882-887.

[9] Xu Y, Mahmood M, Fejleh A, Li Z, Watanabe F, Trigwell S, et al. Carbon-covered magnetic nanomaterials and their application for the thermolysis of cancer cells. Int J Nanomedicine 2010 Apr 7;5:167-176.

[10] Levi-Polyachenko NH, Merkel EJ, Jones BT, Carroll DL, Stewart JH, 4th. Rapid photothermal intracellular drug delivery using multiwalled carbon nanotubes. Mol Pharm 2009 Jul-Aug;6(4):1092-1099.

[11] Kostarelos K, Bianco A, Prato M. Promises, facts and challenges for carbon nanotubes in imaging and therapeutics. Nature Nanotechnology 2009;4(10): 627-633.

[12] Meng J, Duan J, Kong H, Li L, Wang C, Xie S, et al. Carbon nanotubes conjugated to tumor lysate protein enhance the efficacy of an antitumor immunotherapy. Small 2008;4(9):1364-1370.

[13] Pantarotto D, Partidos CD, Hoebeke J, Brown F, Kramer E, Briand JP, et al. Immunization with peptide-functionalized carbon nanotubes enhances

virus-specific neutralizing antibody responses. Chem Biol 2003;10(10):961-966.

[14] Fadel TR, Steenblock ER, Stern E, Li N, Wang X, Haller GL, et al. Enhanced cellular activation with single walled carbon nanotube bundles presenting antibody stimuli. Nano letters 2008;8(7):2070-2076.

[15] Begley J, Ribas A. Targeted therapies to improve tumor immunotherapy. Clinical Cancer Research 2008;14(14):4385.

[16] Rosenberg SA, Yang JC, Restifo NP. Cancer immunotherapy: moving beyond current vaccines. Nat Med 2004;10(9):909.

[17] Li Y, Yao Y, Sheng Z, Yang Y, Ma G. Dual-modal tracking of transplanted mesenchymal stem cells after myocardial infarction. Int J Nanomedicine 2011;6:815-823.

[18] Dong W, Du J, Shen H, Gao D, Li Z, Wang G, et al. Administration of embryonic stem cells generates effective antitumor immunity in mice with minor and heavy tumor load. Cancer Immunology, Immunotherapy 2010:1-9.

[19] Mocan T, Iancu C. Effective colon cancer prophylaxis in mice using embryonic stem cells and carbon nanotubes. International Journal of Nanomedicine 2011;6:1945.

[20] Mahmood M, Casciano DA, Mocan T, Iancu C, Xu Y, Mocan L, et al. Cytotoxicity and biological effects of functional nanomaterials delivered to various cell lines. Journal of Applied Toxicology 2010;30(1):74-83.

[21] Mocan T, Clichici S, Agoşton-Coldea L, Mocan L, Şimon Ş, Ilie IR, et al. Implications of oxidative stress mechanisms in toxicity of nanoparticles (review). Acta Physiol Hung2010;97(3):247-255.

[22] Mocan T, Clichici S, Biris AR, Simon S, Catoi C, Tabaran F, et al. Dynamic effects over plasma redox ballance following subcutaneous injection of single walled carbon nanotubes functionalized with single strand DNA. Dig J Nanomat Bios 2011;6(3):1207-1214.

[23] Iancu C, Mocan L, Bele C, Orza AI, Tabaran FA, Catoi C, et al. Enhanced laser thermal ablation for the in vitro treatment of liver cancer by specific delivery of multiwalled carbon nanotubes functionalized with human serum albumin. International Journal of Nanomedicine 2011;6:129.

[24] Mocan L, Tabaran F, Mocan T, Bele C, Orza A, Lucan C, et al. Selective ex-vivo photothermal ablation of human pancreatic cancer with albumin functionalized multiwalled carbon nanotubes. International Journal of Nanomedicine 2011 28 April 2011;6(1):915-928.

[25] Mocan T, Clichici S, Biris A, Simon S, Catoi C, Tabaran F, Et Al. Dynamic Effects Over Plasma Redox Ballance Following Subcutaneous Injection Of Single Walled Carbon Nanotubes Functionalized With Single Strand DNA.

[26] Zuzana M, Alessandra R, Lise F, Maria D. Safety Assessment of Nanoparticles Cytotoxicity and Genotoxicity of Metal Nanoparticles In Vitro. Journal of Biomedical Nanotechnology 2011;7(1):20-21.

[27] AshaRani P, Low Kah Mun G, Hande MP, Valiyaveettil S. Cytotoxicity and genotoxicity of silver nanoparticles in human cells. ACS nano 2008;3(2):279-290.

[28] Taylor-Papadimitriou J, Burchell J, Miles D, Dalziel M. MUC1 and cancer. Biochimica et Biophysica Acta (BBA)-Molecular Basis of Disease 1999; 1455(2-3):301-313.

[29] Brossart P, Schneider A, Dill P, Schammann T, Grünebach F, Wirths S, et al. The epithelial tumor antigen MUC1 is expressed in hematological malignancies and is recognized by MUC1- specific cytotoxic T-lymphocytes. Cancer Res 2001;61(18):6846.

[30] Noto H, Takahashi T, Makiguchi Y, Hayashi T, Hinoda Y, Imai K. Cytotoxic T lymphocytes derived from bone marrow mononuclear cells of multiple myeloma patients recognize an underglycosylated form of MUC1 mucin. Int Immunol 1997;9(5):791.

[31] Mukherjee P, Ginardi AR, Tinder TL, Sterner CJ, Gendler SJ. MUCl-specific cytotoxic T lymphocytes eradicate tumors when adoptively transferred in vivo. Cancer Res 2001;7(3 Supplement):848s.

Chapter 4

Techniques Used for Cytotoxicity Evaluation of Nanoparticles

Meda Cosma, Diana Gonciar

Gastroenterology Institute; Department of Nanomedicine, "Iuliu Hatieganu" University of Medicine and Pharmacy 19-21 Croitorilor Street, Cluj-Napoca, Romania

Introduction

There have been many comprehensive studies on the use of nanoparticles in biomedical applications over the past decade. Some of these include drug and gene delivery, diagnosis and treatment of cancer and biosensors. The use of nanoparticles helps improve the delivery of anticancer drugs to cancer cells. One of the underlying problems of anticancer drugs is the narrow therapeutic index, accompanied by severe cumulative and acute toxicities in healthy tissues. (1-5) There are also nanoparticles which are used in preclinical and in vitro studies in order to enhance the delivery of cytotoxic chemotherapeutic agents to cancer cells and to decrease toxicity by restricting drug exposure to healthy tissues. For a better management of chemotherapy-induced cytotoxicity in cancers (lung, colon, squamous, pancreas), hydroxycamptothecin, 5-fluorouracil, docetaxel and gemcitabine encapsulated nanoparticles have been used in preclinical studies. (1)

Besides their therapeutic use, nanoparticles might improve cancer detection and diagnosis. Magnetic iron oxide nanoparticles have proved to improve the performance of magnetic resonance imaging (MRI) in diagnosing cancers, as compared to the current cancer imaging contrast agents. (1, 6-9) Protein-targeted antibody-conjugated magnetic iron oxide nanoparticles expressed on the surface of human cancer cells may further improve the accuracy of MRI for the early detection of cancer. Models of fluorine-18-deoxyglucose encapsulated carbon and polymeric nanoparticles have been examined in preclinical studies in order to increase tumor diagnosis and detection rates using positron emission tomography. (10-12) Carbon nanotubes have been used for protein and gene delivery via non-specific endocytosis in cancer cells. (13-19) As other cytotoxic chemotherapy agents, gold and other metal nanoparticles have proved to increase the therapeutic efficacy of external beam therapy in preclinical models. There will be further studies on the use of nanoparticles as vectors for the delivery of biological and pharmacological agents. (20-28)

Besides their use in the delivery of cytotoxic and biological agents, nanoparticles may also be used as anticancer therapeutics. Gold nanoparticles with a diameter of 5–10 nm have innate antiangiogenic properties. These gold nanoparticles bind to pro-angiogenic heparin- binding growth factors, such as VEGF165 and bFGF, and inhibit their activity. In a preclinical model of ovarian cancer, gold nanoparticles demonstrated to reduce ascites, inhibit the Proliferation of multiple myeloma cells and induce apoptosis in *B-cell chronic* lymphocytic *leukemia*. (29)

Semiconductor quantum dots surface modification, known for their emission of fluorescence when excited at the appropriate wavelength, is investigated for a better detection of lymph nodes and other sites of metastases during surgical procedures. Tumor-specific peptide or antibody-conjugated quantum dots may enhance tumor targeting and increase the diagnostic accuracy of this optical imaging technique. There are various studies on the potential of imaging techniques using selective targeted fluorescent nanoparticles to allow in vivo localization of cancer cells. There is hope that such imaging techniques will increase the accuracy of different types of diagnostic imaging modalities used for cancer detection and treatment. TNF-alpha- coated colloidal gold nanoparticles are used in early phase cancer clinical trials. (30) Preclinical studies showed that the delivery of tumor necrosis factor-alpha (TNF-α) to malignant tumors was improved by the use of the nanoparticle-based drug delivery system, preventing systemic toxicities that usually restrict the clinical utility of this biological agent. The conjugation of nanoparticles to targeting agents is also researched to deliver gene therapy payloads into cancer cells. (30)

Lastly, immunocomplexes of antibody-coated gold nanoparticles have proved to enhance the detection of certain serum tumor markers, such as carcinoembryonic antigen (CEA), carcinoma antigen 125 (CA125), and carbohydrate antigen 19-9 (CA19-9), more rapidly and more accurately than currently available techniques. There will definitely be extensive use of nanoparticles to enhance cancer detection. (31)

The development of nanoparticles for use in nanomedicine is also in progress and has grown significantly over the past years. The National Science Foundation (NSF) estimated that between 2010 and 2015, the market for pharmaceutical nanoproducts will be of approximately US$ 180 billion per year. (32) Moreover, nanoparticles are already largely dispersed in the air and in hundreds of nanoparticle-containing products on the market, including cosmetics, printer toners, varnishes, drugs and even food. However, there is little knowledge on the risks and toxicity of these nanomaterials. Because of the extensive use of nanoparticles in various fields, there is also a growing concern on their unexpected adverse effects, both academically and socially. Some studies have examined the toxicity of nanoparticles based on their shape, size, surface chemistry, chemical composition, surface activity and solubility. The use of nanoparticles in various fields has been recommended as a result of these initial toxicity studies. Still, it is necessary to rigorously evaluate their toxicity in order to legislate the safe use of all types of nanoparticles. Even if nanoparticles and their effects on the human body are of great scientific interest, there is no standardized procedure framework for the evaluation of their toxicity. (33-36)

Cytotoxicity

Cytotoxicity is the property of a chemical compound (food, cosmetics or pharmaceuticals) or mediator cell (cytotoxic T cell) to kill cells. (37)

Compared to necrosis and apoptosis, cytotoxicity does not indicate a distinct cell death mechanism. T cell-mediated cytotoxicity or natural killer cell-mediated cytotoxicity incorporate aspects of both necrosis and apoptosis.

There has been an exponential growth of apoptosis publications over the past years. About 30 new molecules have been discovered, all related to the initiation and regulation of apoptosis. Other 20 molecules, related to DNA signalling to DNA replication, transcription or repair, have been demonstrated to affect apoptosis regulation. (38)

Both necrosis and apoptosis can cause cell death. Moreover, certain chemical compounds and cells are toxic to cells and cause their death. (39)

Necrosis and Apoptosis

Necrosis (unprogrammed cell death) is the pathological process due to cell exposure to exposed to acute physical or chemical events.

Apoptosis (programmed cell death) is the physiological process resulting in the elimination of unwanted or useless cells during their development or other biochemical events. (40)

Some of the main morphological features are cell shrinkage, with violent bubbling and surface blebbing, resulting in cell separation into clusters of membrane-bound bodies.

Organelle structure is usually unharmed, but the nucleus shows chromatin condensation, initiated at sublamellar foci and often generating heavily heterochromatic regions.

Changes in cell surface molecules determine the instantaneous recognition and phagocytosis of apoptotic cells by their neighbours. Therefore, many cells can quickly disappear from tissues without much evidence provided by conventional microscopic samples. This process accounts for cell death, normal tissue homeostasis, endocrine atrophy, negative selection in immune system and considerable T-cell death. It is also responsible for extensive cell death after exposure to cytotoxic compounds, hypoxia or viral infection. It is an important factor in the kinetics of tumor cell growth and regression. (41)

Many effects of cancer therapeutic agents are displayed through initiation of apoptosis and carcinogenesis itself seems to depend on selective, critical failure of apoptosis that allows cell survival after DNA damage and mutagenesis.

Caspase gene CED3 is the prototype of the family of cysteine proteases necessary for mammalian apoptosis, known for their predilection for cutting adjacent to aspartate residues. Mammalian caspases appear as autocatalytic cascades and some members (caspase 8 or FLICE) are "apical" and more susceptible for endogenous regulatory protein changes, while others (caspase 3 – also known as CPP32, Yama and apopain) achieve final death. Studies on caspase substrates give details on how cells destroy their structure and function. (42)

Examples of such substrates include cytoskeletal proteins - actin and fodrin and the nuclear lamins, but also a multitude of regulatory and chaperone-like proteins with cleavage and functional alteration. A good example is *ICAD* (inhibitor of caspase-activated deoxyribonuclease), the nuclease chaperone, whose cleavage allows distinctive apoptotic nuclease, responsible for chromatin cleavage into oligonucleosomal fragments. (43)

Caspases seem to appear as inactive proenzymes in most if not all cells, undergoing activation by cleavage.

Granzyme B is a protease delivered to T cell-target cells which triggers these latent proenzymes and constitues one of the killing mechanisms of cytotoxic T cells. (44)

There are endogenous triggers as well, such as C. elegans CED4 and its protein homologue, of mitochondrial origin, possibly initiating apoptosis in mammalian cells, inhibiting the cellular energy metabolism, causing critical cell injury and affecting mitochondrial respiration. Thus,

CED4 may interact with agents associated with mitochondrial injury, such as calcium and reactive oxygen species, and initiate apoptosis. (45)

Another mitochondrial protein of great significance in initiating apoptosis is the *mammalian CED-9 homologue* BCL-2. BCL-2 has the tertiary structure typical for a bacterial pore-forming protein, targeted to the mitochondrial outer membrane. It abrogates apoptosis, probably by binding CED4 and the Bcl-2–associated X *protein* (BAX) and forming heterodimers. Like CED4, this is another killer protein. BCL2 and BAX have structurally and functionally similar homologues and are also inserted into the outer nuclear membrane (ONM) and the endoplasmic reticulum (ER). (46)

There are other examples of death receptor signal transducers.

P53 is a tumor suppressive protein activated by DNA damage which triggers apoptosis. This can occur by transcriptional activation of BAX. (47)

Ceramide, found in cell membrane, can lead to the activation of acid sphingomyelinase in the cell, signaling plasma membrane damage. (48)

Tumor necrosis factor receptors (fas/apo-1/CD95, TNF receptor I) mediate the activation of caspase. (49)

When these receptors bind to a ligand, they receive a death stimulus and initiate a series of protein-protein interactions, forming the death inducing signalling complex (DISC) that recruits and activates caspases.

These mechanisms connecting cell injury to apoptosis are determined by the activation of preformed proteins. Transcriptional mechanisms can also initiate apoptosis, but not much is known about them.

A good example is cell killing is that induced by the Drosophila gene reaper, transcriptionally activated two hours before injury-induced death in the organism. Apoptosis in Drosophila can occur without reaper transactivation, but with increased stimuli, showing the existance of a *threshold* for *reaper*-induced apoptosis. (50)

Another death initiating gene is the immediate-early gene, c-myc. Transcriptional activation of c- myc induces DNA synthesis and, when lacking concurrent cytokine support, c-myc activation initiates apoptosis. This can be seen as a threshold regulatory mechanism, as c-myc expression increases the need for insulin-like growth *factor* 1, *required for survival*. (51)

Studies on cell transformation by viruses prove the significance of these apoptosis pathways. These strong survivors have found many ways of escaping cell death. Therefore, papovavirus SV40, adenovirus type 12, Human Papilloma Virus type 16 and Epstein-Barr Virus, all express proteins that inactivate apoptosis by p53 inactivation or BAX binding. (52) Lytic viruses also possess death postponing mechanisms, such as the cowpox virus serpin crmA and the baculovirus p35 caspase inhibitors. (53)

Differences Between Necrosis and Apoptosis

Necrosis and apoptosis are different in terms of morphology and biochemistry. (54) Necrosis is induced by cell exposure to extreme physiological factors (hypothermia, hypoxia) which may result in plasma membrane damage. Under physiological conditions, direct plasma membrane damage is induced by high doses of nanoparticles. Necrosis brings along some major morphological changes, such as cell swelling, cytoplasmic vacuoles, distended endoplasmic reticulum, cytoplasmic blebbing, condensed, swollen or ruptured mitochondria, ribosome disaggregation and detachment, organelle disruption, swollen and ruptured lysosomes, and finally cell membrane disruption. (55) There is no inflammatory reaction as apoptotic cells do not deliver their chemical constituents into the surrounding interstitial tissue and rapidly undergo phagocytosis by macrophages or adjacent healthy cells. (56) Necrosis is determined by cell exposure to severe deviation from physiological conditions, resulting in plasma membrane damage. It is characterized by cell swelling and organelle disruption, with little initial change in chromatin. Due to final plasma membrane rupture, cytoplasmic contents including lysosomal enzymes are delivered into the extracellular fluid. Thus, there is a correlation between in vivo necrotic cell death and extensive tissue damage, determining a strong inflammatory response. (57)

On the other side, apoptosis occurs under normal physiological conditions, the cell being an active participant in its own programmed death. It mostly appears during normal cell turnover and tissue homeostasis, embryogenesis, induction and maintenance of immune tolerance, development of the nervous system and endocrine atrophy. (58) There are typical morphological and biochemical features of cells undergoing apoptosis. Morphological changes occuring during apoptosis have been observed by light and electron microscopy. Cell shrinkage and pyknosis can be identified by light microscopy in the early phases of apoptosis. (59) Cell shrinkage is represented by smaller cells, dense cytoplasm and tightly packed organelles. Pyknosis results from chromatin condensation, which is the most typical characteristic of apoptosis. Histologic examination of samples stained with hematoxylin and eosin shows that apoptosis involves both individual cells and small cell clusters. The image of the apoptotic cell is that of a dark round or oval eosinophilic mass with dense purple fragments of nuclear chromatin. (57) Subcellular changes can better be identifed by electron microscopy. In the early phase of chromatin condensation, the electron and nuclear dense material tipically accumulates peripherally under the nuclear membrane, with possible nuclei of uniform density. Macrophages or adjacent epithelial cells quickly recognise and phagocytose these apoptotic bodies in vivo. This efficient mechanism of in vivo removal of apoptotic cells does not evoke any inflammatory response. Apoptotic bodies and remaining cell fragments ultimately swell and lyse in vitro. This final phase of in vitro cell death is called secondary necrosis or apoptotic necrosis. Apoptosis can be initiated by both transcriptional and non-transcriptional pathways which have similar effector mechanisms mediated by caspases and regulated by BCL2 family members. Low doses determine a variety of harmful stimuli. Nanoparticles, heat, radiation, hypoxia and cytotoxic anticancer drugs can initiate apoptosis but can also induce serious necrosis. (59-64) The coordinated energy-dependent process of apoptosis implies the activation of caspases, a family of cysteine proteases, together with a series of events that correlate initial stimuli with final cell death.

Cell Proliferation Assay MTT Assay

Introduction

Cell viability and proliferation assays are the ground for many in vitro studies on the response of cell populations to external factors. Cell growth determination is conventionally accomplished by counting viable cells after vital dye staining. There have been different approaches. Trypan blue staining is a simple method of assessing cell membrane integrity (estimating cell proliferation or cell death) but it is not sensitive and cannot be adapted for high-throughput screening (HTS). A radioactive uptake assay, such as *thymidine incorporation assay*, is accurate but also time-consuming and requires handling of radioactive substances. (65) The reduction of tetrazolium salts is a widely accepted procedure for measuring cell proliferation. (66) Yellow tetrazolium MTT (3-(4, 5-dimethylthiazolyl-2)-2,5-diphenyltetrazolium bromide), a well-known tetrazole, is reduced to purple formazan in living cell mitochondria. The absorbance of this colored solution can be assessed by spectrophotometry (between 500 and 600 nm wavelength). The absorption maximum depends on the solvent employed. This reduction only occurs when mitochondrial reductase enzymes are active, being directly related to the number of viable (living) cells. When the amount of purple formazan produced by treated cells is compared with that produced by untreated cells, the effectiveness of the death-inducing agent can be understood by creating a dose-response curve. MTT solutions absorbed in tissue culture media or balanced salt solutions without phenol red, had a yellowish color. Mitochondrial dehydrogenases of viable cells are converted to purple MTT formazan crystals by cleavage of the tetrazolium ring, insoluble in aqueous solutions. The crystals can be solubilized in acidified isopropanol. The resulting purple solution is spectrophotometrically measured. An increase in cell number leads to an increase in the amount of MTT-formazan formed and in absorbance. (67)

The MTT assay measures the cell proliferation rate and the reduction of cell viability when metabolic events induce apoptosis or necrosis. There small number of phases in this assay facilitates sample processing. The MTT reagent used yield low background absorbance.

The correlation between cell number and produced signal is assessed for each type of cell, thus allowing an accurate evaluation of changes in cell proliferation rate. (66)

Protease Activity Assays

Caspase activation is a unique characteristic of early stage apoptosis. Members of the ICE/CED-3 family of aspartate-*specific cysteine proteases* are important intermediaries of the complex biochemical events accompanying apoptosis. Caspase cleavage sites are marked by three to four amino acids followed by an aspartate residue. Caspases are normally synthesized as inactive precursors (procaspases). Caspases are activated by ihibitor release or cofactor binding through cleavage at internal aspartate residues determined by either autocatalysis or the action of another protease. There is a wide selection of fluorogenic caspase substrates to choose from. (68)

Caspase-3 (CPP32/apopain) plays a dominant role in the apoptosis pathway, amplifying the signal from initiator caspases (such as caspase-8) and showing full commitment to cell disaggregation. Besides cleaving other caspases in the cascade, caspase-3 has proven to cleave other proteins, such as poly (ADP-ribose) polymerase (PARP), DNA-dependent protein kinase, protein kinase Cδ and actin. (69)

CellEvent Caspase-3/7 Green detection reagent (C10423) is a new generation of caspase substrates, very useful for the study of apoptosis. The cell-permeant CellEvent reagent consists of the four–amino acid peptide DEVD (containing the recognition site for caspases 3 and 7) conjugated to a nucleic acid–binding dye. As DEVD inhibits the ability of the dye to bind to DNA, CellEvent Caspase-3/7 Green detection reagent is basically nonfluorescent. In the presence of activated caspase 3/7, the dye is cleaved from the DEVD peptide and binds DNA, producing a bright green-fluorescent signal (absorption/emission maxima ~502/530 nm) suggesting apoptosis. This powerful assay is highly specific for caspase 3/7 activation and it detects an almost total inhibition of the CellEvent Caspase-3/7 Green detection reagent signal in the cells pretreated with a caspase 3/7 inhibitor. (70)

Assays based on CellEvent Caspase-3/7 Green Apoptotic Detection Reagents can be accomplished easily. Cells are incubated with the CellEvent reagent in complete culture medium for 30 minutes and then evaluated using fluorescence microscopy (high-content screening). While apoptotic cells showing activation of caspase 3/7 exhibit bright green-fluorescent nuclei, cells without activation of caspase 3/7 exhibit minimal fluorescence. Cleaved reagents identifiy caspase 3/7–positive cell nuclei and thus, the stain can supply data on nuclear morphology, including condensed nuclei typical of late-stage apoptosis.

One of the main benefits of assays based on CellEvent caspase-3/7 green detection reagent is that there is no need for washing, which results in the protection of sensitive apoptotic cells that are typically lost during these rinses. Apoptotic cell loss during washing can generate the underestimation of the extent of apoptosis in the sample, resulting in poor assay accuracy. Moreover, formaldehyde fixation and detergent permeabilization do not harm the fluorescent signal resulting from the cleavage of CellEvent Caspase-3/7 detection reagent, giving flexibility for conducting endpoint assays and investigating other proteins using immunocytochemical methods.

One of the first methods employing flow cytometry was cell cycle analysis by quantitation of DNA content. Various DNA binding dyes can be used to stain the DNA of mammalian, yeast, plant or bacterial cells. These dyes are stoichiometric meaning that they bind according to the amount of DNA present in the cell. Thus, cells in S phase will have more DNA than cells in G1 phase. They will take up equivalently more dye and will be of brighter fluorescence until they have doubled their DNA content. The cells in G2 phase will be approximately twice as bright as cells in G1 phase. Apoptosis is a classical form of programmed cell death in eukaryotes, of great importance during embryogenesis, in the homeostatic control of tissue integrity, tumor regression and immune response development. When receiving specific signals, several distinctive biochemical and morphological changes take place inside the cell. A family of proteins known as caspases, and perhaps other proteases, are activated in the early stages of apoptosis. These proteins divide key cellular substrates that are required for normal cellular function, including structural proteins in the cytoskeleton and nuclear proteins. Caspases can also activate other degrading enzymes such as DNases, which begin to cause DNA fragmentation at the linker regions between oligonucleosomes. These biochemical events result in morphological changes inside the cell and extensive DNA fragmentation. The products of DNA fragmentation are nucleosomal and oligonucleosomal DNA fragments (180 bp and multiples of 180 bp), generating a characteristic ‘‘ladder’’ pattern during agarose gel electrophoresis. Due to the partially damaged DNA from apoptotic cells, the fraction of low-molecular-weight DNA can be extracted, whereas the non-damaged DNA remains in the cell nucleus. Because DNA fragments are lost from apoptotic nuclei and nuclear DNA content can be easily measured by flow cytometry, after nucleic acid staining with specific fluorochromes, there are several methods to assess apoptotic nuclei from a quantitative point of view. When staining apoptotic cells with PI and analyzing them with a flow cytometer, they exhibit a broad hypodiploid (sub-G1) peak, which can easily be differentiated from the narrow peak of cells with normal (diploid) DNA content in the red fluorescence channels. This method has a few advantages. It provides (i) a rapid, reliable and reproducible estimation of apoptosis, (ii) a simultaneous analysis of cell-cycle parameters of surviving cells and (iii) when necessary, a simultaneous analysis of cell surface antigens recognized by fluorescein isothiocyanate- or Alexa 488-conjugated monoclonal antibodies and the extent of apoptosis. However, there are many types of apoptosis and the extensive DNA fragmentation and the loss of DNA fragments are not universal in apoptotic death. (71) Moreover, necrotic cells sometimes exhibit certain degrees of DNA fragmentation that might result in hypodiploid nuclei. (72) In addition, besides apoptotic cells, the 'sub-G1' peak can display nuclear fragments, clumps of chromosomes, micronuclei or nuclei with normal DNA content but different chromatin structure and diminished accessibility of fluorochrome to DNA (i.e., cells undergoing differentiation). In conclusion, the presence of a hypodiploid DNA peak is not an authentic proof of apoptotic death. In order to confirm apoptosis, use morphological (microscopic observation of apoptotic bodies), biochemical (DNA ladder in agarose gel) or specific demonstration of DNA breaks (terminal deoxynucleotidyl transferase assay) before the quantitative analysis by flow cytometry. Another major issue in the quantitative assessment of apoptotic cells by flow cytometry is the differentiation between true apoptotic nuclei and nuclear debris. An appropiate determination of acquisition parameters (volume of particles, usually measured as forward scatter (FSC) and of diploid

DNA peak by using a calibration standard (DNA check beads), and negative and positive cell controls is essential before using the method for a cell line that has not been evaluated before. Keep in mind that apoptosis is a dynamic process and that there is a short ‘‘time-window’’ when apoptotic cells display their characteristic features. Therefore, different methods can produce different results according to the time of the apoptotic process. For example, in early phases of apoptosis, terminal deoxynucleotidyl transferase can be positive for DNA breaks and cell membrane can display Annexin-V positive phosphatidylserine. (73) However, morphological observation can be negative for apoptotic bodies and flow cytometric analysis can be negative for the sub-G1 peak, as DNA fragments are still maintained in the nucleus. Correspondingly, the DNA ladder cannot be detected by agarose gel electrophoresis. Still, when used properly, the propidium iodine (PI) flow cytometric assay is a rapid and easily reproducible method that can be adjusted for assessment of apoptosis in various cell types. (74)

Lysed mitotic cells, micronuclei and chromosome aggregates can be mistakenly recognized as apoptotic cells, especiallly when using hypotonic propodium iodine solution (quick method). A better exclusion of objects/events with minimal DNA content is obtained if using a linear rather than logarithmic scale in the PI emission histogram. (74) If cell debris still strongly influences the percentage of hypodiploid nuclei, evaluate the samples by fluorescence microscopy, and in case of extensive cell lysis, use an alternative method. Flow cytometric analysis that cannot indicate a hypodiploid peak despite the presence of apoptosis as demonstrated by other methods (morphological observation and/or Annexin-V positivity) can be related to absent or very low DNA loss from apoptotic nuclei because of the presence of large DNA fragments. In this situation, use a specific extraction procedure as shown above. (75)

References

[1] Biswas S, Dodwadkar NS, Deshpande PP, Torchilin VP. Liposomes loaded with paclitaxel and modified with novel triphenylphosphonium-PEG-PE conjugate possess low toxicity, target mitochondria and demonstrate enhanced antitumor effects in vitro and in vivo. J Controlled Release 2012;159(3):393-402.

[2] Chen N, He Y, Su Y, Li X, Huang Q, Wang H, et al. The cytotoxicity of cadmium-based quantum dots. Biomaterials 2012;33(5):1238-1244.

[3] Kim T, Kim M, Park H, Shin US, Gong M, Kim H. Size-dependent cellular toxicity of silver nanoparticles. Journal of Biomedical Materials Research Part A 2012;100(4):1033-1043.

[4] Jena P, Mohanty S, Mallick R, Jacob B, Sonawane A. Toxicity and antibacterial assessment of chitosancoated silver nanoparticles on human pathogens and macrophage cells. International journal of nanomedicine 2012;7:1805.

[5] Kumari M, Rajak S, Singh SP, Kumari SI, Kumar PU, Murty US, et al. Repeated oral dose toxicity of iron oxide nanoparticles: biochemical and histopathological alterations in different tissues of rats. Journal of Nanoscience and Nanotechnology 2012;12(3):2149-2159.

[6] Corot C, Warlin D. Superparamagnetic iron oxide nanoparticles for MRI: contrast media pharmaceutical company R&D perspective. Wiley Interdisciplinary Reviews: Nanomedicine and Nanobiotechnology 2013.

[7] Durmus NG, Taylor EN, Kummer KM, Webster TJ. Enhanced Efficacy of Superparamagnetic Iron Oxide Nanoparticles Against Antibiotic-Resistant Biofilms in the Presence of Metabolites. Adv Mater 2013;25(40):5706-5713.

[8] Kucheryavy P, He J, John VT, Maharjan P, Spinu L, Goloverda GZ, et al. Superparamagnetic Iron Oxide Nanoparticles with Variable Size and an Iron Oxidation State as Prospective Imaging Agents. Langmuir 2013;29(2):710-716.

[9] Yang H, Zhao F, Li Y, Xu M, Li L, Wu C, et al. VCAM-1-targeted core/shell nanoparticles for selective adhesion and delivery to endothelial cells with lipopolysaccharide-induced inflammation under shear flow and cellular magnetic resonance imaging in vitro. International journal of nanomedicine 2013;8:1897.

[10] Jingting C, Huining L, Yi Z. Preparation and characterization of magnetic nanoparticles containing Fe(3)O(4)-dextran-anti-beta-human chorionic gonadotropin, a new generation choriocarcinoma-specific gene vector. Int J

Nanomedicine 2011;6:285-294.

[11] Malhotra M, Lane C, Tomaro-Duchesneau C, Saha S, Prakash S. A novel method for synthesizing PEGylated chitosan nanoparticles: strategy, preparation, and in vitro analysis. Int J Nanomedicine 2011;6:485-494.

[12] Saltan N, Kutlu HM, Hur D, Iscan A, Say R. Interaction of cancer cells with magnetic nanoparticles modified by methacrylamido-folic acid. Int J Nanomedicine 2011;6:477-484.

[13] Lee P, Chiou Y, Wong J, Peng C, Shieh M. Targeting colorectal cancer cells with single- walled carbon nanotubes conjugated to anticancer agent SN-38 and EGFR antibody. Biomaterials 2013;34(34):8756-8765.

[14] Mulvey JJ, Villa CH, McDevitt MR, Escorcia FE, Casey E, Scheinberg DA. Self-assembly of carbon nanotubes and antibodies on tumours for targeted amplified delivery. Nature nanotechnology 2013;8(10):763-771.

[15] Niu L, Meng L, Lu Q. Folate-Conjugated PEG on Single Walled Carbon Nanotubes for Targeting Delivery of Doxorubicin to Cancer Cells. Macromolecular bioscience 2013;13(6):735- 744.

[16] Ilie I, Ilie R, Mocan T, Tabaran F, Iancu C, Mocan L. Nicotinamide-functionalized multiwalled carbon nanotubes increase insulin production in pancreatic beta cells via MIF pathway. International Journal of Nanomedicine 2013;8:3345-3353.

[17] Chou H, Wang T, Lee C, Tai N, Chang H. Photothermal effects of multi-walled carbon nanotubes on the viability of BT-474 cancer cells. Materials Science and Engineering: C 2013;33(2):989-995.

[18] Song M, Zeng L, Yuan S, Yin J, Wang H, Jiang G. Study of cytotoxic effects of single- walled carbon nanotubes functionalized with different chemical groups on human MCF7 cells. Chemosphere 2013;92(5):576-582.

[19] Iancu C, Mocan L, Bele C, Orza AI, Tabaran FA, Catoi C, et al. Enhanced laser thermal ablation for the in vitro treatment of liver cancer by specific delivery of multiwalled carbon nanotubes functionalized with human serum albumin. International Journal of Nanomedicine 2011;6:129.

[20] Eniola-Adefeso O, Heslinga MJ, Porter TM. Design of Nano Vectors for Therapy and Imaging of Cardiovascular Diseases. Methodist DeBakey cardiovascular journal 2012;8(1):13.

[21] Puvanakrishnan P, Park J, Chatterjee D, Krishnan S, Tunnell JW. In vivo tumor

targeting of gold nanoparticles: effect of particle type and dosing strategy. Int J Nanomedicine 2012;7:1251-1258.

[22] Shan Y, Luo T, Peng C, Sheng R, Cao A, Cao X, et al. Gene delivery using dendrimer- entrapped gold nanoparticles as nonviral vectors. Biomaterials 2012;33(10):3025-3035.

[23] Banerjee D, Harfouche R, Sengupta S. Nanotechnology-mediated targeting of tumor angiogenesis. Vasc Cell 2011 Jan 31;3(1):3.

[24] Chen XA, Zhang LJ, He ZJ, Wang WW, Xu B, Zhong Q, et al. Plasmid-encapsulated polyethylene glycol-grafted polyethylenimine nanoparticles for gene delivery into rat mesenchymal stem cells. Int J Nanomedicine 2011;6: 843-853.

[25] Ruan J, Shen J, Wang Z, Ji J, Song H, Wang K, et al. Efficient preparation and labeling of human induced pluripotent stem cells by nanotechnology. Int J Nanomedicine 2011;6:425-435.

[26] Ferrari M. Frontiers in cancer nanomedicine: directing mass transport through biological barriers. Trends Biotechnol 2010 Apr;28(4):181-188.

[27] Zhong Z, Wan Y, Han J, Shi S, Zhang Z, Sun X. Improvement of adenoviral vector- mediated gene transfer to airway epithelia by folate-modified anionic liposomes. Int J Nanomedicine 2011;6:1083-1093.

[28] Cheng Y, C. Samia A, Meyers JD, Panagopoulos I, Fei B, Burda C. Highly efficient drug delivery with gold nanoparticle vectors for in vivo photodynamic therapy of cancer. J Am Chem Soc 2008;130(32):10643-10647.

[29] Cherukuri P, Glazer ES, Curley SA. Targeted hyperthermia using metal nanoparticles. Adv Drug Deliv Rev 2010;62(3):339-345.

[30] Libutti SK, Paciotti GF, Byrnes AA, Alexander HR, Jr, Gannon WE, Walker M, et al. Phase I and pharmacokinetic studies of CYT-6091, a novel PEGylated colloidal gold-rhTNF nanomedicine. Clin Cancer Res 2010 Dec 15;16(24): 6139-6149.

[31] Tang D, Su B, Tang J, Ren J, Chen G. Nanoparticle-based sandwich electrochemical immunoassay for carbohydrate antigen 125 with signal enhancement using enzyme-coated nanometer-sized enzyme-doped silica beads. Anal Chem 2010;82(4):1527-1534.

[32] Roco MC. National nanotechnology initiative-past, present, future. Handbook on

nanoscience, engineering and technology 2007;2.

[33] AshaRani P, Low Kah Mun G, Hande MP, Valiyaveettil S. Cytotoxicity and genotoxicity of silver nanoparticles in human cells. ACS nano 2008;3(2):279-290.

[34] Chen C, Cheng YC, Yu CH, Chan SW, Cheung MK, Yu PHF. In vitro cytotoxicity, hemolysis assay, and biodegradation behavior of biodegradable poly (3-hydroxybutyrate)–poly (ethylene glycol)–poly (3-hydroxybutyrate) nanoparticles as potential drug carriers. Journal of Biomedical Materials Research Part A 2008;87(2):290-298.

[35] Dong L, Joseph KL, Witkowski CM, Craig MM. Cytotoxicity of single-walled carbon nanotubes suspended in various surfactants. Nanotechnology 2008;19:255702.

[36] Sayes CM, Wahi R, Kurian PA, Liu Y, West JL, Ausman KD, et al. Correlating nanoscale titania structure with toxicity: a cytotoxicity and inflammatory response study with human dermal fibroblasts and human lung epithelial cells. Toxicological sciences 2006;92(1):174.

[37] Messori L, Abbate F, Marcon G, Orioli P, Fontani M, Mini E, et al. Gold (III) complexes as potential antitumor agents: solution chemistry and cytotoxic properties of some selected gold (III) compounds. J Med Chem 2000;43(19): 3541-3548.

[38] Lawen A. Apoptosis—an introduction. Bioessays 2003;25(9):888-896.

[39] Bonfoco E, Krainc D, Ankarcrona M, Nicotera P, Lipton SA. Apoptosis and necrosis: two distinct events induced, respectively, by mild and intense insults with N-methyl-D-aspartate or nitric oxide/superoxide in cortical cell cultures. Proc Natl Acad Sci U S A 1995 Aug 1;92(16):7162-7166.

[40] Lemasters JJ, Nieminen A, Qian T, Trost LC, Elmore SP, Nishimura Y, et al. The mitochondrial permeability transition in cell death: a common mechanism in necrosis, apoptosis and autophagy. Biochimica et Biophysica Acta (BBA)-Bioenergetics 1998;1366(1):177-196.

[41] Al-Rubeai M, Singh R, Goldman M, Emery A. Death mechanisms of animal cells in conditions of intensive agitation. Biotechnol Bioeng 1995;45(6):463-472.

[42] Los M, Herr I, Friesen C, Fulda S, Schulze-Osthoff K, Debatin KM. Cross-resistance of CD95- and drug-induced apoptosis as a consequence of deficient activation of caspases (ICE/Ced-3 proteases). Blood 1997 Oct 15;90(8):3118-3129.

[43] Enari M, Sakahira H, Yokoyama H, Okawa K, Iwamatsu A, Nagata S. A caspase-activated DNase that degrades DNA during apoptosis, and its inhibitor ICAD. Nature 1998;391(6662):43- 50.

[44] Shi L, Kam CM, Powers JC, Aebersold R, Greenberg AH. Purification of three cytotoxic lymphocyte granule serine proteases that induce apoptosis through distinct substrate and target cell interactions. J Exp Med 1992 Dec 1;176(6):1521-1529.

[45] Spector MS, Desnoyers S, Hoeppner DJ, Hengartner MO. Interaction between the C. elegans cell-death regulators CED-9 and CED-4. 1997.

[46] Hengartner MO, Horvitz HR. C. elegans cell survival gene ced-9 encodes a functional homolog of the mammalian proto-oncogene bcl-2. Cell 1994;76(4): 665-676.

[47] Chipuk JE, Kuwana T, Bouchier-Hayes L, Droin NM, Newmeyer DD, Schuler M, et al. Direct activation of Bax by p53 mediates mitochondrial membrane permeabilization and apoptosis. Science 2004 Feb 13;303(5660):1010-1014.

[48] Ferri KF, Kroemer G. Organelle-specific initiation of cell death pathways. Nat Cell Biol 2001;3(11):E255-E263.

[49] Wallach D, Varfolomeev E, Malinin N, Goltsev YV, Kovalenko A, Boldin M. Tumor necrosis factor receptor and Fas signaling mechanisms. Annu Rev Immunol 1999;17(1):331-367.

[50] Gagic M. Identification and functional analysis of interaction partners of the apoptosis inhibitor DIAP1 in Drosophila 2005.

[51] Dominguez-Sola D, Ying CY, Grandori C, Ruggiero L, Chen B, Li M, et al. Non- transcriptional control of DNA replication by c-Myc. Nature 2007;448(7152): 445-451.

[52] Gori WC, Roost ME, Kmsev CM, MICHAEL SF. HIV-1 Vpr increases viral expression by manipulation of the cell cycle: a mechanism for selection of Vpr in vivo. 1998.

[53] Zhao J, Punj V, Matta H, Mazzacurati L, Schamus S, Yang Y, et al. K13 blocks KSHV lytic replication and deregulates vIL6 and hIL6 expression: a model of lytic replication induced clonal selection in viral oncogenesis. PLoS One 2007 Oct 24;2(10):e1067.

[54] Kroemer G, Galluzzi L, Vandenabeele P, Abrams J, Alnemri E, Baehrecke E, et al. Classification of cell death: recommendations of the Nomenclature Committee on

Cell Death 2009. Cell Death & Differentiation 2009;16(1):3-11.

[55] Dong Z, Saikumar P, Weinberg JM, Venkatachalam MA. Internucleosomal DNA cleavage triggered by plasma membrane damage during necrotic cell death. Involvement of serine but not cysteine proteases. Am J Pathol 1997 Nov;151(5):1205-1213.

[56] Ten VS, Pinsky DJ. Endothelial response to hypoxia: physiologic adaptation and pathologic dysfunction. Curr Opin Crit Care 2002 Jun;8(3):242-250.

[57] Kanduc D, Mittelman A, Serpico R, Sinigaglia E, Sinha AA, Natale C, et al. Cell death: apoptosis versus necrosis (review). Int J Oncol 2002;21(1):165-170.

[58] Cotter TG, Lennon SV, Glynn JG, Martin SJ. Cell death via apoptosis and its relationship to growth, development and differentiation of both tumour and normal cells. Anticancer Res 1990 Sep-Oct;10(5A):1153-1159.

[59] Kannan K, Jain SK. Oxidative stress and apoptosis. Pathophysiology 2000;7(3):153-163. (60)

[60] Colognato R, Bonelli A, Ponti J, Farina M, Bergamaschi E, Sabbioni E, et al. Comparative genotoxicity of cobalt nanoparticles and ions on human peripheral leukocytes in vitro. Mutagenesis 2008;23(5):377-382.

[61] AshaRani P, Low Kah Mun G, Hande MP, Valiyaveettil S. Cytotoxicity and genotoxicity of silver nanoparticles in human cells. ACS nano 2008;3(2):279-290.

[62] Sharma HS, Ali SF, Hussain SM, Schlager JJ, Sharma A. Influence of engineered nanoparticles from metals on the blood-brain barrier permeability, cerebral blood flow, brain edema and neurotoxicity. An experimental study in the rat and mice using biochemical and morphological approaches. Journal of nanoscience and nanotechnology 2009;9(8):5055-5072.

[63] Pokharkar V, Dhar S, Bhumkar D, Mali V, Bodhankar S, Prasad B. Acute and subacute toxicity studies of chitosan reduced gold nanoparticles: a novel carrier for therapeutic agents. Journal of Biomedical Nanotechnology 2009;5(3):233-239.

[64] Nair S, Sasidharan A, Rani VD, Menon D, Nair S, Manzoor K, et al. Role of size scale of ZnO nanoparticles and microparticles on toxicity toward bacteria and osteoblast cancer cells. J Mater Sci Mater Med 2009;20(1):235-241.

[65] Griffiths M, Sundaram H. Drug design and testing: profiling of antiproliferative agents for cancer therapy using a cell-based methyl-[3H]-thymidine incorporation assay. Cancer Cell Culture: Springer; 2011. p. 451-465.

[66] Stockert JC, Blázquez-Castro A, Cañete M, Horobin RW, Villanueva Á. MTT assay for cell viability: Intracellular localization of the formazan product is in lipid droplets. Acta Histochem 2012;114(8):785-796.

[67] Abid NBS, Rouis Z, Nefzi F, Souelah N, Aouni M. Evaluation of dimethylthiazol diphenyl tetrazolium bromide and propidium iodide inclusion assays for the evaluation of cell viability by flow cytometry. 2012.

[68] Jolivel V, Arthaud S, Botia B, Portal C, Delest B, Clavé G, et al. Biochemical Characterization of a Caspase-3 Far-red Fluorescent Probe for Non-invasive Optical Imaging of Neuronal Apoptosis. Journal of Molecular Neuroscience 2014;54(3):451-462.

[69] Reed JC. Apoptosis-regulating proteins as targets for drug discovery. Trends Mol Med 2001;7(7):314-319.

[70] Huang T, Lee J, Chen J. Pardaxin, an antimicrobial peptide, triggers caspase-dependent and ROS-mediated apoptosis in HT-1080 cells. Marine drugs 2011;9(10):1995-2009.

[71] Gerschenson LE, Rotello RJ. Apoptosis: a different type of cell death. FASEB J 1992 Apr;6(7):2450-2455.

[72] Berghe TV, Grootjans S, Goossens V, Dondelinger Y, Krysko DV, Takahashi N, et al. Determination of apoptotic and necrotic cell death in vitro and in vivo. Methods 2013;61(2):117- 129.

[73] Barroso G, Morshedi M, Oehninger S. Analysis of DNA fragmentation, plasma membrane translocation of phosphatidylserine and oxidative stress in human spermatozoa. Hum Reprod 2000 Jun;15(6):1338-1344.

[74] Riccardi C, Nicoletti I. Analysis of apoptosis by propidium iodide staining and flow cytometry. Nature protocols 2006;1(3):1458-1461.

[75] Nicoletti I, Migliorati G, Pagliacci M, Grignani F, Riccardi C. A rapid and simple method for measuring thymocyte apoptosis by propidium iodide staining and flow cytometry. J Immunol Methods 1991;139(2):271-279.

Chapter 5

Spectroscopic Techniques Used in Nanomedicine

Diana Gonciar[1], Teodora Mocan[2], Lucia Agoston[3]

[1]Gastroenterology Institute, "Iuliu Hatieganu" University of Medicine and Pharmacy, 19-21 Croitorilor Street, Cluj-Napoca, Romania

[2]Department of Physiology, "Iuliu Hatieganu" University of Medicine and Pharmacy, 5-7 Clinicilor Street, Cluj-Napoca, Romania

[3]Department of Medical Sciences, Iuliu Hatieganu University of Medicine & Pharmacy, 2–4 Clinicilor, 400006, Cluj-Napoca, Romania

In this chapter we propose to report several optical spectroscopy techniques and their Nanomedicine applications (1). The overview of spectroscopy requires clear distinction between absorption and emission. When electromagnetic radiation is in contact with a sample, the photons are absorbed and the molecules of the atoms suffer a transition from the ground state to the excited state. The plot obtained from the absorbance values according to the wavelengths represents the absorbance spectrum. The transition from the excited state to the ground state implies energy emission, the basic principle in emission spectroscopy (2).

UV-Vis Spectroscopy

Due to the property of molecules or ions to absorb electromagnetic radiation in the UV and visible domain, 4 types of transition in the configuration of valence electrons may be evidenced. The most important transitions are $n \rightarrow \pi^*$ and $\pi \rightarrow \pi^*$ through the implication of functional groups. Chromophores are functional groups and bands which are able to induce the increase in absorption of a substance. Furthermore, transitions occurred in metal ions may lead to a visible color change, which is the principle of the qualitative detection. UV-vis spectroscopy may be also performed in quantitative manner, based on

Bouguer-Lambert-Beer law and on the parameters of attenuation of incident radiation- transmittance and absorbance, directly dependent on the concentration of the analyte (2, 3).

In order to obtain novel eco-friendly nanomaterials, Ahmad A et al used Rhodococcus sp., Actinomycetales order, which was cultured in specific medium. After the separation of the mycelial mass and a washing step, the biomaterial was resuspended in a HAuCl4 solution for 24 hours. UV/VIS spectra were performed before and after resuspention. Whilst the spectrum before immersion showed no evident absorption, the one obtained after contains a detached peak at around 540 nm. Considering that gold nanoparticles (GNPs) have a maximum absorption between 520 and 580 nm according to the literature (4), the result asserts the presence of GNPs aggregates. On a macroscopic scale, it was observed that the colour of the mixture changed in intense purple after AuCl4- ions were added, which indicates that Au ions were reduced. Moreover, the HAuCl4 solution is transparent. Taking together, it was emphasized that the formation of GNP take place within the cells. The observation is strengthen by the UV/VIS spectrum of the HAuCl4 solution after the bioreaction because the absorption at approximatively 540 nm was absent. The intracellular synthesis of GNP was demonstrated and the result was completed by another techniques to validate the precise localization of GNPs, which was founded to be on the cell wall and in the cytoplasmic membrane (5).

Previously, a similar approach was performed by Mukherjee P et al by culturing a fungus, Verticillium. The biomass was obtained and immersed in aqueous AgNO3 solution for 72 hours. UV-vis spectroscopy was performed before and after the reaction and it was suggested the presence of a silver nanoparticle (SNP) aggregate, taking into consideration the presence of the absorption peak around 450 nm and the known maximum absorption of SNP to be between 380 and 450 nm. The intracellular reduction of Ag^+ ions was suggested by the color conversion into brown and by the UV-vis spectrum performed before the completion of the reaction. It is of particular importance that the formation of silver sulfide nanoparticles was excluded by the characteristic aspect of the spectra. The novel SNPs and GNPs may be further used for different purposes, according to their electronical, optical, chemical and physical properties (6).

In order to develop an accessible and non-expensive diagnosis method for cancer, El- Sayed HI and co-workers designed GNPs coated with anti-EGFR antibody and the payload was added into HaCaT cells (nonmalignant cell line), respectively into HOC and HSC (malignant cell line) and compared to the uptake of colloidal gold in the same cell lines. Scattering images were performed based on the surface plasmon resonance (SPR) property of GNPs and absorption spectra were recorded. It was revealed that single GNPs form aggregates into cells, finding sustained by the bands observed around 700 nm. In comparison, no bands were observed in the absorption spectra of the conjugated nanoparticles. Moreover, the adroitness to perform specific binding was observed on malignant cancerous cells, due to the overexpression of EGFR molecules in cancerous cells. The binding process was increased by 6 and 7 folds when compared to nonmalignant cells. The results were straightened by the scattering imaging results. Because of the facility of the tools proposed, SPR spectroscopy and scattering imaging may be used in cancer diagnosis as fast and low-cost method (7).

Drug delivery systems are consisting of tremendous designs forms. GNPs polymers were conjugated with folate-PEG-thiol to deliver with high specificity doxorubicin by Banu H et al. UV-vis spectrum has been recorded before and after functionalization and the results were according to the visible change of colour in reddish brown. Before coating with folate-PEG-thiol a maximum peak was registered at around 540 nm. After the conjugation process, the increase in dimensions of the particles were suggested by rising the peak at 560 nm (8).

Several colorimetric methods have been developed, starting from the advantages offered by UV-vis spectroscopy: ELISA (enzyme linked immunosorbent assay) (9), MTT (3-(4,5- dimethylthiazol-2yl)-2,5-diphenyl tetrazolium bromide) assay (10).

Mosmann T provided a quantitative assay to evaluate cell survival. The method is based on the capacity of living mitochondria to form formazan compound from MTT. The formed purple compound has an absorption peak at 570 nm. (10) Several tetrazolium assays were developed, starting from the limitations observed in metabolizing the MTT by different cell types. 3-(4,5-dimethylthiazol-2-yl)-5-(3-carboxymethoxyphenyl)-2- (4- sulfophenyl)-2H-tetrazolium (MTS) was found to be well metabolized, especially by mouse 3T3 fibroblasts and human colon tumor cells, in the presence of PMS- phenazine methosulfate (11). XTT- 2,3-bis(2-methoxy-4-nitro-5-sulfophenyl)-5-[(phenylamino)carbonyl]-2H-tetrazolium hydroxide was also tested as an alternative to MTT with a well enhancement of cellular reduction of tetrazolium salts (12).

Tuzlakoglu K and co-workers developed a combined scaffold by mixing micro and nanofibers with a payload of human osteoblast-like osteosarcoma and rat bone marrow stromal cells. MTS assay was performed to evaluate cell viability after one and two weeks and it was observed a marked cell proliferation by increasing the growth rate. The authors concluded that the nano/micro scaffold promises to be an achievable material for bone tissue engineering (13). Nanoparticles designed by Anitha A et al based on chitosan (CS)- O-carboxymethyl CS and N,O-carboxymethil CS- were added on MCF-7 cells and MTT assay revealed no modification in cell growth rate, upholding the absence of cytotoxicity of the chitosan based nanoparticles (14). Nano-hydroxyapatite/chitosan scaffolds were seeded with preosteoblastic cells and MTT revealed significant increase in cell proliferation suggesting also a suitable strategy for bone loss management (Kong L et al (15)).

Despite the fact that tetrazolium salts assays are currently wide-used, several observations have been reported. It was revealed that superoxide anions (SOD) interfere with tetrazolium reduction and MTT or XTT assays may lead to a misinterpretation of cell toxicity. Moreover, nano-TiO_2 induce SOD formation and applying MTT/XTT assays to evaluate cell survival is, therefore, wildly inacurrate (16). In astrocytes and HeLa cells subjected to mesoporus silica nanoparticles (MSN) endocytosis, the stimulation of exocytosis of formazan was observed and it was correlated with the overestimation of MSN cytotoxicity (17). Thus, researchers should use another cell viability techniques, as ATP assay concept, currently wide used (18).

Enzyme linked immunosorbent assay has been reported by Perlmann P and Engvall E, as a quantitative method for determination of rabbit IgG (9). The method is based on the principle of antigen-antibody interactions and it is currently wide-used especially in diagnosis. The antigen or antibody is fixed on a solid plate and then is added the liquid- phase containing the particle needed to be quantified, which will specific bind to the antibody or antigen fixed. Then, another antibody is added to bind to the analyzed molecules with an enzyme, usually horseradish peroxidase (HRP). After adding the substrate for enzyme, it occurs a color reaction, readable by spectrophotometer.

The applications of ELISA in nanotechnology field is tremendous. Vast nanoparticles have been validated. IL-10, IL-12 and TNF-α were determined by ELISA after mice infected with Paracoccidioides brasiliensis were treated with nanoparticles loaded with Amphotericin B (19).

The induction of bone formation by silica nanoparticles with a fluorescent core-shell was emphasized by quantitation of carboxy-terminal telopeptide of type I collagen and osteocalcin, whilst creatinine, alanine aminotransferase and TNFα were determined as markers for organ function. It was revealed that the proposed nanoparticles enhance bone formation without inducting organ damages. (20)

In order to improve the results obtained by ELISA, Ambrosi A et al used GNP as potential carrier-agents for anti-CA15-3-HRP, which binds to CA15-3 plasmatic breast cancer marker. The nanoparticles were characterized by UV-vis and TEM. To prevent the formation of aggregates, UV-vis was performed to determine the optimal concentration of anti-CA15-3-HRP which may be bound to GNP. When the optimization was completed, the novel assay was compared to classic ELISA assay and it was observed that the presence of GNP significantly increase the sensitivity (21).

Raman spectroscopy implies light scattering with loss or gain of energy-inelastic scattering (Raman scattering) (22). It is a vibrational spectroscopy method and the spectrum obtained from the difference between the wavelength of the scattered and incident light is consisting of characteristic bands (23), which are usually complementary to IR spectroscopy bands. The most used technique is Stokes Raman, in which the transition from ground to excited state is followed by energy emission to a superior vibrational energy level than the initial point. The phenomenon is more likely to happen because at normal conditions molecules are usually in the ground state. In comparison, anti-Stokes Raman spectroscopy relies on the transition from a higher energy level to the ground state. (24)

Qian X et al employed a novel technique for spectroscopic detection using GNPs functionalized with ScFv B10, a specific antibody fragment for EGFR.

GNPs with and without PEG layer were analyzed by Raman spectra under different medium conditions: concentrated salts, strong acids and bases and different organic solvents and it was established that PEG-coated nanoparticles exhibit a higher stability. The nanocomposites were incubated with an EGFR positive and an EGFR negative cell lines (Tu686 and NCI- H550 respectively) and surface-enhanced Raman scattering (SERS) spectra have been recorded to emphasize the binding specificity. Strong SERS bands were observed when ScFv-conjugated particles were incubated with EGFR positive cells. In contrast, strong signals could not be emphasized when EGFR negative cells were incubated with the proposed nanosystem, suggesting that the binding process is based on specific affinity. In vivo testing was performed for mice inoculated with Tu686 cells and injected with conjugated or non-conjugated GNPs. Strong signals have been emphasized with a gradually accumulation of nanoparticles in the tumor, suggesting that ScFv-GNPs may be used as key agents for in vivo targeting and SERS analyses (25).

In order to improve tip-enhanced Raman spectroscopy (TERS), the Au tip is replaced by a GNPs layer. The nanoparticles employed were coated with silica or with alumina. Li JF et al established the aspects of their novel technique- shell-isolated nanoparticle-enhanced Raman spectroscopy (SHINERS)- which has a higher sensitivity. The method has been applied to emphasize the Pt-H signal, on Pt(111) when a strong band may be observed when silica/GNPs are used. The silica shell was replaced with an Al_2O_3 coat and no notable changes in the recorded spectra have been observed. SHINERS may be used successfully in semi-conductor industry, due to the capability to emphasize the Si-H band after the treatment with HF, and also is a potential technique to detect pesticide residues in situ. Another possible application may be the detection of cell wall proteins in situ because it was observed for yeast cells that the spectra recorded following by SHINERS technique are different from references Raman spectra, but are similar to those obtained from mannoproteins. As a conclusion, SHINERS may be an adequate technique to be world-wide used in a wide range of fields (26).

Cao YWC et al designed nanoparticles-based probes, labeled with Cy3 (Raman active dye), which are able to promote SERS for oligonucleotide targeting. Raman spectroscopy was founded to be an useful tool after elicit with Ag. Special chips were prepared with different DNA strands incorporated, the probe based on GNPs, oligonucleotides and Cy3 was added. Following the treatment with Ag, gray spots may be observed. Raman spectroscopy performed after Ag enhancement sustained the presence of Raman response, whilst no response was detected before Ag treatment. Cy3 dye was replaced from the nanoprobe with six other dyes and the detection method was performed for human immunodeficiency, hepatitis A and B, Ebola, variola viruses and Bacillus anthracis. The targets were mixed and were removed strategically to emphasize the selectivity of the method. The gray signals appeared were validated by Raman spectroscopy. RNA detection was also assessed and a semi-quantitative result was estimated. GNPs targeted with Raman active dye and specific oligonucleotide strain are veritable instruments in DNA or RNA detection, with advantages of great importance, such as the large variety of dyes, the wide range of probes and the possibility to obtain the ratio of specific intensity directly from the spectrum (27).

Starting from this, achievement, the team further investigated the possibility to develop protein probes. They designed two types of probes, with GNP core. The first probe designed, has an alkylthiol-capped oligoadenotides-biotin-Raman dye label, and it was used to assess screening of protein-small molecule interactions by using biotin, digoxigenin and dinitrophenyl as oligoadenotides. The chip was prepared containing specific antibodies. Following the enhancement with Ag, the gray spots were visible and were furher validated by Raman spectroscopy, indicating that the binding between probe and target took place. The experiment was performed also with only two probes to emphasize the selectivity. The second type of probe contains an antibody interposed between the GNP core and Raman dye and it was used to assess protein-protein interactions. The probes contained specific ubiquitin, mouse IgG and human protein C antibodies and the correspondent antigen was placed on slides. The experiment went further in the same manner as the first part, with the appearance of the gray spots and further confirmation via Raman spectroscopy. The method was founded to have a marked selectivity, it is also flexible, with no cross-reaction detected and it is also feasible as a protein detection technique. (28)

Schwartzberg AM et al developed GNP aggregates to be used as SERS substrate. The design of the surface is unique, due to the presence of sulfur species, confirmed by eletron energy loss spectroscopy. UV-vis was used to characterize the particles. The spectrum exhibited two bands, the transverse plasmon band and the extended plasmon band, whether the spherical, non-aggregated particles have an unique transverse band. The interactions between the particles was revealed by TEM images. Furthermore, Rh6G was founded to increase SERS activity by 107 times. SERS signals have been registered in the presence of GNP aggregates for various amino acids and also for adenine and uridine. Clear distinct peaks never reported before have been registered, probably due to the unique properties of aggregates surface, or due to the maintenance of the pH at a value of 3, which is characteristic for GNP aggregates. (29)

In order to develop an effective method for bioimaging, Yin D et al developed Ag and SiO_2- based nanoparticles, labeled with sialic acid (SA). The nanoparticles were characterized by UV-vis. To evaluate the capacity to differentiate normal from abnormal cells, normal liver cells (L-02) and human hepatocarcinoma cells (HepG2) were employed. After the nanoparticles were added, intense SERS signals may be evidenced in HepG2, whilst L-02 exhibited only weak signals. By incubation with non-labeled nanoparticles, no SERS signals may be evidenced. Glucose was also tested as an imprinting agent, but it was founded that it cannot differentiate normal from cancerous cells. Moreover, pre-blocking with glucose had no influence, whilst pre-blocking with SA led to the absence of response. By replacing SA with boronic acid, intense signals may be observed for both cell lines, suggesting the lack of selectivity. It may be concluded that the apparition of SERS signals, conditioned by specific binding, is related to the properties offered by SA. Furthermore, the method was performed for liver tissue, normal and abnormal. SA-targeted nanoparticles lead to intense SERS signals in damaged liver tissue. The results obtained from liver tissue are in well concordance with those obtained from cells experiments. Imprinted nanotags may represent key agents for improving bioimaging and cancer studies. (30)

Wan Xu et al proposed a design to incorporate lapatinib into human serum albumin nanoparticles as an effective agent in breast cancer with HER2 overexpression. The novel nanoparticles (LHNPs) have been characterized by Raman spectroscopy, which revealed that LHNPs lost the specific bands of lapatinib during incapsulation. The result is strengthen by XPS and XRS, leading to the conclusion that the incapsulation process took place conducting to a structure similar to human serum albumin. (31)

Fourier Transform Infrared Spectroscopy (FTIR) is also subjected to vibrational spectroscopy techniques, due to the excitation of oscillatory motions when the incident radiation has a frequency in the IR region (1-100 μm). The spectrum has nine bands: amide I-VII, A and B, which are characteristic for the repeated units of proteins and polypeptide. FTIR spectroscopy is useful to determine the protein secondary structure with the great advantage that the amount required of sample is small. It is also appropriate for the study of dynamics and stability. The mention that the bands are superposed at the edges implies that the interpretation of the specific spectra should be performed with caution (32).

Sarmento B et al proposed a delivery system for insulin, composed by alginate and chitosan (6:1), which was characterized by FTIR spectroscopy in order to assess chemical interactions. The spectra from chitosan, alginate and also from the alginate-chitosan complex has been reported, and revealed that an ionic interaction between carboxyl and amino groups of alginate and chitosan respectively occurred. The interactions recorded by adding the insulin payload were observed and it was concluded that are specific for protein entrapping (33).

FTIR has been used to evaluate silver NPs synthesis from papaya fruit extract. UV-vis spectra was registered to pursue the reduction process of Ag^{+}, also macroscopic visible. FTIR performed before and after the bioreaction occurrence revealed that the reduction is probably due to the oxidation of C-O groups of polyos because the corresponding bands completely disappeared by adding Ag^{+} ions and carbonyl bands were emphasized on the spectra (Jain D et al) (34).

Magnetite nanoparticles coated with PEG were used as a drug delivery system for methotrexate, which was immobilized on the surface of the NPs by an amine bond to improve the pharmacokinetics of the drug. FTIR was used to assert the success of the proposed structure. Moreover, UV-vis emphasized the cleavage process of the drug and the amount released. Considering the validation techniques performed, magnetite nanoparticles covered with PEG may be effectively used to improve methotrexate usage (35).

Several other nanoparticles and nanoscaffolds were characterized by FTIR:

collagen/nano-hydroxiapatite scaffolds (36), citric acid modified Fe_3O_4 and magnetic zeolitic imidazolate framework 8 (37), CdS QDs (38), $CoFe_2O_4$, $NiFe_2O_4$, $MnFe_2O_4$ (39).

Emission Spectroscopy

Photoluminescence and chemiluminescence are particular cases of emission. In first case, the emission appears after absorption and in the second case, the excited state is the result of a chemical reaction (2).

Photoluminescence spectroscopy

Both fluorescence and phosphorescence reunite photoluminescence spectroscopy field. In the first case, the energy emission is due to the transition in singlet excited state caused by photon absorption, in which the spin orientation of the excited electron is different from the ground electron. Phosphorescence appears as a consequence of energy emission from triplet excited state, in which the two spins have the same orientation. The spectra may be express in two different manners, emission and excitation spectra, according to the varied wavelength (2, 40).

Aslan K et al designed silver core nanoparticles with different silica shell thickness, which were bounded to various fluorophores- Rhodamine 800 (Rh800), Eu- [Tris (dibenzoylmethane) mono (5-amino phenanthroline) europium] (Eu-TDPA) and Alexa Fluor 647. Fluorescence spectra were realized and was compared to nanoparticles synthesized without the silver core. It was observed an increase by 8 fold and 20 fold in emission intensity for the nanoparticles labeled with Eu-TDPA and with Rh800 when compared to the control. Considering the decrease registered in the lifetime of the developed systems, it suggested the capacity of the nanocomposites to enhance particle sensing by 200 folds (41).

Fluorescence spectroscopy has been used for characterization of a variate types of nanoparticles. Due to the hydrophobicity exhibited, curcumin was encapsulated into polyester nanoparticles. UV-vis and fluorescence spectra were performed and suggested that curcumin is located inside the nanosystem (Leung MHM et al) (42). CdS quantum dots (QDs) were used to form a nanosystem with chitosan and with a tripeptide labeled with chitosan (arginine-glycine-aspartic acid). Photoluminescent proprieties were evaluated by fluorescence spectroscopy, which revealed green fluorescence at 405 nm (Mansur AAP et al) (43).

A novel strategy for the assay of organophosphorus (OPP) has been reported (Zhang R et al). It is based on the inner filter effect (IFE) of GNPs, which quenches MnZnS QDs phosphorescence and also on the inhibition effect of OPP on acetylcholinesterase. In the presence of OPP, the production of acetylthiocholine is decreased and GNPs form aggregates which stimulate the restauration of the phosphorescence. Phosphorescence spectra suggested that the increase of GNPs concentration produces the decrease of phosphorescence MnZnS QDs emission. Moreover, the lifetime of QDs showed no noticeable change when AuNPs were added, suggesting that the complex is not relayed on hydrogen bounding and electrostatic forces but is due to the IFE of GNPs. The experimental data sustained the theoretical principles, which may lead to the assertion that an assay of OPP which implies phosphorescence spectroscopy is feasible (44).

Chemiluminescence (CL) is another emission spectroscopy technique. The excited state is due to a chemical reaction, which may occur directly from two reagents and cofactors forming excited state compounds. Bioluminescence is the result of biological or enzymatic reactions. Another mechanism of CL generation is the transfer of energy from the excited compound to fluorophores (2, 45).

Lee D et al have reported a novel method for in vivo imaging of hydrogen peroxide. The technique involves nanoparticles with CL proprieties, made of peroxalate esters and fluorescent dyes. CL spectra was recorded from the peroxalate nanoparticles labeled with perylene, pentacene or rubrene in the presence of hydrogen peroxide. The spectra emphasized that the emission of light was recorded at a similar wavelength as the fluorescent emission of the dyes used. Moreover, the intensity of light exhibited a linear relation with the hydrogen peroxide concentration. The CL proprieties of the nanoparticles promises to be a key factor in in vivo imaging (46).

Due to the tremendous features of GNPS, CL have been studied by Cui H et al. GNPs react with KIO_4-NaOH-Na_2CO_3 and are able to elicit CL. The authors provided an insight into the correlation between the diameter of the nanoparticles and the CL intensity and it was observed that 68 nm GNP exhibited the strongest intensity. The spectra were also recorded and emphasized 3 different emission bands. The increase in CL intensity was observed by increasing the GNP concentration and by replacing the citrate ions of the surface with SCN-. Further research is needed to establish the implication of GNPs in bioimaging. (47)

X-ray fluorescence spectroscopy (XRF) provides a qualitative and also a quantitative method by using measurements focused on specific wavelength and intensity of fluorescent emission energy, as a result of X-ray electromagnetic radiation (48). Even if the method is not destructive, the preparation process requires structural alternation of the analyte. A variant of XRF is micro-XRF, which offers the advantage to probe samples with irregular shape, by focusing on a small part of the sample (49).

In order to enquire into the destructions methods of tumor cells directly in the blood flow, Hossain M et al employed iron oxide and bismuth nanoparticles, which were functionalized with FA. The binding process was confirmed by

FTIR. HeLa and MG-63 cells were purchased, having overexpression of FA receptors (FAR) and an insignificant level respectively. The authors designed an in vitro system to simulate the blood flow in organism, in which HeLa cells treated with nanoparticles were added. The tube was engineered with a magnet on the internal wall, which is able to capture conjugated HeLa cells and by exposing to X-ray radiation, to destroy them. The experiment was performed also by replacing the PBS inside the tube with human blood cells containing HeLa and MG-63. XRF was performed after X-ray exposure and emphasized the selectivity of the system to capture HeLa cells, suggesting that the binding process took part because of the interaction between FA and FAR. Moreover, the affinity for FA-bismuth nanoparticles to bind to HeLa cells was asserted by XRF. The system proposed may have a well applicability on destroying cancerous cells in the blood flow by using targeted X-ray radiation and functionalized nanoparticles. (50)

$CaCO_3$ (51), arsenic acid-presenting iron oxide (52), selenium (53), Ag/SiO_2 (54) nanoparticles have also been used for various achievements and XRF was used as a method of validation.

Future Perspectives

Magnetic resonance spectroscopy (MRS) is a wide-available technique, used as a noninvasively, repetitively and painlessly diagnostic method, complementary to magnetic resonance imaging. It may indicate the concentration of a wide range of metabolites: N- acetyl aspartate, ATP, choline, creatine, phosphocreatine, lactate, applications that have tremendous importance especially in brain disorders (55, 56). By placing a nucleus in an uniform magnetic radiofrequency field (usually 10-100 MHz), it tend to register alignment and rotation movements and it also exhibits a transition process (57).

The resonance signal is the spectral line recorded after energy absorption, conducting to the spectrum registration (58).

The reaction between arsoncacetic acid and dithiothreitol was evaluated by 1H-MRS (52).

However, current data indicate that the potential of MRS has not been enquired in nanomedicine as it is other domains. Functionalized nanoparticles may be further studied regarding their ability to overcome MRS limitations and to improve the specificity of the presented technique.

References

[1] Williams D, Fleming I, Pretsch E. Spectroscopic Methods. Organic Chemistry 1989(1989).

[2] Harvey D. Modern analytical chemistry; 2000.

[3] Perkampus H, Grinter H, Threlfall T. UV-VIS Spectroscopy and its Applications: Springer; 1992.

[4] Pelton M, Bryant GW. Introduction to metal-nanoparticle plasmonics. John Wiley Wiley & Sons; 2013.

[5] Ahmad A, Senapati S, Khan MI, Kumar R, Ramani R, Srinivas V, et al. Intracellular synthesis of gold nanoparticles by a novel alkalotolerant actinomycete, Rhodococcus species. Nanotechnology 2003;14(7):824.

[6] Mukherjee P, Ahmad A, Mandal D, Senapati S, Sainkar SR, Khan MI, et al. Fungus- mediated synthesis of silver nanoparticles and their immobilization in the mycelial matrix: a novel biological approach to nanoparticle synthesis. Nano Letters 2001;1(10):515-519.

[7] El-Sayed IH, Huang X, El-Sayed MA. Surface plasmon resonance scattering and absorption of anti-EGFR antibody conjugated gold nanoparticles in cancer diagnostics: applications in oral cancer. Nano Letters 2005;5(5):829-834.

[8] Banu H, Sethi DK, Edgar A, Sheriff A, Rayees N, Renuka N, et al. Doxorubicin loaded polymeric gold nanoparticles targeted to human folate receptor upon laser photothermal therapy potentiates chemotherapy in breast cancer cell lines. Journal of Photochemistry and Photobiology B: Biology 2015;149:116-128.

[9] Engvall E, Perlmann P. Enzyme-linked immunosorbent assay (ELISA) quantitative assay of immunoglobulin G. Immunochemistry 1971;8(9):871-874.

[10] Mosmann T. Rapid colorimetric assay for cellular growth and survival: application to proliferation and cytotoxicity assays. J Immunol Methods 1983;65(1):55-63.

[11] Cory AH, Owen TC, Barltrop JA, Cory JG. Use of an aqueous soluble tetrazolium/formazan assay for cell growth assays in culture. Cancer Commun 1991 Jul;3(7):207-212.

[12] Scudiero DA, Shoemaker RH, Paull KD, Monks A, Tierney S, Nofziger TH, et al. Evaluation of a soluble tetrazolium/formazan assay for cell growth and drug sensitivity in culture using human and other tumor cell lines. Cancer Res 1988 Sep 1;48(17):4827-4833.

[13] Tuzlakoglu K, Bolgen N, Salgado A, Gomes ME, Piskin E, Reis R. Nano-and micro- fiber combined scaffolds: a new architecture for bone tissue engineering. J Mater Sci Mater Med 2005;16(12):1099-1104.

[14] Anitha A, Rani VD, Krishna R, Sreeja V, Selvamurugan N, Nair S, et al. Synthesis, characterization, cytotoxicity and antibacterial studies of chitosan, O-carboxymethyl and N, O-carboxymethyl chitosan nanoparticles. Carbohydr Polym 2009;78(4):672-677.

[15] Kong L, Gao Y, Cao W, Gong Y, Zhao N, Zhang X. Preparation and characterization of nano-hydroxyapatite/chitosan composite scaffolds. Journal of Biomedical Materials Research Part A 2005;75(2):275-282.

[16] Wang S, Yu H, Wickliffe JK. Limitation of the MTT and XTT assays for measuring cell viability due to superoxide formation induced by nano-scale TiO 2. Toxicology in Vitro 2011;25(8):2147-2151.

[17] Fisichella M, Dabboue H, Bhattacharyya S, Saboungi M, Salvetat J, Hevor T, et al. Mesoporous silica nanoparticles enhance MTT formazan exocytosis in HeLa cells and astrocytes. Toxicology in vitro 2009;23(4):697-703.

[18] Riss TL, Moravec RA, Niles AL, Benink HA, Worzella TJ, Minor L, et al. Cell Viability Assays. In: Sittampalam GS, Coussens NP, Nelson H, Arkin M, Auld D, Austin C, et al, editors. Assay Guidance Manual Bethesda (MD); 2004.

[19] Souza A, Nascimento A, de Vasconcelos N, Jerônimo M, Siqueira I, R-Santos L, et al. Activity and in vivo tracking of Amphotericin B loaded PLGA nanoparticles. Eur J Med Chem 2015;95:267-276.

[20] Weitzmann MN, Ha S, Vikulina T, Roser-Page S, Lee J, Beck GR. Bioactive silica nanoparticles reverse age-associated bone loss in mice. Nanomedicine: Nanotechnology, Biology and Medicine 2015;11(4):959-967.

[21] Ambrosi A, Airo F, Merkoçi A. Enhanced gold nanoparticle based ELISA for a breast cancer biomarker. Anal Chem 2009;82(3):1151-1156.

[22] Long DA. Raman spectroscopy. New York 1977:1-12.

[23] Morris MD, Mandair GS. Raman assessment of bone quality. Clinical Orthopaedics and Related Research® 2011;469(8):2160-2169.

[24] Wartewig S. IR and Raman Spectroscopy: Fundamental Processing (Spectroscopic Techniques: An Interactive Course). 2003.

[25] Qian X, Peng X, Ansari DO, Yin-Goen Q, Chen GZ, Shin DM, et al. In vivo tumor targeting and spectroscopic detection with surface-enhanced Raman nanoparticle tags. Nat Biotechnol 2008;26(1):83-90.

[26] Li JF, Huang YF, Ding Y, Yang ZL, Li SB, Zhou XS, et al. Shell-isolated nanoparticle-enhanced Raman spectroscopy. Nature 2010;464(7287):392-395.

[27] Cao YC, Jin R, Mirkin CA. Nanoparticles with Raman spectroscopic fingerprints for DNA and RNA detection. Science 2002 Aug 30;297(5586):1536-1540.

[28] Cao YC, Jin R, Nam JM, Thaxton CS, Mirkin CA. Raman dye-labeled nanoparticle probes for proteins. J Am Chem Soc 2003;125(48):14676-14677.

[29] Schwartzberg AM, Grant CD, Wolcott A, Talley CE, Huser TR, Bogomolni R, et al. Unique gold nanoparticle aggregates as a highly active surface-enhanced Raman scattering substrate. The Journal of Physical Chemistry B 2004;108(50): 19191-19197.

[30] Yin D, Wang S, He Y, Liu J, Zhou M, Ouyang J, et al. Surface-enhanced Raman

scattering imaging of cancer cells and tissues via sialic acid-imprinted nanotags. Chemical Communications 2015.

[31] Wan X, Zheng X, Pang X, Zhang Z, Zhang Q. Incorporation of lapatinib into human serum albumin nanoparticles with enhanced anti-tumor effects in HER2-positive breast cancer. Colloids and Surfaces B: Biointerfaces 2015;136:817-827.

[32] Kong J, Yu S. Fourier transform infrared spectroscopic analysis of protein secondary structures. Acta Biochim Biophys Sin (Shanghai) 2007 Aug;39(8): 549-559.

[33] Sarmento B, Ferreira D, Veiga F, Ribeiro A. Characterization of insulin-loaded alginate nanoparticles produced by ionotropic pre-gelation through DSC and FTIR studies. Carbohydr Polym 2006;66(1):1-7.

[34] Jain D, Daima HK, Kachhwaha S, Kothari S. Synthesis of plant-mediated silver nanoparticles using papaya fruit extract and evaluation of their anti microbial activities. Digest journal of nanomaterials and biostructures 2009;4(3):557-563.

[35] Kohler N, Sun C, Fichtenholtz A, Gunn J, Fang C, Zhang M. Methotrexate-Immobilized Poly (ethylene glycol) Magnetic Nanoparticles for MR Imaging and Drug Delivery. Small 2006;2(6):785-792.

[36] Cao S, Li H, Li K, Lu J, Zhang L. In-vitro mineralization of MC3T3-E1 osteoblast-like cells on collagen/nano-hydroxyapatite scaffolds coated carbon/carbon composites. Journal of Biomedical Materials Research Part A 2015.

[37] Hou C, Wang Y, Ding Q, Jiang L, Li M, Zhu W, et al. Facile synthesis of enzyme-embedded magnetic metal–organic frameworks as a reusable mimic multi-enzyme system: mimetic peroxidase properties and colorimetric sensor. Nanoscale 2015.

[38] Yao J, Yang M, Liu Y, Duan Y. Fluorescent CdS Quantum Dots: Synthesis, Characterization, Mechanism and Interaction with Gold Nanoparticles. Journal of Nanoscience and Nanotechnology 2015;15(5):3720-3727.

[39] Nooris M, Aparna D, Radha S. Synthesis and characterization of MFe_2O_4 (M= Co, Ni, Mn) magnetic nanoparticles for modulation of angiogenesis in chick chorioallantoic membrane (CAM). European Biophysics Journal 2015:1-10.

[40] Lakowicz JR. Principles of fluorescence spectroscopy: Springer Science &

Business Media; 2013.

[41] Aslan K, Wu M, Lakowicz JR, Geddes CD. Fluorescent core-shell Ag@ SiO_2 nanocomposites for metal-enhanced fluorescence and single nanoparticle sensing platforms. J Am Chem Soc 2007;129(6):1524-1525.

[42] Leung MH, Harada T, Dai S, Kee TW. Nanoprecipitation and Spectroscopic Characterization of Curcumin-Encapsulated Polyester Nanoparticles. Langmuir 2015.

[43] Mansur AA, de Carvalho SM, Mansur HS. Bioengineered Quantum Dot/Chitosan-Tripeptide Nanoconjugates for Targeting the Receptors of Cancer Cells. Int J Biol Macromol 2015.

[44] Zhang R, Li N, Sun J, Gao F. A Colorimetric and Phosphorimetric Dual-Signaling Strategy Mediated by Inner Filter Effect for Highly Sensitive Assay of Organophosphorus Pesticides. J Agric Food Chem 2015.

[45] Garcia-Campana AM. Chemiluminescence in analytical chemistry: CRC Press; 2001.

[46] Lee D, Khaja S, Velasquez-Castano JC, Dasari M, Sun C, Petros J, et al. In vivo imaging of hydrogen peroxide with chemiluminescent nanoparticles. Nature materials 2007;6(10):765-769.

[47] Cui H, Zhang Z, Shi M. Chemiluminescent reactions induced by gold nanoparticles. The Journal of Physical Chemistry B 2005;109(8):3099-3103.

[48] Jenkins R. Quantitative X-ray spectrometry. : CRC Press; 1995.

[49] Haschke M. Laboratory Micro-X-Ray Fluorescence Spectroscopy. Laboratory Micro-X-Ray Fluorescence Spectroscopy: Instrumentation and Applications, Springer Series in Surface Sciences, Volume 55. ISBN 978-3-319-04863-5. Springer International Publishing Switzerland, 2014;1.

[50] Hossain M, Luo Y, Sun Z, Wang C, Zhang M, Fu H, et al. X-ray enabled detection and eradication of circulating tumor cells with nanoparticles. Biosensors and Bioelectronics 2012;38(1):348-354.

[51] Horie M, Nishio K, Kato H, Endoh S, Fujita K, Nakamura A, et al. Evaluation of cellular influences caused by calcium carbonate nanoparticles. Chem Biol Interact 2014;210:64-76.

[52] Minehara H, Narita A, Naka K, Tanaka K, Chujo M, Nagao M, et al. Tumor cell- specific prodrugs using arsonic acid-presenting iron oxide nanoparticles with high sensitivity. Bioorg Med Chem 2012;20(15):4675-4679.

[53] Ramamurthy C, Sampath K, Arunkumar P, Kumar MS, Sujatha V, Premkumar K, et al. Green synthesis and characterization of selenium nanoparticles and its augmented cytotoxicity with doxorubicin on cancer cells. Bioprocess Biosyst Eng 2013;36:1131-1139.

[54] Abdal-hay A, Hamdy AS, Abdel-Jaber G, Barakat NA, Ebnalwaled A, Khalil KA. A facile manufacturing of Ag/SiO 2 nanofibers and nanoparticles composites via a simple hydrothermal plasma method. Ceram Int 2015;41(9):12447-12452.

[55] Gujar SK, Maheshwari S, Björkman-Burtscher I, Sundgren PC. Magnetic resonance spectroscopy. Journal of neuro-ophthalmology 2005;25(3):217-226.

[56] Taylor D. Magnetic resonance spectroscopy. Inborn Metabolic Diseases: Springer;1990. p. 55-65.

[57] Nixon C, Ormerod I, Johnson G. Nuclear magnetic resonance. Anaesthesia 1986;41(2):131-137.

[58] Günther H. NMR spectroscopy: basic principles, concepts and applications in chemistry: John Wiley & Sons; 2013.

Chapter 6

Hybridization Techniques in Nanotechnology-Present State and Future Trends

Diana Gonciar[1], Lucia Agoston[2], Teodora Mocan[3]

[1]Gastroenterology Institute; "Iuliu Hatieganu" University of Medicine and Pharmacy, 19-21 Croitorilor Street, Cluj-Napoca, Romania, tel/fax: +40264-439696

[2]Department of Medical Sciences, Iuliu Hatieganu University of Medicine & Pharmacy, 2–4 Clinicilor, 400006, Cluj-Napoca, Romania

[3]Department of Physiology, "Iuliu Hatieganu" University of Medicine and Pharmacy, 5-8 Clinicilor Street, Cluj-Napoca, Romania

The process of hybridization involves mixing two nucleic acids strands. The two strands are coming from two different molecules of DNA or RNA. To separate the chains, the molecules are usually treated with alkaline substances or heated. To identify and isolate the target nucleic acid, one of the chains is labeled with a radioactive tracer or a fluorescent compound, known as probe. The probe will reassociate with the target nucleic acid sequence by the complementarity of the bases principle (adenine is paired with thymine or with uracil and guanine is paired with cytozine) and the DNA or RNA chains may be simply detected. Based on this process, several laboratory techniques as fluorescence in situ hybridization, polymerase chain reaction, northern, western and southern blot were developed.

Fluorescence in situ hybridization (FISH) is a cytogenetic molecular technique, used to detect a specific sequence of DNA or RNA, usually in the packaged form (chromosome), but not necessarily. The probe is marked with fluorescent dye and it is complementary with the target DNA sequence which will hybridize to. It can be used to localize a gene position, for karyotyping, to detect the chromosomal abnormalities, gene-mapping, to mark the entire chromosomes, or to label the interphase DNA. As a disadvantage, FISH does not offer information about the cell type (1), but it brings the possibility to use simultaneously more than one probe to examine different targets (2).

Roger M et al. used polylactic acid nanoparticles (PLA-NPs) and lipidnanocapsuls (LNCs) to highlight if marrow-isolated adult multilineage inducible cells (MIAMI) can be used as a drug vehicle system in brain tumor therapy. They injected athymic mice with human glioma cells and then, MIAMI cells, loaded or not with PLA-NPs or LNCs, were injected in the tumor. The rodents were sacrificed. MIAMI cells were detected using FISH assay. Y-chromosome probe is employed. Unloaded MIAMI cells were localized between the normal and the affected tissue. No signals were seen in the normal brain and similar migration of the loaded MIAMI cells was observed. Authors concluded that MIAMI cells are veritable carriers for NPs in brain tumor (3).

Quantum dots (QDs), nanocrystalline semiconductors, have an advantageous photostability, longer fluorescence emission period (4) and have a narrow emission peak when are excited with different wavelengths (5). When are labeled with specific oligonucleotides, the nanoparticles can be used as veritable FISH probes and have the ability to reduce the signal/noise ratio (6).

QDs FISH probes designed by Y Choi et al are employed to target specific Drosophila Rp49 mRNA. To test the specificity, negative controls were performed. When human telomere specific DNA sequence was used, no signal was observed. By adding RNase A, the intensity of the fluorescent signal decreased. The FISH assay performed for Dif gene, suggested that QDs probes are able to identify low levels of mRNA. Lipopolysaccharide (LPS) induces transcription of the Dpt gene. To suggest the relation between intensity of the signals and the level of transcription, Drosophila cells were treated with different amounts of LPS. An increase of the intensity of the signals was observed when FISH was performed for the specific mRNA, suggesting that it can be used as a quantitative method. The authors also tested the ability to use two different QDs probes to target specific mRNA to assess the potential in multiplex imaging. The signals for the specific Act5C and Rp49 mRNA were highlighted (7).

QDs based molecular beacon (QDs- based MBs) developed by SM Wu et al. were used to target the β-lactamase gene, located in the plasmid pUC18 in Escherichia coli. β-lactamase gene is involved in the antibiotic resistance. FISH was performed using the designed nanoprobes, which are able to preserve their bioactivity even reassociated with complementary DNA sequence. The authors observed that the background noise was eliminated and clearer focusing was achieved. The nanosystem described might be veritable FISH probe for detecting antibiotic-resistant bacteria because it has the ability to penetrate the cell, to hybridize with the target DNA and to generate specific and clear signals (8).

Bentolila and Weiss designed QDs based FISH probes, containing DNA oligonucleotides against minor and major mouse satellites. First, one type of probe was used to target the minor satellite of the mouse mast cells. To evaluate the specificity of this method, negative control was also performed, by adding the QD probe against mouse major satellite on human HeLa cells and an irrelevant probe. No signal was detected. Then, two different labeled probes were simultaneously added to target the major satellite. Co-localization was observed. As a conclusion, the designed FISH probes can be used in multicolor FISH assay with the advantage that only one excitation wavelength is required (6).

Chromogenic in situ hybridization CISH assay is a laboratory technique similar with FISH but it also brings the immunohistochemistry advantages, to visualize the tissue morphology. DNA probes, labeled usually with digoxigenin, are used to hybridise with the target DNA sequence. The primary antibody binds to digoxigenin and then the secondary antibody combined with peroxidase is added. The substrate for peroxidase is diaminobenzidine. Hematoxylin staining is then performed and the slides are analyzed using a dark-field microscopy (9).

Polymerase chain reaction (PCR) is a wide-used technique, based also on the hybridization process. It allows amplification of small DNA sequences which will be further used. PCR has a variable number of repeated cycles and each cycle contains three steps. First, the reaction mixture, composed by the target DNA, the primers, free nucleotides and the DNA polymerase is heated, to let the complementary strands to separate. Second, because of the temperature decrease, the primers will hybridize with the target DNA chains. On the third step, DNA polymerase will add complementary nucleotides to the forming-chains. These steps are repeated and the DNA is exponentially amplified. PCR can be used as a qualitative method and also as a quantitative one (qPCR). To determine the amount of RNA, reverse transcriptase is required to transcript the information into a complementary DNA fragment. This method is known as revers transcription PCR (RT-PCR). (http://www.roche.com/pcr_e.pdf) Quantitative real time PCR uses fluorescent dyes to keep under observation in real time the total amount of the probe. First used fluorescent dye was ethidium bromide (Higuchi et al (10)), but SYBR Green I is currently one of the most preferred fluorescent dye

Exosomes are nano-scale vesicles, secreted by all type of cells, in vivo and in vitro, in both normal and affected cells. The vesicles contain RNA and proteins and are found in body fluids. Exosomes were isolated from the serum of patients with metastatic prostate cancer, who have undergone prostatectomy and from patients without any history of prostate cancer, serving as control (M Li et al). miRNA was isolated from the nano-vesicles and then qRT-PCR was performed and the cycle threshold (Ct) values were determined. The Ct values corresponding to the twelve amplificated types of miRNA were compared and it was revealed that no significant difference was observed between the control and the prostate cancer group related to miR16, 20a, 96, 107, 141, 145, 183, 221 and 409. For miR21, 375 and 574, the Ct values were lower for the patients with prostatectomy than the others from the control group, but higher than the values from the prostate cancer group. Considering the inverse proportionality relationship between the Ct value and the amount of specific amplificated miR, the authors suggested that miR21, 375 and 574, which are founded to be in higher levels in the serum samples from the prostate cancer patients, associated with exosomes nano-vesicles, may be veritable markers in prostate cancer (11).

R Say et al. synthesized Taq DNA polymerase nanoparticles and compared them to the traditional DNA polimerases. PCR assay was performed to emphasize the properties of the new enzyme. The reusability of the developed-enzyme was suggested by recovery the nano- polymerase using centrifugation. Taq DNA polymerase was reused and, after 5 cycles, the enzyme loss of activity was small. Compared to the traditional enzyme, the synthesized one has a higher stability against chemical and physical agents, due to the cross-linked intrinsic structure and also, a small quantity was required to perform the PCR assay. The nano-polymerase developed by the authors provides a new perspective of an economically and quicker PCR assay because of the important properties presented (12).

Silica-based nanoparticles, developed by Y Guo et al. are coated with streptavidin and then, are labeled with specific 5'-biotin- oligonucleotides. The nanocomplex is designed for hepatitis B virus (HBV) covalently closed circular DNA (cccDNA), which is a considered to be a valid marker for HBV infection. The authors assessed the performance of a quantitative assay for cccDNA, based on based on magnetic capture hybridization and quantitative PCR (MCH-qPCR).

The proposed-method was compared with real-time PCR and it was shown that combining the MCH, the specificity of the method increased. The increase of specificity resulted from the increase of amplicon in serum of HBV infected patients, when it was quantified without the MCH step. The amount of cccDNA detected, was close to the total amount of HBV DNA, suggesting the non-specific amplification process. The cccDNA could not be quantified from all the serum samples because one of them has a low-concentration of DNA. Between the cccDNA log10 concentrations and the log10 expected concentrations a good linearity relationship was identified, suggesting that the introduction of the MCH step could increase the parameters of the detection assays for cccDNA (13).

KP Miller et al. designed silicon dioxide nanoparticles (Si-NP) to reduce bacterial communication. To achieve the aim of the study, Vibrio fisheri, Gram-negative bacterium, was used. It has the property to generate bioluminescence, via the lux operon. N-acyl-L-homoserine lactone (HSL) is a signaling molecule generated by Gram-negative bacteria, able to activate the bioluminescence process. The nanoparticles were coated with β-cyclodextrin (β-CD) because HSL is allowed to bind to β-CD. The bacteria were treated with the proposed biosystem. To assess the efficiency of SI-NP in silencing bacterial communication, qPCR was performed to detect the difference between transcription of the lux operon in the treated group and in the control group. Results show that the proposed nanosystem decreased transcription of the lux operon, which indicate that Si-NP is able to down regulate bacterial communication (14).

X Hu et al developed doped-fluorapatite (FA) with Yb^{3+} and Ho^{3+} and then, coated the nanocrystals with dextran. The described nanoparticles were tested for the ability of labeling and tracking the chondrogenic differentiation. To achieve the purpose, rat bone marrow stem cells (BMSCs) with the ability to secret constant amount of green fluorescence proteins (GFP) were employed. BMSCsGFP were treated with different amounts of nanocrystal and chondrogenic differentiation was induced. Gene expression of Sox9, Col II was followed by real-time PCR analysis and it was shown that the transcription level did not change. Based on these data and also on the evidence that no difference was observed when cells treated with nanocrystals were stained with alcian blue after 21 days of chndrogenic differentiation induction, the authors concluded that treated BMSCsGFP are able to differentiate in vitro into chondrocytes (15).

GR Beck et al. performed RT-PCR to demonstrate that silica nanoparticles-NP1 do not elicit an inflammatory response. The murine monocyte cell lines (RAW264.7) were treated with NP1 or with the polyethylene glycol (PEG) coated NP1. It was shown that the nanoparticles employed do not initiate the inflammasome based cleavage of the precursor of IL-1β when compared with the non-treated cells group. A positive control test was performed by treating RAW264.7 with LPS, a molecule able to generate IL-1 β. RT-PCR assay showed that LPS induced IL-1β transcription. The authors concluded that the nanoparticles had no consequences on the immune system activation (16).

MN Weitzmann et al. employed silica-shell nanoparticles, combined them with magnetic cobalt ferrite nanoparticles (MNP) and coated with PEG. The described nanosystem was used to assess the potential to induce differentiation of the osteoblasts and to promote bone mineralization in vivo. To validate if NP1-MNP-PEG specifically influence mineralization on osteoblasts, qRT- PCR for ALK, OSC and Runx2 mRNA was performed on human aortic smooth muscle cells (HASMCs) and human embryonic kidney cells (HEKs), treated with the described nanoparticles. It was shown that no mineralization response was founded on HASMC and HEK, compared to osteoblasts, which proved a good response as a result of the treatment. The proposed nanoparticles are efficient in the specific induction of mineralization and differentiation of the osteoblast cells (17).

Gold nanorod-siRNA nanoplex (GNR-siRNAD) employed by AC Bonoiu et al. was used to investigate the interference withDARPP-32 (adenosine 3’,5’-monophosphate-regulated phosphoprotein) gene silencing in dopaminergic neuronal cells (DAN). DARPP-32, key protein in DAN cells, is activated by opiate addiction. DAN cells were treated with GNR-siRNAD and q-PCR was performed to evaluate the levels of PP-1 and ERK, effectors of the DARPP-32 signaling pathway. It was observed that the two proteins significantly decreased in the presence of GNR-siRNAD, which may indicate the potential usage of the proposed nanosystem in addiction therapy (18).

Southern Blot is a laboratory method used to detect DNA molecules from a mixture. The sequences are separated using electrophoresis, according to their size and then, are transferred on a bloating membrane and are let to hybridize with specific DNA probes, which are labeled with fluorescent or radioactive compounds. (http://www.nature.com/scitable/definition/southern-blot-289).

Cationic gold nanoparticles were developed to form a gene carrier complex (T Niidome et al). They were loaded with plasmid DNA containing the luciferase gene and then HeLa cells were treated with the proposed gene delivery system. Southern blotting was performed to determine the amount of DNA transfected into cells. It was observed the correlation between the amount of DNA and the expression level of luciferase and also, a significant proportion of gene transfection was succeeded. The present nano-delivery system may be a veritable compound of a future gene therapy (19).

ES Hwang et al employed single walled carbon nanotubes (SWCNTs), which advantageous optical properties for bioimaging, labeling and tracking- the nanotubes do not blink and are able to eliminate photobleaching. SWCNTs express stable Raman scattering. Based on these data, the authors conjugated SWCNTs with specific single-strained DNA oligonucleotides, complementary with the DNA sequences of Escherichia coli, used as a control, and human fibroblasts. Southern blotting assay was adjusted and Raman scattering was used instead of fuorescent staining. It was observed that the method is sensitive and specific. G peaks had lower amplitude when the amount of target DNA decreased. The borderline of detection the target DNA was evaluated to be 0.18 pg μl-1 which may suggest that Southern blot was improved by using SWCNT probes and it has achieved a comparable sensitivity with PCR. Future perspective of the technique includes adjusting the nanotubes length because DNA sequences may bind to them, instead of hybridizing with specific nucleic acid sequences (20).

Northern blot derivers from Southern blot analysis and it also used to detect specific nuclei acid from a mixture of molecules. In this case, the nucleic acid is RNA. It requires electrophoresis separation, transferring on a blotting membrane and labeled specific probe to detect the RNA sequence. (http://www.nature.com/scitable/definition/northern-blot-287)

GR Beck et al. used Northern blot to determine the expression of characteristic osteoblast genes in pre-osteoblastic cells (MC3T3), fibroblastic cells (NIH3T3) and RAW264.7 cells, treated with NP1. The nanoparticles were also validated by PCR to determine if they are able to elicit an immune response. It was founded that NP1, after 7 days of treatment, increase the expression of sialoprotein, osteopontin, osteocalcin and osterix in a dose dependent manner in MC3T3 cells. In non-osteoblastic cells (NIH3T3 and RAW264.7), no significant effect related to the upregulation of the bone matrix proteins was observed, which may indicate that NP1 promote specific differentiation. The authors concluded that presented nanoparticles are able to enhance transcription of specific osteoblast genes in MC3T3 cells, promoting the differentiation process (16).

Y Peng et al. designed an electrochemical biosensor for direct detection of miRNAs. The action process of the nanocomplex is based on the deposition of polyaniline after the proposed system hybridize with the target miRNA. The deposition is determined by RuO2. Northern blot was performed to evaluate the capacity of the proposed biosensor to identify let-7miRNAs. To achieve the aim, HeLa and lung cancer cells were employed. The results showed that specific miRNA was founded to be in a lower level when compared to normal cells. The method promotes a high sensitivity because the borderline of detection was founded to be 1 ng of RNA for less than 100 cells (21).

Mice experimental Ewing sarcoma was achieved by A Maksimenko et al. in order to emphasize the effect of antisense oligonucleotides (AON) loaded in nanospheres or nanocapsules against EWs-Fli-1 oncogene. After the intratumorally injection with AON free or loaded, the tumor were removed and northern blot was performed. It was revealed that both nanodelivery tools were efficient in release AON and the presented nanosystem is able to elicit specific down regulation of EWS-Fli-1 mRNA, indicating the role as feasible agents in Ewing sarcoma and also as effective delivery systems (22).

The development process of identifying RNA illustrates a tend towards inquiring into nanoparticles properties. Several assays for detecting specific miRNA were developed with the involvement of nanoparticles-based probes, optimizing the sensibility, specificity, reducing the background artifacts and providing time-saving detecting methods (23-25).

Western Blot combines the advantages of electrophoresis and the specificity of detection brought by the usage of antibodies to attain a precisely method to identify and quantify the amount of proteins. After the separation of proteins via electrophoresis, according to the molecular weight and to the isoelectric point, they are transferred on a membrane on which specific antibodies for the target proteins are added to be easily identified. The thickness of the bands seen are proportional with the amount of protein detected (26).

To relieve the usage of cationic albumin-conjugated pegylated nanoparticles (CBSA-NP) as an effective gene delivery system, western blot assay was performed by W Lu et al. The novel nanosystem was preferred to be used in gliomas because it can cross the brain-blood barrier as compared to the viral vectors. It was loaded with plasmid Porf-hTRAIL which encodes Apo2L/TRAIL to induce a selective apoptotic pathway. Mice were treated with C6 glioma cells and divided in three groups, one injected with CBSA-NP-hTRAIL, the other one with NP- hTRAIL, and the third one was used as control. The highest protein level was detected in the second day after treatment and it remains raised in the sixth day after the injection. The proposed system may be a feasible agent in glioma therapy (27).

Amine-modified single walled carbon nanotubes (a-SWNTs) were engineered by HJ Lee et al to scrutiny the implications in stroke. To achieve the purpose, rats were employed and divided in two groups, one pre-treated with a-SWNTs and the other with PBS. Following the administration, brain ischemia was inducted by middle cerebral artery occlusion surgery (MCAO). One week after the procedure, tissue from the ischemic area was used for western blot. On a first step, blots were immunoprobed for p53 and Bax and it was revealed that the expression level was downregulated in the treated group. P-ERK, a kinase involved in cell survival and a regulatory factor for apoptosis process, was higher in the control group than in the treated group, result which may indicate that the infarct area was larger in PBS-group. P-Akt expression level was founded to be comparable for both groups. Moreover, rats received an injection with LY294002, an antagonist for Akt and it conducted to the death of PBS-treated rats after the MCAO procedure. The finding conducts to the conclusion that Akt is a key component in the limitation of brain damage. In addition, N-Cad levels were higher in a-SWNTs treated rats, indicating that the protective effect is realized by sustaining cellular adhesion. Moreover, HIF-1α, VEGF (involved in angiogenesis) and DCX (neurogenesis marker) were downregulated in treated group, sustaining the conclusion that a-SWNT pre-treatment reduce the brain injury amplitude which leads to a diminishment of the angiogenesis and neurogenesis processes (28).

Y Huang et al. tested the efficiency of SeNPs coated with transferrin and loaded with deoxorubicin on MCF-7 (breast adenocarcinoma human cells) as a potential anti-tumor agent. After the cellular uptake of the developed nanosystem, western blot was performed to establish the apoptotic pathway activated. Results show an upregulation of the histone phosphorylation which indicates that the DNA is damaged, so it may induce apoptosis via p53 pathway. The upregulation of the phosphorylated p53 is also registred and demonstrates the implication of p53 in the apoptotic process induced by the proposed nanosystem, which is also sustained by the MAPK signaling cascade. Western blot was also performed for the in vivo study and results suggested the correlation with the MCF-7 experiments. Authors concluded that the novel nanosystem may be successfully used in cancer therapy and it was shown that it is able to activate p53 mediated apoptosis (29).

Silica NP1 employed by GR Beck Jr et al were added on MC3T3 and western blot was performed to evaluate the capacity of suppression the osteoclastogenesis function. It was found that the nanoparticles are able to prevent activation of subunits p50 and p52 of NF-Kb, which indicates that silica NP1 suppress differentiation of osteoclasts. Western blot assay was performed for Runx2 level in MC3T3 cells treated with NP1 and it was shown that the nanosystem upregulated the expression of the transcription factor, which is involved in the differentiation process of the osteoblasts. Taking into consideration the results validated by PCR and northern blot, the authors concluded that NP1 promise an effective agent against bone loss (16).

As the drug resistance phenomenon is one major cause of failure in cancer therapy, novel strategies are developing to fight against it. Based on the fact that tumor cells often have an increased numer of folate-receptors, T Liu et al coated SeNP with folate and added a payload of ruthenium polyridyl (RuPOP) with fluorescence and anticancer activity. Western blot was used to evaluate if the level of folate receptors (FAR) interfere with the cellular uptake because it was observed that R-HepG2 exhibited the strong fluorescence at the same moment, when compared to HepG2 and L02 cells treated with FA-SeNp. Results revealed that the FAR level was the highest in R-HepG2. The authors performed western blotting for the ABC family in R-HepG2, HepG2 and L02 cells and observed that the highest expression level is in R-HepG2. Furthermore, the assay was performed in R-HepG2 cells treated with different concentrations of FA-SeNPs and it was revealed the downregulation of ABC family related to concentration of nanoparticles used, result which lead to the conclusion that the proposed nanodrug may prevent drug resistance. To examine the anti-tumor effect, western blot assay for caspase 3, caspase 8, caspase 9 and PARP revealed that both intrinsic and extrinsic apoptotic pathways were activated. Moreover, the increase of p53, Ser 15, p-ATM, p-BRCA1, H2A.X, p38 and JNK reinforce the idea that FA-SeNp promotes apoptosis via p53 signaling cascade (30).

P Liu et al employed an efficient drug delivery for cancer therapy, based on amphiphilic graft copolymer poly (lactic-co-glycolic acid)-g-dextran (Dex-PLGA). Nanoparticles were loaded with paclitaxel (Dex-PLGA/PTX). P-gp is an efflux pump and it is often overexpressed in the membrane of cancer cells, phenomenon which leads to drug resistance. After the uptake of the presented nanodrugs into MCF-7(breast cancer cells) and MCF-7/Adr (multidrug-resistant breast cancer cells), western blotting was performed to evaluate the level of P-gp to demonstrate if overcoming drug resistance is dependent on downregulation P-gp. Without the uptake of Dex- PLGA/PTX, it was shown that MCF-7 cells do not express P-gp. After the treatment with Dex- PLGA loaded or not with PTX, western blot assay indicates that P-gp level was not affected. Moreover, flow cytometry sustains the results and lead to the conclusion that the developed nanosystem do not overcome drug resistance by reducind the P-gp levels (31).

GNR-siRNAD employed by Bonoiu et al was also validated by western blot to scrutiny the effect in addiction. After the uptake of the present nanoparticles in DAN cells, DARPP-32 level was quantified and it was observed that the expression level decreased. The result lead to the conclusion that the proposed nanosystem enhance gene silencing. Moreover, PCR testing straighten the idea that GNR-siRNAD may be successfully used in addiction treatment (18).

In order to assess the effect of MWCNTs on DNA, mouse embryonic stem cells were employed by L Zhu et al and treated with present nanotubes. Blots were immunoprobed for Oct4 both in treated and untreated cells. The elevation observed in treated cells suggests that MWCNTs initiate cell differentiation. An increase in a dose-dependent manner was observed in treated cells regarding to the p53 expression levels, which indicates that the nanotubes elicit apoptosis. It was founded that MWCNTs also promotes p53 phosphorylation. Furthermore, the increase of both isoforms of 8-oxoguanine-DNA-glycosylase1 (OGG1) was observed, indicating that MWCNTs cause damage in nuclear and mitochondrial DNA by a guanine lesion. Expression levels of Rad51 and X-ray cross-complementation group 4(XRCC4) were also founded to be elevated in treated cells, revealing that nanotubes induce double stranded DNA subsequent breakdown. Moreover, SUMO (small ubiquitin-like-modifier) -modified XRCC4 expression level was increased. MWCNTs were founded to cause DNA damage, conclusion that enhances the importance of analysis the toxicity of nanomaterials (32).

References

[1] Price C. Fluorescence in situ hybridization. Blood Rev 1993;7(2):127-134.

[2] Bartlett JM. Fluorescence in situ hybridization. Molecular Diagnosis of Cancer: Springer; 2004. p. 77-87.

[3] Roger M, Clavreul A, Venier-Julienne M, Passirani C, Sindji L, Schiller P, et al. Mesenchymal stem cells as cellular vehicles for delivery of nanoparticles to brain tumors. Biomaterials 2010;31(32):8393-8401.

[4] Jamieson T, Bakhshi R, Petrova D, Pocock R, Imani M, Seifalian AM. Biological applications of quantum dots. Biomaterials 2007;28(31):4717-4732.

[5] Ma L, Wu S, Huang J, Ding Y, Pang D, Li L. Fluorescence in situ hybridization (FISH) on maize metaphase chromosomes with quantum dot-labeled DNA conjugates. Chromosoma 2008;117(2):181-187.

[6] Bentolila LA, Weiss S. Single-step multicolor fluorescence in situ hybridization using semiconductor quantum dot-DNA conjugates. Cell Biochem Biophys 2006;45(1):59-70.

[7] Choi Y, Kim HP, Hong SM, Ryu JY, Han SJ, Song R. In situ Visualization of Gene Expression Using Polymer-Coated Quantum–Dot–DNA Conjugates. Small 2009;5(18):2085-2091.

[8] Wu S, Tian Z, Zhang Z, Huang B, Jiang P, Xie Z, et al. Direct fluorescence in situ hybridization (FISH) in Escherichia coli with a target-specific quantum dot-based molecular beacon. Biosensors and Bioelectronics 2010;26(2):491-496.

[9] Tanner M, Gancberg D, Di Leo A, Larsimont D, Rouas G, Piccart MJ, et al. Chromogenic in situ hybridization: a practical alternative for fluorescence in situ hybridization to detect HER-2/neu oncogene amplification in archival breast cancer samples. The American journal of pathology 2000;157(5):1467-1472.

[10] Higuchi R, Dollinger G, Walsh PS, Griffith R. Simultaneous amplification and detection of specific DNA sequences. Bio/technology 1992;10(4):413-417.

[11] Li M, Rai AJ, DeCastro GJ, Zeringer E, Barta T, Magdaleno S, et al. An optimized procedure for exosome isolation and analysis using serum samples: Application to

cancer biomarker discovery. Methods 2015.

[12] Say R, Biçen Ünlüer Ö, Ersöz A, Öziç C, Kılıç V. Reusable nanocopy machine particles for the replication of DNA. Biotechnol Prog 2015;31(1):119-123.

[13] Guo Y, Sheng S, Nie B, Tu Z. Development of Magnetic Capture Hybridization and Quantitative Polymerase Chain Reaction for Hepatitis B Virus Covalently Closed Circular DNA. Hepatitis monthly 2015;15(1).

[14] Miller KP, Wang L, Chen Y, Pellechia PJ, Benicewicz BC, Decho AW. Engineering nanoparticles to silence bacterial communication. Frontiers in microbiology 2015;6.

[15] Hu X, Zhu J, Li X, Zhang X, Meng Q, Yuan L, et al. Dextran-coated fluorapatite crystals doped with Yb 3 /Ho 3 for labeling and tracking chondrogenic differentiation of bone marrow mesenchymal stem cells in vitro and in vivo. Biomaterials 2015;52:441-451.

[16] Beck GR, Ha S, Camalier CE, Yamaguchi M, Li Y, Lee J, et al. Bioactive silica-based nanoparticles stimulate bone-forming osteoblasts, suppress bone-resorbing osteoclasts, and enhance bone mineral density in vivo. Nanomedicine: Nanotechnology, Biology and Medicine 2012;8(6):793-803.

[17] Weitzmann MN, Ha S, Vikulina T, Roser-Page S, Lee J, Beck GR. Bioactive silica nanoparticles reverse age-associated bone loss in mice. Nanomedicine: Nanotechnology, Biology and Medicine 2015;11(4):959-967.

[18] Bonoiu AC, Mahajan SD, Ding H, Roy I, Yong KT, Kumar R, et al. Nanotechnology approach for drug addiction therapy: gene silencing using delivery of gold nanorod-siRNA nanoplex in dopaminergic neurons. Proc Natl Acad Sci U S A 2009 Apr 7;106(14):5546-5550.

[19] Niidome T, Nakashima K, Takahashi H, Niidome Y. Preparation of primary amine-modified gold nanoparticles and their transfection ability into cultivated cells. Chemical Communications 2004(17):1978-1979.

[20] Hwang E, Cao C, Hong S, Jung H, Cha C, Choi J, et al. The DNA hybridization assay using single-walled carbon nanotubes as ultrasensitive, long-term optical labels. Nanotechnology 2006;17(14):3442.

[21] Peng Y, Yi G, Gao Z. A highly sensitive microRNA biosensor based on ruthenium

oxide nanoparticle-initiated polymerization of aniline. Chemical Communications 2010;46(48):9131-9133.

[22] Maksimenko A, Malvy C, Lambert G, Bertrand J, Fattal E, Maccario J, et al. Oligonucleotides targeted against a junction oncogene are made efficient by nanotechnologies. Pharm Res 2003;20(10):1565-1567.

[23] Yang SW, Vosch T. Rapid detection of microRNA by a silver nanocluster DNA probe. Anal Chem 2011;83(18):6935-6939.

[24] Liang RQ, Li W, Li Y, Tan CY, Li JX, Jin YX, et al. An oligonucleotide microarray for microRNA expression analysis based on labeling RNA with quantum dot and nanogold probe. Nucleic Acids Res 2005 Jan 31;33(2):e17.

[25] Gao Z, Yang Z. Detection of microRNAs using electrocatalytic nanoparticle tags. Anal Chem 2006;78(5):1470-1477.

[26] Mahmood T, Yang P. Western blot: technique, theory, and trouble shooting. North American journal of medical sciences 2012;4(9):429.

[27] Lu W, Sun Q, Wan J, She Z, Jiang XG. Cationic albumin-conjugated pegylated nanoparticles allow gene delivery into brain tumors via intravenous administration. Cancer Res 2006 Dec 15;66(24):11878-11887.

[28] Lee HJ, Park J, Yoon OJ, Kim HW, Kim DH, Lee WB, et al. Amine-modified single-walled carbon nanotubes protect neurons from injury in a rat stroke model. Nature nanotechnology 2011;6(2):121-125.

[29] Huang Y, He L, Liu W, Fan C, Zheng W, Wong Y, et al. Selective cellular uptake and induction of apoptosis of cancer-targeted selenium nanoparticles. Biomaterials 2013;34(29):7106-7116.

[30] Liu T, Zeng L, Jiang W, Fu Y, Zheng W, Chen T. Rational design of cancer-targeted selenium nanoparticles to antagonize multidrug resistance in cancer cells. Nanomedicine: Nanotechnology, Biology and Medicine 2015;11(4):947-958.

[31] Liu P, Situ J, Li W, Shan C, You J, Yuan H, et al. High tolerated paclitaxel nano-formulation delivered by poly (lactic-co-glycolic acid)-g-dextran micelles to efficient cancer therapy. Nanomedicine: Nanotechnology, Biology and Medicine 2015;11(4):855-866.

[32] Zhu L, Chang DW, Dai L, Hong Y. DNA damage induced by multiwalled carbon nanotubes in mouse embryonic stem cells. Nano letters 2007;7(12):3592-3597.

Chapter 7

Gold Nanoparticles for Multimodal Imaging in Nanomedicine

Lucian Mocan[1], Teodora Mocan[2], Cristian T. Matea[1], Flaviu A. Tabaran[3], Lucia Agoston[4], Ofelia Mosteanu[5], Teodora Pop[5], Dana Bartos[1], Cornel Iancu[1]

[1]Gastroenterology Institute; “Iuliu Hatieganu” University of Medicine and Pharmacy, 19-21 Croitorilor Street, Cluj-Napoca, Romania, 400162

[2]Department of Physiology, "Iuliu Hatieganu" University of Medicine and Pharmacy, Clinicilor 5-7, Cluj-Napoca, Romania

[3]Department of Pathology, University of Agricultural Sciences and Veterinary Medicine, Faculty of Veterinary Medicine, 3-5 Manastur Street, 400372 Cluj-Napoca, Romania

[4]Department of Medical Sciences, Iuliu Hatieganu University of Medicine & Pharmacy, 2–4 Clinicilor, 400006, Cluj-Napoca, Romania

[5]3rd Medical Clinic, University of Medicine and Pharmacy Cluj Napoca 19-21 Croitorilor Street, Cluj-Napoca, Romania, 400162

Introduction

Due to advance developments in functionalization chemistry, novel gold nanoparticles-based nanosystems with applications in diagnosis and treatment of various human patologies have been reported. (1-5) During the last decade, gold nanoparticles (AuNPs) have been extensively explored as an x-ray contrast agents. Gold nanoparticles exhibit unique properties that makes them suitable candidates as x-ray contrast agents in clinical practice having a relatively high x- ray attenuation coefficient compared with both barium sulfate and iodine. Another major advantage of the GNPs is represented by increased vascular retention time compared with iodinated molecules. Generally, the safety/toxicity of the nanoparticles depends on shape, surface coating and their size. (6-9) This paper illustrates the latest achievements in the applications of gold nanoparticles as multimodal imaging agents for diagnosis of human diseases.

A multifunctional AS1411-functionalized fluorescent gold nanoparticle system (named NAANPs) was synthesized and successfully applied for both targeted cancer cell imaging and efficient photodynamic therapy (PDT). The NAANPs bionanosystems were developed by functionalization of the gold nanoparticles with AS1411 aptamer and then bound with one porphyrin derivative N-methylmesoporphyrin IX (NMM). Next, using HeLa cells over expressing nucleolin as representative cancer cells, the authors proved that the formed NAANPs can target to the cell surface via the specific AS1411-nucleolin interaction. They also observed a linear correlation between fluorescence intensity of NMM and binding to AS1411 G-quadruplex. (10)

Several authors devoped polymer-coated gold nanoparticles using glycol chitosan as a reducing agent and a stabilizer. Next tomographic displays of malign lesions were successfully obtained in the tumor-xenografted animal model when the GC-AuNPs were used as a CT contrast agent. The authors showed that specific targeting of the gold nanoparticles was due to the properties of GC because GC-AuNPs were accumulated in the tumor, in contrast with control nanoparticles. The phantom images were highly contrasted with GC-AuNPs, and the X-ray absorption increased linearly according to the concentration of GC-AuNP. The in vitro behavior of GC- AuNPs was assessed on two types of cells, colon cancer cells (CT-26) and macrophage cells (RAW264.7) showing that GCAuNPs were found exclusively in CT-26 colon cancer cells, not in macrophage cells. (11)

In another paper a new platform for in vivo CT molecular imaging, using immuno-targeted gold nanoprobes that selectively and sensitively target tumor specific antigens was described. (12) The authors successfully developed gold nanoprobes that forms clusters inside cancer cells, yielding a distinguishable X-ray attenuation, feature that was not observed in normal cells or tissue. Using this technique the targeted cancer tissue was easy to be identified. In the present research the authors synthesized 15/45 nm AuNR using the seed mediated growth method and further conjugated with UM-A9 antibody. Next UM-SCC-1 and UM-SCC-5 human head and neck cancer cell lines and the negative control samples of fibrosarcoma (UM-FS-1) and melanoma (UM-Mel-1), which are known not to express the A9 were treated with antibody- coated AuNR solution (2.5 mg/mL), and allowed to interact for 90 min at room temperature. The authors observed that the attenuation coefficient (with respect to water) of the SCC cancer cells that were targeted by the A9 antibody coated gold nanorods was more than 5 times higher than that of the non-targeted SCC cancer cells (32 and 28 HU vs. 168 and 172 HU, respectively). In contrast, the attenuation values observed for the negative control samples that were targeted with gold nanorods (larynx and oral cancer cells targeted with nanorods that were coated with non matching antibodies, and normal fibroblast and melanoma cells targeted with A9 antibodies) were significantly lower (58, 54, 50, 62 HU, respectively). This finding strongly suggested that head and neck tumors may show a likely enhancement of 3-4 times the local contrast of non- targeted tissue in vivo. (12)

In their paper Reuveni and al investigated the delivery of 30 nm GNP-EGF towards head and neck squamous cell carcinoma (SCC), since such tumors express an extremely high level of EGFR. The ability of anti-EGFR-targeted GNPs to form a concentrated assembly exclusively on the SCC cancer cells in tumor-bearing mice was investigated. The authors stated that the strong selective X-ray attenuation by gold nanobiosystems, which is distinct from the attenuation of other cell types and tissues, makes the targeted tumor highly distinguishable and easy to diagnose in CT imaging. A very important feature was also shown: active tumor targeting was more efficient than passive targeting (at specific time points) in authors opinion because of its elevated tumor uptake and retention forces. (13)

A nanoprobe (M-NPAPF-Au) co-loaded with an aggregation-induced emission (AIE) red dye and gold nanoparticles into DSPE-PEG2000 micelles for dual-modal fluorescence/CT imaging was also developed using the method of “one-pot ultrasonic emulsification”. *In vivo* tests of this novel nanobiosystem demonstrated their excellent tumor-targeting ability, high fluorescence, long blood circulation half-life, superior tumor-targeting ability and CT imaging effects. (14)

Several authors reported the development of a lactobionic acid (LA)-modified dendrimer- entrapped gold nanoparticle (LA-Au DENPs) nanosystem for in vitro and in vivo targeted CT imaging of human hepatocellular carcinoma. These amine-terminated poly (amidoamine) dendrimers of generation 5 pre-modified with fluorescein isothiocyanate and poly(ethylene glycol)-linked LA showed good stability under different pH (5–8) and temperature (4–50 ℃) conditions and in different aqueous media, and showed noncytotoxic efect to normal cells but cytotoxic to the targeted hepatocarcinoma cells. In addition the authors proved that LA-Au DENPs complexes can be used as a highly effective nanoprobe for specific CT imaging of hepatocarcinoma cells in vitro and the xenoplanted tumor model in vivo even greater than clinically employed iodine-based CT contrast. (15)

Karmany et al conjugated the anti-CD105 antibody radiolabeled with 89Zr bound to gold nanoparticles (AuNPs) for further testing their biodistribution in mice with a focus on tumor targeting. Using quantitative PET imaging and ICP-MS analysis the authors assessed in vivo distribution and specific tumor targeting of these tracers showing that the tumor uptake of immunoconjugates was preserved up to 24 h after injection, with high tumor contrast and selective tumor targeting. In contrast, no major tracer accumulation was observed over time in nonspecific organs. (16)

In another study, several authors used hyperspectral imaging to assess the uptake and distribution of phosphatidylcholine-coated citrate gold nanoparticles (CGN) and silica-gold nanoshells (SGN) after tail-vein injection in mice bearing orthotopic pancreatic adenocarcinoma. For CGN, the liver and tumor showed 26.5±8.2 and 23.3±4.1 particles/100μm^2 within 10μm from the nearest source and few nanoparticles beyond 50μm, respectively. The spleen tissue had 35.5±9.3 particles/100μm^2 within 10μm with penetration also limited to 50μm. For SGN, the liver showed 31.1±4.1 particles/100μm^2 within 10μm of the nearest source with penetration hindered beyond 30μm. The spleen and tumor showed uptake of 22.1±6.2 and 15.8±6.1 particles/100μm^2 within 10μm, respectively, with penetration similarly hindered. CGH average concentration (nanoparticles/μm2) was 1.09±0.14 in the liver, 0.74±0.12 in the spleen, and 0.43±0.07 in the tumor. SGN average concentration (nanoparticles/μm^2) was 0.43±0.07 in the liver, 0.30±0.06 in the spleen, and 0.20±0.04 in the tumor. (17)

Several authors developed and tested Arg-Gly-Asp-D-Phe-Lys peptide-modified PEGylated dendrimer-entrapped gold nanoparticles for targeted CT imaging of breast carcinoma. The 2.8 nm PEGylated Au DENPs-RGD were spherical, water dispersible and biocompatible and displayed a higher x-ray attenuation intensity than Omnipaque at the same Au or I concentrations. The authors also showed that conjugated RGD ligand can specifically identify and target overexpressed integrin receptors on MDA-MB-435 cells. Following their parenteral administration, these nanoprobes accumulated in the targeted area of mice with MDA-MB-435 xenograft tumors, allowing the tumor to be detected by CT imaging. (18)

In another paper, synthesis and characterization of 1.9-4.6 nm gold nanoparticles (AuNPs) entrapped within polyethylene glycol (PEG)-modified polyethylenimine (PEI) for blood pool and tumor computed tomography (CT) imaging was reported. Following the intravenous administration of the [(Au0) 200-PEI•NHAc-mPEG] NPs via the tail vein, the tumor-bearing mice were scanned by a clinical CT imaging system at different time points showing a better X- ray attenuation property than that of clinically used iodinated small molecular contrast agent (e.g., Omnipaque) and the prolonged half-decay time (11.2 h in rat) confirmed by pharmacokinetics studies. (19)

Chanda et al developed biocompatible gum arabic stabilized gold nanocrystals (GA-AuNPs) and further tested their role as X-ray contrast agent in tumor bearing mice and dog. Following intratumoral injections of GA-AuNP the authors obtained a X-ray contrast change of 26 HU in the tumor region after 1 hour post-injection period that reached a threshold limit within a short time period (5 h), and was retained in the tumor tissue for the rest of the period of investigation. Next, GA-AuNP was injected intratumorally in dog and a contrast enhancement of 12 HU was observed. The CT images of both mice and dog showed that GA-AuNP was effectively distributed and retained throughout the tumor site. (20)

Conclusion

We may assert that multimodal imaging using functionalized gold nanoparticles represents a feasible therapeutic method for the diagnosis of human diseases. However further studies are required to fully understand the biological interactions of nanoparticles inside biological systems.

References

[1] Lehner R, Wang X, Marsch S, Hunziker P. Intelligent Nanomaterials for Medicine: Carrier platforms and targeting strategies in the context of clinical application. Nanomedicine: Nanotechnology, Biology and Medicine 2013.

[2] Parveen S, Misra R, Sahoo SK. Nanoparticles: a boon to drug delivery, therapeutics, diagnostics and imaging. Nanomedicine: Nanotechnology, Biology and Medicine 2012;8(2):147-166.

[3] Banerjee D, Harfouche R, Sengupta S. Nanotechnology-mediated targeting of tumor angiogenesis. Vasc Cell 2011 Jan 31;3(1):3.

[4] Jiao PF, Zhou HY, Chen LX, Yan B. Cancer-targeting multifunctionalized gold nanoparticles in imaging and therapy. Curr Med Chem 2011;18(14):2086-2102.

[5] Shi J, Votruba AR, Farokhzad OC, Langer R. Nanotechnology in drug delivery and tissue engineering: from discovery to applications. Nano letters 2010.

[6] Stern S, Adiseshaiah P, Crist R. Autophagy and lysosomal dysfunction as emerging mechanisms of nanomaterial toxicity. Particle and Fibre Toxicology 2012;9(1):20.

[7] Mittal S, Sharma V, Vallabani NV, Kulshrestha S, Dhawan A, Pandey AK. Toxicity evaluation of carbon nanotubes in normal human bronchial epithelial cells. J Biomed Nanotechnol 2011 Feb;7(1):108-109.

[8] Soenen SJ, Rivera-Gil P, Montenegro J, Parak WJ, De Smedt SC, Braeckmans K. Cellular toxicity of inorganic nanoparticles: common aspects and guidelines for improved nanotoxicity evaluation. Nano Today 2011;6(5):446-465.

[9] Mocan T, Clichici S, Agoşton-Coldea L, Mocan L, Şimon Ş, Ilie IR, et al. Implications of oxidative stress mechanisms in toxicity of nanoparticles (review). Acta Physiol Hung 2010;97(3):247-255.

[10] Ai J, Xu Y, Lou B, Li D, Wang E. Multifunctional AS1411-functionalized fluorescent gold nanoparticles for targeted cancer cell imaging and efficient photodynamic therapy. Talanta 2014;118:54-60.

[11] Sun I, Na JH, Jeong SY, Kim D, Kwon IC, Choi K, et al. Biocompatible glycol chitosan-coated gold nanoparticles for tumor-targeting CT imaging. Pharm Res 2014;31(6):1418-1425.

[12] Popovtzer R, Agrawal A, Kotov NA, Popovtzer A, Balter J, Carey TE, et al. Targeted gold nanoparticles enable molecular CT imaging of cancer. Nano letters 2008;8(12):4593-4596.

[13] Reuveni T, Motiei M, Romman Z, Popovtzer A, Popovtzer R. Targeted gold

nanoparticles enable molecular CT imaging of cancer: an in vivo study. Int J Nanomedicine 2011;6:2859-2864.

[14] Zhang J, Li C, Zhang X, Huo S, Jin S, An F, et al. In vivo tumor-targeted dual- modal fluorescence/CT imaging using a nanoprobe co-loaded with an aggregation- induced emission dye and gold nanoparticles. Biomaterials 2015;42:103-111.

[15] Liu H, Wang H, Xu Y, Guo R, Wen S, Huang Y, et al. Lactobionic acid-modified dendrimer-entrapped gold nanoparticles for targeted computed tomography imaging of human hepatocellular carcinoma. ACS applied materials & interfaces 2014;6(9):6944-6953.

[16] Karmani L, Bouchat V, Bouzin C, Levêque P, Labar D, Bol A, et al. 89Zr-labeled anti-endoglin antibody-targeted gold nanoparticles for imaging cancer: implications for future cancer therapy. Nanomedicine 2014;9(13):1923-1937.

[17] England CG, Huang JS, James KT, Zhang G, Gobin AM, Frieboes HB. Detection of Phosphatidylcholine-Coated Gold Nanoparticles in Orthotopic Pancreatic Adenocarcinoma using Hyperspectral Imaging. PloS one 2015;10(6):e0129172.

[18] Li K, Zhang Z, Zheng L, Liu H, Wei W, Li Z, et al. Arg-Gly-Asp-D-Phe-Lys peptide- modified PEGylated dendrimer-entrapped gold nanoparticles for targeted computed tomography imaging of breast carcinoma. Nanomedicine 2015;10(14):2185-2197.

[19] Zhou B, Zheng L, Peng C, Li D, Li J, Wen S, et al. Synthesis and Characterization of PEGylated Polyethylenimine-Entrapped Gold Nanoparticles for Blood Pool and Tumor CT Imaging. ACS applied materials & interfaces 2014;6(19):17190-17199.

[20] Chanda N, Upendran A, Boote EJ, Zambre A, Axiak S, Selting K, et al. Gold nanoparticle based X-ray contrast agent for tumor imaging in mice and dog: A potential nanoplatform for computer tomography theranostics. Journal of biomedical nanotechnology 2014;10(3):383-392.

Short Introduction to the Book

During the past decade advances in functionalization chemistry have been one of the driving forces in the development of new classes of novel nanomaterials for applications in biology and medicine. Despite the impressive scientific efforts towards the development of novel nanomediated therapies, at the current time there is a tremendous need for standardizing cellular and molecular protocols used in Nanomedicine. this is the first attempt to gather in a single book the most common molecular techniques used in Nanomedicine. Since Nanomedicine field is expanding and becomes part of the curricula in many universities, the present book with protocols will be extremely useful for the researchers, students and medicaldoctors. This book intends to publish the most common cellular and molecular techniques (presented in a reproducible manner) used in Nanomedicine (at the interface of nanoparticles with biological systems).

Short biography of author

Lucian Mocan is Associate Professor in General Surgery (Digestive Oncologic Surgery) at 3-rd Surgical University Hospital-"Prof. O. Fodor" Gastroenterology Intitute Iuliu Hatieganu University of Medicine and Pharmacy Cluj-Napoca, Romania. He is also the vicepresident of Romanian Society of Nanomedicine, cofounder of the Nanomedicine Department at 3-rd Surgical Clinic. Among clinical studies in the field of digestive surgical oncology, during the last three years, Dr. Mocan's research was also focused in the area of nanotechnology, bio-nano-medical research, nano-toxicology, cancer visualization and treatment by bioconjugated nanomaterials with priority on the selective laser ablation and optical damage of the pancreatic and liver cancer cells by antibody functionalized nanoparticles.

To order additional copies of this book, please contact:
Science Publishing Group
book@sciencepublishinggroup.com
www.sciencepublishinggroup.com

ISBN 978-1-940366-05-0

9 781940 366050 >

Price: US $90